E.O. Paton Electric Welding Institute of the National Academy of Sciences of Ukraine

International Scientific-Technical and Production Journal

The Paton WELDING JOURNAL

December **2016**
No. 12

Published since 2000

English translation of the monthly «Avtomaticheskaya Svarka» (Automatic Welding) journal published in Russian since 1948

Address
E.O. Paton Electric Welding Institute,
International Association «Welding»
11 Kazimir Malevich Str. (former Bozhenko Str.),
03680, Kiev, Ukraine
Tel.: (38044) 200 60 16, 200 82 77
Fax: (38044) 200 82 77, 200 81 45
E-mail: journal@paton.kiev.ua
www.patonpublishinghouse.com

State Registration Certificate
KV 4790 of 09.01.2001
ISSN 0957-798X

Subscriptions
$348, 12 issues per year,
air postage and packaging included.
Back issues available.

CONTENTS

doi.org/10.15407/tpwj2016.12.01

JOINING PARTS FROM SHAPE-MEMORY ALLOY OF Cu–Al SYSTEM AND STRUCTURAL METALS BY ARC-CONTACT WELDING

B.E. PATON[1], **D.M. KALEKO**[1], **S.N. KEDROVSKY**[2], **Yu.N. KOVAL**[2], **L.M. NEGANOV**[2] and **V.N. SLEPCHENKO**[2]

[1] E.O. Paton Electric Welding Institute, NASU
11 Kazimir Malevich Str., 03680, Kiev, Ukraine. E-mail: office@paton.kiev.ua
[2]G.V. Kurdyumov Institute for Metal Physics, NASU
36 Acad. Vernadsky Blvd., 03680, Kiev, Ukraine. E-mail: metal@imp.kiev.ua

Shape-memory alloys changing part configuration at heating, as well as preserving their elasticity at up to 8–10 % deformation, are becoming ever wider applied in industrial products and apparatuses as thermally-activated elements. Commercial application of alloys of Cu–Al system instead of well-studied alloy of Ti–Ni system (nitinol) allows lowering product cost and expanding the application area up to high temperatures (about 400 °C). Widening the range of products with elements from shape-memory alloys requires studying the possibility of joining metals of this system with structural metals, in particular, with stud-type fasteners. Proceeding from available experience, joints of studs from low-carbon steel of St.3 grade and 12Kh18N9T stainless steel, as well as L63 brass and AMg3 aluminium alloy produced by the methods of arc-contact welding by a capacitor discharge and by DC pulse were studied. Good results were obtained at capacitor welding of studs from the above materials, except for AMg3. The latter is attributable to greater mismatch of thermophysical properties of the metals joined. In DC welding, strong joints were produced only with studs from St.3 steel, because of greater time of welding. It is shown that pulsed welding methods enable preserving functional properties of parts from shape-memory alloys. Inhomogeneity of butt metal structure was found in dissimilar metal welding, which is attributable to short-time existence of the melt (incomplete mixing) and heterogeneity and non-simultaneity of joint cluster solidification. A positive consequence of that is absence of brittle intermetallics of $FeAl_3$ type in the butt and preservation of ductility at deformation of joints with steel studs. 5 Ref., 1 Table, 9 Figures.

Keywords: *shape-memory alloys, copper-aluminium alloys, arc-contact welding, structural materials, thermoelastic martensitic transformation*

Modern technology is increasingly interested in application of materials with special properties, allowing development of devices, self-activating at the change of external conditions. Specific characteristics of such materials enable simplifying the design, and consequently, improving the operating reliability of machine activators. Such materials include, in particular, shape-memory alloys (SMA).

These alloys attract growing interest in different sectors of industry, medicine and culture, owing to the possibility of practical utilization of their thermoelastic characteristic, namely their ability to recover the preset shape at heating, after deformation in the cold state. In addition to thermoelasticity (form change under the impact of stresses, arising at crystallographic transformations), these alloys are also characterized by widely applied properties of superelasticity, namely preservation of elastic properties at relatively high deformations.

From the large number of known shape-memory alloys, the best studied and the most widely accepted now are alloys based on two systems, namely Ti–Ni and Cu–Al. Each of them has its advantages and disadvantages. Nitinol meets the requirements of medical applications better than do other alloys, namely it has high corrosion resistance, bioinertness and biocompatibility, as well as good mechanical properties (yield point is higher than 1 GPa, elastic deformation is up to 8 %, modulus of elasticity is about 70 MPa). At the same time, in most of non-medical applications less expensive copper-based alloys can be used, the technology of manufacturing and heat treatment of which is well-known. In addition to relatively low cost, copper-aluminium SMA, compared to nitinol, have higher limit temperature range of martensitic transformations that allows them to be used in devices, operating at high temperatures, for instance, in automatic fire extinguishing systems or in thermal plants of the type of furnaces, boilers or steam lines.

Industrial application of any materials, including SMA, requires solving the problems of joining them to each other or to other materials. Earlier [1, 2], we showed that characteristics of SMA of Ni–Ti or Cu–Al systems are preserved at pulse welding, and, therefore, this class of welding processes can be applied for

joining these alloys, when used in thermally-activated structures.

It should be noted that the earlier considered welding methods and characteristic small dimensions of the samples allowed limiting current pulse duration to several milliseconds. This was convenient to produce welded joints in medical products and in instrument-making. However, application of copper-aluminium alloy in power engineering requires increasing the welded cross-section, and duration of welding heating and energy input, respectively.

This work is a study of the possibility of joining plates from SMA of Cu–Al system to fasteners in the form of studs from structural alloys of different grades. The complexity of the problem was determined not only by behaviour of the alloy with shape-memory effect in the joint, but also by metallurgical compatibility of dissimilar metals, including combinations of iron alloys and non-ferrous metals. Traditional stud welding techniques, namely capacitor-discharge welding («contact» and «gap» methods) and DC arc welding are also considered [3]. Experiments on capacitor stud welding were performed in K-747MB machine [4], arc welding experiments were conducted in GLV 650 machine of HBS Company (Germany).

Capacitor stud welding. At selection of the mode of capacitor stud welding the variable parameters were capacitor capacitance, their charging voltage, lift height (in welding by «gap» method) and upset force (Table). Results of rupture testing showed that it was not possible to produce strong joints with all the materials. This pertains, in particular, to welding studs from AMg3 aluminium alloy. Strong and stable joints were produced only with studs from this alloy of not more than M3 diameter by «contact» welding method. In standard stud, in keeping with ISO 13918, the ratio of joint area (area of the flange at the stud end to be welded) to stud cross-sectional area is maximum for M3* (Figure 3). Presence of a flange on the stud at capacitor welding is due to the need to increase the joint strength up to that of base metal without increasing the energy required to create a reinforcement around the stud body. Lowering of welding current enables capacitor welding of studs to a thin sheet, preservation of decorative or functional coating on the sheet reverse side and welding of dissimilar metals.

At determination of welding mode, providing strong welded joints, correspondence of welded samples quality to the condition of fracture running across the stud body, was verified by a rapid method: stud bending in keeping with ISO Standard 14555.

Modes of welding different studs to sheet material from Cu–Al system alloys

Stud material	Threaded stud	Capacitor capacitance, mF	Capacitor charging voltage, V	Upset force, N	Lift height, mm
«Contact» welding					
St.3 steel	M3	96	60	15	–
	M6	96	100	15	–
	M8	96	150	15	–
12Kh18N9T steel	M3	72	75	15	–
	M6	96	125	10	–
	M8	96	150	10	–
L63 brass	M3	48	100	10	–
	M6	60	125	10	–
	M8	96	175	10	–
AMg3 alloy	M3	72	80	15	–
«Gap» welding					
St.3 steel	M3	96	80	–	3
	M8	96	150	–	3
L63 brass	M3	36	75	–	2
	M6	72	125	–	2

Dependence of tensile strength of joints on welding mode parameters was studied on studs of M6 diameter. Results of these measurements are shown in Figure 2.

Influence of capacitor capacitance on joint strength in «contact» welding was determined at constant value of capacitor charging voltage, which corresponds to optimum value given in the Table, namely, 100 V for St.3 steel, 125 V — for studs from 12Kh18N9T steel and L63 brass. Analysis of curves of rupture force dependence on capacitor capacitance (Figure 2, *a*) showed that for steel studs at maximum capacitor capacitance the welding mode still remains energetically unexhausted, but the achieved strength already corresponds to specific characteristics of the material. At the same time, welding studs from lower-melting

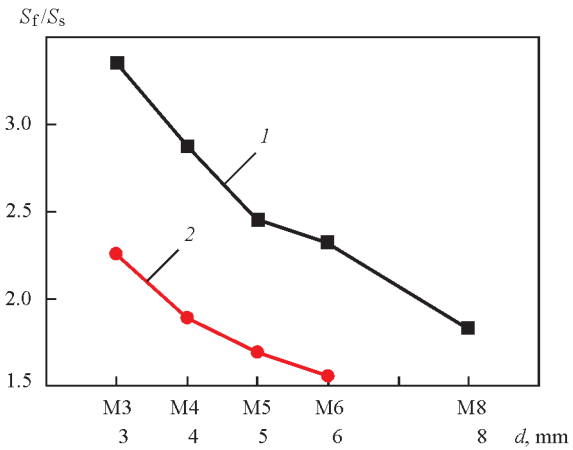

Figure 1. Standard ratio of the area of flange end face on the stud to section of threaded (*1*) and smooth (*2*) studs

*That is most probably related to conditions of stud manufacturing by cold upset forging.

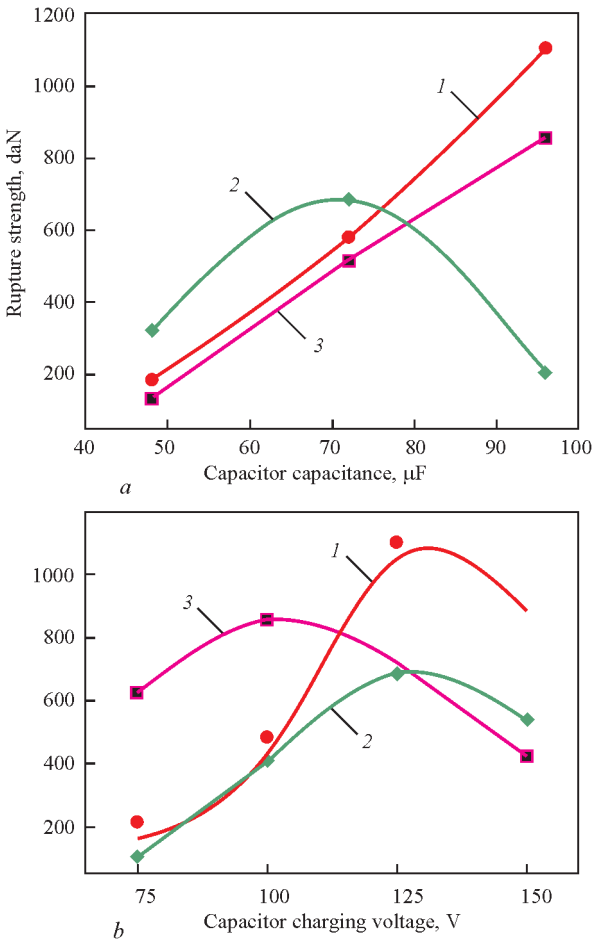

Figure 2. Dependence of strength of welded joints of M6 studs from different metals with plates from SMA of Cu-Al system on capacitance (*a*) and charging voltage (*b*) of capacitors: *1* — 12Kh18N9T steel; *2* — L63 brass; *3* — St.3 steel

brass with exceeding the optimum value of energy, accumulated in the capacitors, leads to lowering of sample strength. As shown by visual analysis, this is due to melting out of a considerable part of the flange being welded. At tension, fracture runs across the flange body with stud tearing out.

As the energy accumulated in the capacitors has a quadratic dependence on charging voltage, influence of the latter is more significant than that of the capacitance values. This is illustrated by Figure 2, *b*. Determination of joint strength dependence on capacitor charging voltage was performed with M3 studs at capacitor capacitance found to be the optimum one (Table). The curves and sample examination showed that at a low capacitor charge the stored energy is insufficient for melting the entire abutted surface of the flange at the stud end face. Here, an undercut is preserved in the welded joint at the flange periphery. When the optimum value of stored energy in the butt is exceeded, pores are formed, as shown by fracture analysis, reducing the joint area. Visual analysis revealed simultaneous intensification of liquid overheated metal splashing, that also reduces the joint area and creates a slot between the stud and the sheet.

Upset force is one of the determining parameters of the mode of capacitor stud welding. In welding by the «contact» method, the results of which are discussed below, and in which upsetting is performed before arc excitation by explosion of a thin protrusion at the stud end face, the force is determined by the time of stud holding at discharge current (Figure 3). The influence of contact resistance on duration of heating the exploding protrusion (section 1) is clearly seen in voltage oscillogram. Comparison of oscillograms shows that the delay of arc excitation (Figure 4, *b*) leads to shorter duration of arc stage of the discharge (section II in voltage curve).

Shown oscillograms also demonstrate lowering of amplitude value of current and voltage between the parts being welded (arc electrodes) at increase of pressure of welding head spring. These changes are caused by counter-action of spring upsetting pressure and exploding protrusion vapour pressure. Increase of vapour pressure at protrusion overheating by prolonged current passage leads to greater electric resistance of the arc gap (comparable with discharge circuit resistance) that causes current lowering, whereas increase of spring pressure reduces the arc length, while changing its voltage.

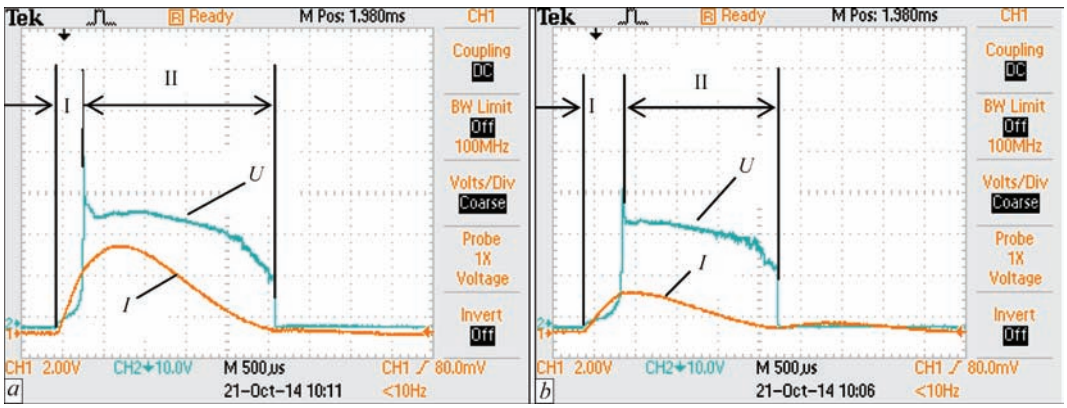

Figure 3. Oscillograms of current *I* and voltage *U* between the parts being welded during welding M8 studs from stainless steel by «contact» method with spring pressure of 50 (*a*) and 60 N (*b*) (96 mF capacitor capacitance, 150 V charging voltage)

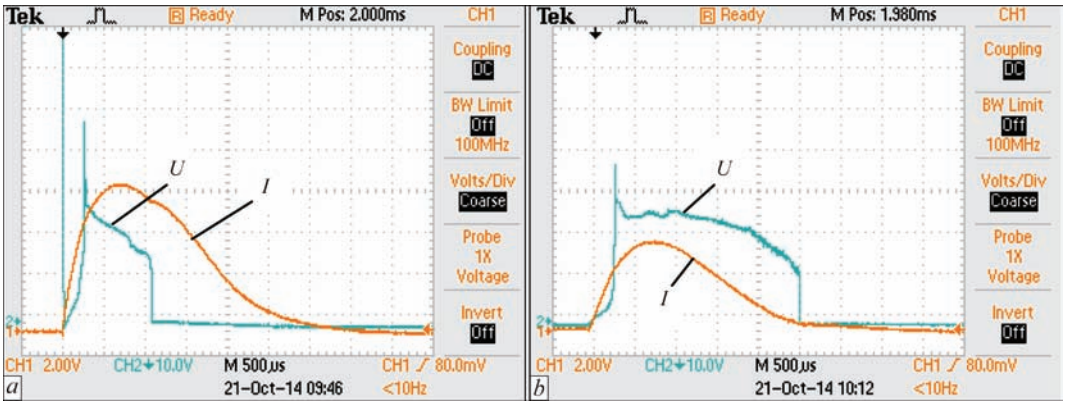

Figure 4. Oscillograms of welding current *I* and arc voltage *U* at capacitor welding of M8 studs from low-carbon steel by «gap» (*a*) and «contact» (*b*) methods (96 mF capacitor capacitance, 150 V charging voltage)

The next experimental series belongs to arc-contact capacitor stud welding by «gap» method. This method differs from the earlier considered one by that the discharge current is switched on when the stud, which has been removed from the sheet at the start of the welding process (in de-energized state), comes into contact with the sheet under the impact of welding device spring. At this moment current loop is closed and burning-out of roughnesses begins at the tip of the thin protrusion of the stud.

The main features of the processes of arc excitation at capacitor stud welding and arc excitation by exploding protrusion are demonstrated by oscillograms of welding current and arc voltage (Figure 4).

First, in welding by the «gap» method the stage of arc excitation (arc gap formation) is shorter than in welding by «contact» method. This can be judged by a delay of voltage rise, accompanying protrusion «explosion». In the given oscillograms this difference is about 20 ms at 3 mm initial gap*. Note that voltage surge at the moment of arc excitation in «gap» welding is higher than that in «contact» welding, as the initial volume of plasma is smaller in the first case than it is in the second case, and, more over, it is pressed by a mobile clamp to the stud. This leads to greater resistance at the moment of arc excitation, which drops quickly to a characteristic resistance value at regular voltage of the arc discharge.

Secondly, duration of the discharge stage of the arc in «gap» welding is much smaller that it is in «contact» welding. This feature is attributable to arc excitation at burning out of microroughnesses in the point of contact in the first variant and protrusion «explosion» in the second one. At protrusion evaporation, vapour pressure is greater than at arc running between the protrusion and the sheet that leads to greater arc length, as follows from the above-said. This assumption is confirmed by higher arc voltage in Figure 4, *b*. In addition, arcing time also influences the inertia of movable mass of welding device that counteracts metal vapour pressure. Therefore, in welding with a moving stud by «gap» method, the arc stage of the discharge is shorter than that in «contact» welding, when «hanging» of movable mass occurs at the start of the process, and, thus, arcing time is increased. Arc shortening in «gap» welding and respective reduction of discharge loop resistance lead to increase of amplitude value of current.

Peculiarities of processes of capacitor welding of studs by different methods determined the limited success of welding studs to sheets from SMA of Cu–Al system by «gap» method. As shown by the Table, this method allowed welding only studs from low-carbon steel in the M3-M8 diameter range that corresponds to limit capacity of K747MB machine, as well as those from brass of M3 and M6 diameter. In experiments with other metals undercuts and cracks in butt joint metal could not be avoided.

Known are the difficulties of joining iron alloys to aluminium alloys, associated with butt metal embrittlement as a result of formation of Fe–Al intermetallics of different stoichiometric composition. However, at impact bend testing to ISO 14555 of our joints of steel studs with an alloy of Cu–Al system, the samples withstood plastic bending through 90°. No other intermetallic inclusions were revealed, either. Apparently, such compounds are absent, or they are scattered through the matrix in the form of dispersed particles, not detectable by metallographic analysis, that is confirmed also by durometry investigations in the butt joint area.

Typical microstructure of the zone of welding steel studs to a sheet of SMA of Cu–Al system is shown

*Initial gap value influences the force at which roughnesses at the end face are deformed. The greater the gap, the greater the force of compression, and the lower the contact resistance, which causes thermal excitation of the arc at roughnesses evaporation from the end face.

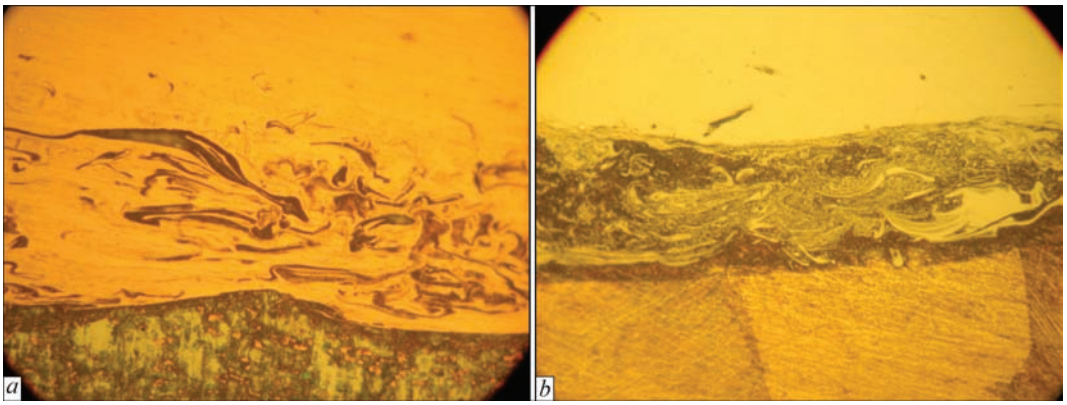

Figure 5. Microstructure (×500) of joints of M6 studs from low-carbon (*a*) and stainless (*b*) steel

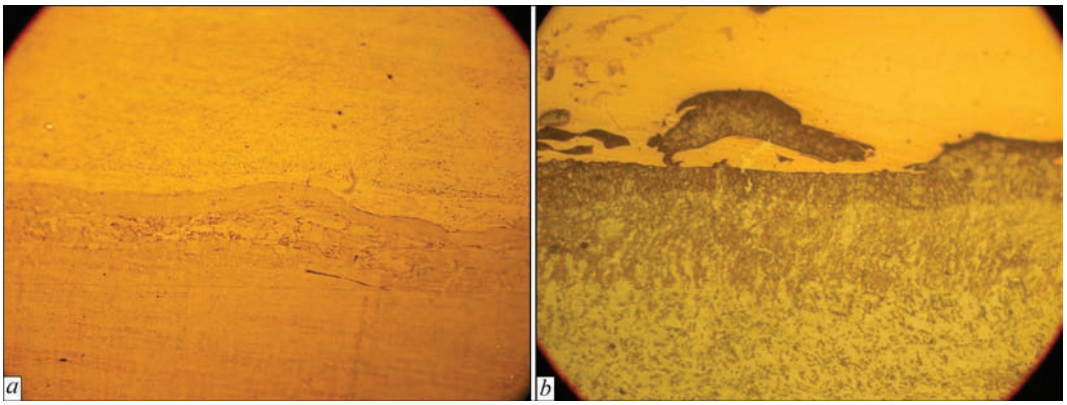

Figure 6. Microstructure (×500) of joints of M6 studs from brass L63 (*a*) and aluminium alloy AMg3 (*b*)

in Figure 5. It is characterized by presence of a layer, in which molten metal of the stud is mixed with sheet metal (dark-coloured zone). As SMA melting temperature is lower (by almost 400 °C) than that of stud material, the latter is the first to solidify, jamming SMA metal. This is also manifested in that the butt joint of St.3 steel with melting temperature of 1530 °C, has less jammed alloy, than the butt joint of stainless steel with melting temperature of about 1400 °C, closer to SMA melting temperature, which is about 1000 °C.

Microstructures of stud joints from metals, related to Cu–Al alloy components, namely brass L63 and aluminium alloy AMg3, have less contrast (Figure 6). In view of closeness of melting temperatures, the metals being welded to each other, solidify in the butt almost simultaneously, so that only a small quantity of the low-melting phase is jammed. This is illustrated by comparison of microstructures of joints of L63 studs (Figure 6 *a*), in which molten metal of both the joint elements solidified almost simultaneously, and those of AMg3 alloy (Figure 6, *b*) — a lower melting alloy than complex alloy of Cu–Al system, so that the latter was preserved as an islet in the aluminium alloy. The given microstructure photos show that the joint surface is dense, without pores or other discontinuities.

DC welding of studs. Current value at capacitor stud welding is equal to several kiloamperes, while in DC welding of the same stud cross-sections current value is not more than 1 kA. Duration of the process of arc-contact stud welding is more than an order of magnitude greater than capacitor welding time. As a result, each of these arc-contact welding processes has its applications.

Owing to short duration of the process, capacitor welding has its advantages, namely possibility of stud joining to a thin sheet with thickness to stud diameter ratio of 1:10 (in DC welding this ratio is 1:6 for up to M12 studs and 1:4 for larger diameter studs) and possibility of joining with parts having heat-sensitive coatings, for instance, those from polymer, layer paint or another decorative material. However, a disadvantage of this welding process, which is also related to short duration of the process, is the need for precisely keeping the perpendicularity of stud axis to the surface of the sheet, to which it is welded, within 7°. This, certainly, requires higher welder's qualifications, and limits operation efficiency.

The method of arc-contact stud welding by DC current is devoid of such a drawback to a certain extent.

Experiments were conducted with threaded studs from low-carbon steel St.3 and stainless steel 12Kh18N9T, as well as aluminium alloy AMg3 of a standard shape, having a flange greater than the stud cross-section by a value given in the Table, which is tapered at the tip with apex angle of 165°.

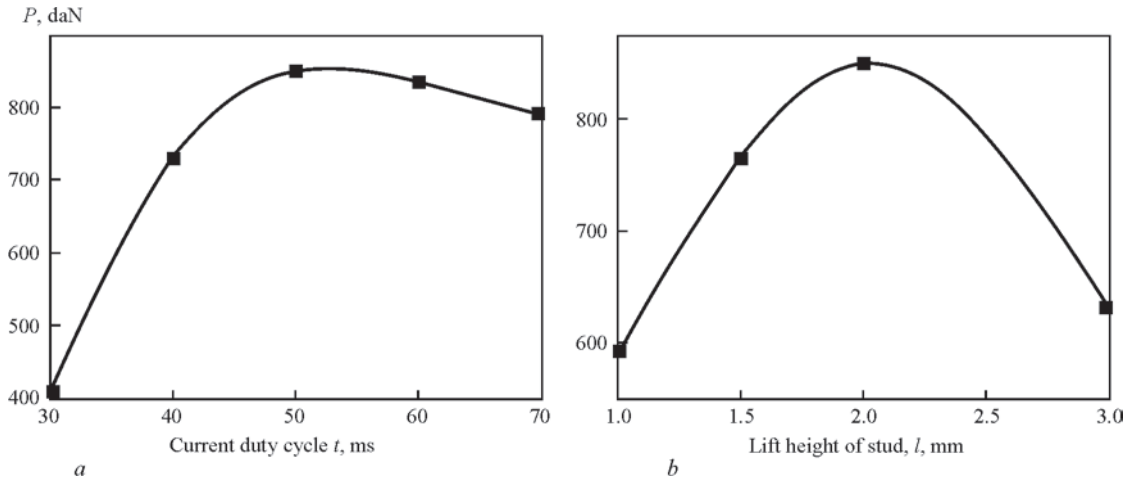

Figure 7. Influence of mode parameters of arc-contact welding of steel studs M6 to a sheet of SMA of Cu–Al system 8 mm thick on joint strength: *a* —*l* = 2 mm; *b* — *t* = 50 ms

GLV machine, in which experiments were performed, does not allow adjusting welding current value, which nominally is equal to 650 A, or its polarity, which is set as straight in the machine, so that the adjustable parameters were only welding current pulse duration and lift height of the stud. AMg3 studs were welded in argon, fed into the welding zone with 15 l/min flow rate with pre-blowing for 10 s. Joints were evaluated by impact bending and tensile strength, as well as by their appearance. Strong joints could only be obtained on St.3 steel studs.

Considering possible applications of joints with welded studs, their diameter was limited to M6 and M8, so that «short cycle» welding process was selected from all the possible variants of arc-contact stud welding, at which welding time is not more than 100 ms.

Joints with M6 studs from AMg3 alloy failed in the welding area at bending through up to 10° angle. Change of welding mode parameters in a broad range did not allow producing strong joints.

Analysis of fracture area led to the assumption that the cause for failed experiment is the mismatch of thermo-physical characteristics of materials being welded. Energy, sufficient for melting the stud surface, turned out to be insufficient for melting the sheet to a depth that provides a strong joint. If welding current duration is increased up to the value, sufficient for creating a satisfactory volume of molten metal on the sheet surface, then the flange on the stud being welded will be melted completely. This, certainly, lowers the joint strength. Subsequent experiments with steel studs confirmed this assumption.

Influence of welding mode parameters on welded joint strength was studied in welding M6 steel studs to sheet of δ = 8 mm. Obtained results in the form of graphs of joint strength dependence on duration of welding current pulse and lift height of stud at arc excitation stage are given in Figure 7. Analysis of the graphs is indicative of existence of a narrow optimum range of welding mode parameters, corresponding to strength properties of the joint, comparable with peel strength of the material. Deviation from them lowers joint strength, because of insufficient duration of the process (arcing time proportionally depends on the gap between the stud and sheet at the moment of the start of their drawing together and welding current switching on) or excess heating, leading to significant splashing of metal from the welding zone (Figure 8), pore formation and respective reduction of joint area.

Studying and analysis of results of impact bend testing of the joints in keeping with ISO 14555 Standard (Figure 8) and their comparison with the graph (Figure 7, *a*) lead to the conclusion that the joints, which withstood this test, are not always equivalent to base metal in terms of strength.

Investigations of metallographic structure of samples of this composition, revealed non-uniformity of metal of joint solidification zone, namely presence of material in the base matrix, which solidified separately from the main mass (Figure 9). Generalizing these results with the above analysis (Figures 5 and 6) leads to the conclusion that the non-simultaneity of solidi-

Figure 8. Samples of welding M6 steel studs with different heating duration

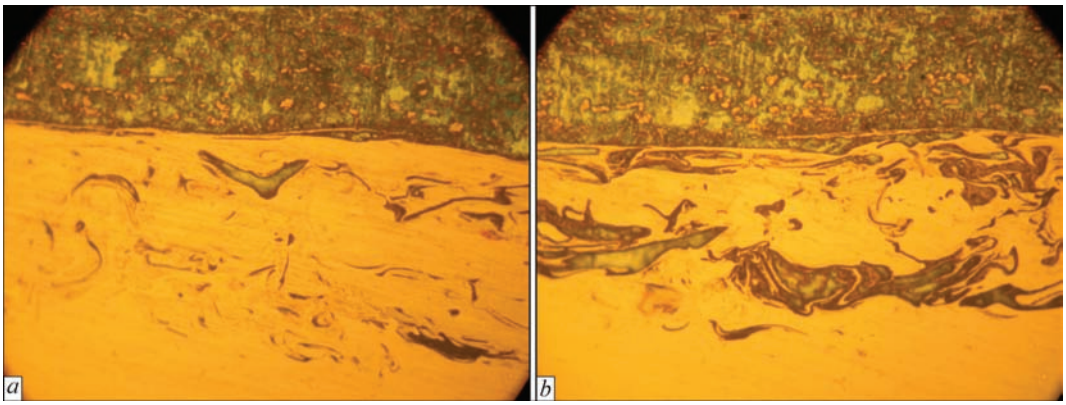

Figure 9. Microstructure (×500) of zone welding of M6 stud from low-carbon steel with an alloy of Cu–Al system (*below*). Duration of welding current pulse of 50 (*a*) and 70 (*b*) ms

fication of materials being joined is typical for pulsed arc-contact welding of dissimilar metals. At increase of welding time, the joint zone becomes more heterogeneous due to its enrichment in the steel component (Figure 9, *b*).

Studying fractures of joints of steel studs with copper-aluminium alloy showed the ductile nature of the fracture. This is indicative of the fact that no brittle intermetallics form in pulsed welding mode. As shown by microstructural analysis of arc-contact welded joints, the HAZ, the size of which was determined by refinement of copper-aluminium alloy grains [5], is not more than 0.2 mm. Preservation of the structure of the main bulk of SMA, as shown by earlier research [2], also ensures preservation of functional characteristics of the weldment.

Conclusions

1. Two methods of arc-contact welding, namely by capacitor discharge and by direct current, known as capacitor and arc stud welding, were tested for joining fasteners from steel and non-ferrous metals to complex alloy of Cu–Al system.

2. Studying strength properties and metallographic structure showed that pulsed methods of arc-contact welding provide strong joints of fasteners in dissimilar combination with an alloy of Cu–Al system, characterized by shape-memory effect. Owing to short duration of welding, the alloy preserves its functional characteristics. This enables an essential expansion of the range of products with these alloy, featuring high corrosion- and wear-resistance at relatively low lost.

3. Of the two variants of capacitor stud welding, it is preferable to apply the «contact» welding method for making dissimilar joints, which allows welding M3–M8 studs from L63 brass, low-carbon and stainless steels owing to relatively low current and greater heating duration. Joints with more than 3 mm diameter studs from AMg3 could not be produced, because of a significant difference in melting temperatures.

4. At direct current arc-contact welding strong joints with SMA of Cu–Al system could be obtained only with low-carbon steel studs, because of significant increase of welding time. Studs from non-ferrous metals and stainless steel melted out without preservation of the standard flange at the welded tip, which improves welded joint strength up to that of base metal.

5. Analysis of microstructure of arc-contact welded joints of dissimilar materials demonstrated heterogeneity of the welding zone. Inclusions of the lower-melting constituent are preserved in the matrix of the solidified phase. Metals being joined do not form a common structure, because of the short time of process and high cooling rate. Positive outcome of this process was manifested in ductility of fracture of joints with steel studs, owing to absence of brittle intermetallics of $FeAl_3$ type in the butt joint.

1. Paton, B.E., Kaleko, D.M., Shevchenko, V.P. et al. (2006) Weldability of shape-memory alloys of Ni–Ti system. *The Paton Welding J.*, **5**, 2–7.
2. Paton, B.E., Kaleko, D.M., Kedrovsky, S.N. et al. (2015) Resistance welding of shape-memory copper-aluminium alloy. *Ibid.*, **12**, 2–7.
3. Lebedev, V.K., Kaleko, D.M., Chvertko, N.A. (1994) Development of technology and equipment for arc-contact welding of fastening parts to sheet and other surfaces of items. *Svarochn. Proizvodstvo*, **4**, 14–16.
4. Kaleko, D.M., Kononets, B.I., Oseledko, N.N. et al. (1991) Unit K747MB for capacitor-discharge stud welding. *Ibid.*, **6**, 25–27.
5. Kaleko, D.M., Kedrovsky, S.N., Koval, Yu.N. et al. (2015) Pulsed capacitor-discharge welding of functional alloys based on Cu–Al system and its influence on joint zone structure *Metallofizika i Novejshie Tekhnologii*, 37(**12**), 1663–1680.

Received 10.10.2016

doi.org/10.15407/tpwj2016.12.02

FINITE-ELEMENT MODELLING OF STRESS-STRAIN STATE IN WELDABILITY TESTS (PVR-TEST)

K.A. YUSHCHENKO, E.A. VELIKOIVANENKO, N.O. CHERVYAKOV, G.F. ROZYNKA and N.I. PIVTORAK
E.O. Paton Electric Welding Institute, NASU
11 Kazimir Malevich Str., 03680, Kiev, Ukraine. E-mail: office@paton.kiev.ua

Hot cracks appearing in process of welding are an important problem determining weldability of number of structural materials. Regardless the fact that this phenomenon is widely investigated in course of many decades a nature of hot crack appearance is still a relevant problem for number of current alloys in fusion welding. To reach wider understanding of a mechanism of hot crack formation a finite-element method was used for mathematical modelling of PVR-Test. Realizing the mathematical model employing the experimental data, received as a result of such testing, allowed getting stress and strain distribution in the crack formation zones. The zones of plastic strain positive increments, promoting crack formation, were found for a range of brittleness temperature interval. Prediction of the zones of higher susceptibility to hot crack appearance as a result of decrease of material ductility well agrees with the experimental investigations. 8 Ref., 1 Table, 4 Figures.

Keywords: *hot cracks, weldability testing, welding, PVR-Test, nickel alloys, finite-element method*

High-alloy steels and nickel alloys are one of the most essential structural materials capable to withstand extreme temperatures and power loads as well as resist effect of aggressive media. They are mostly used in chemical, oil and power machine building and other branches of industry for manufacture of structures operating in a wide temperature range. Overwhelming majority of the high-alloy steels and nickel alloys refer to a structural class of austenite structural materials, characterized with structure stability in a wide range of operating temperatures, high temperature resistance, heat resistance and resistance to aggressive media effect.

Most stably austenite materials have high sensitivity to hot crack formation in fusion welding. The main difficulties in welding of considered materials are caused by their multi-component alloying and variety of operating conditions of the welded structures. The primary and general peculiarity of these materials is susceptibility to formation of hot cracks, having intergranular nature [1], in the weld and near-weld zone. Susceptibility to crack formation is evaluated with the help of current methods for weldability evaluation Varestraint-Test and PVR-Test [2–4].

The PVR-Test method is recommended by the International Institute of Welding for evaluation of weldability of structural materials in single-pass and multi-pass welding, first of all of the materials with stably austenite structure, sufficiently sensitive to crack formation.

Principle of the PVR-Test is based on the grounds of theory of process strength developed by N.N. Prokhorov [5]. The method of crack resistance evaluation is realized by means of non-consumable welding without filler along a central plane axis with simultaneous longitudinal varying in time sample deformation.

A crack formation sensitivity criterion is a critical deformation rate v_{cr}, at which first cracks appear. Simultaneous appearance of the cracks in a weld as well as heat affected zone is possible in welding. Moreover, these cracks appear, as a rule, at different value of critical deformation rate v_{cr}. This allows for having quantitative description of sensitivity to a specific type of cracks. More accurate information on a moment of crack formation start can be received through examination of a weld surface using optical enlargement methods.

An aim of the work was mathematical modelling of a weldability testing method (PVR-Test) for more complete analysis of the peculiarities of stresses and deformations localizing as well as determination of possible zones of crack formation.

Carried investigation was made applicable to alloy of Ni–Cr–Fe alloying system which is widely used in nuclear power engineering.

The experimental data, received at forced deformation for evaluation of crack formation susceptibility [6], were used for development of a PVR-Test mathematical model using finite-element method [7]. This allowed computing temperature, stress and de-

formation fields for different zones of a welded joint at macrolevel.

A computational procedure [8] was used for evaluation of kinetics of stress-strain state of the sample. It is based on sequential tracing of a development of elasto-plastic deformations in *x*, *y* points of considered sample at temperature change during source movement.

A hypothesis of two-dimensional stress state was used. According to it a stress tensor σ_{ij} in any point *x*, *y* in a moment of time *t* is presented as following

$$\sigma_{ij} = \begin{Vmatrix} \sigma_{xx} & \sigma_{xy} \\ \sigma_{yx} & \sigma_{yy} \end{Vmatrix}, (\sigma_{yx} = \sigma_{xy}), \quad (1)$$

where the tensor components σ_{ij} in each point *x*, *y* of considered area satisfy the equilibrium equations

$$\frac{\partial \sigma_{xx}}{\partial x} + \frac{\partial \sigma_{xy}}{\partial y} = 0, \frac{\partial \sigma_{xy}}{\partial x} + \frac{\partial \sigma_{yy}}{\partial y} = 0. \quad (2)$$

Deformation tensor ε_{ij} has structure similar to σ_{ij} tensor, i.e.

$$\varepsilon_{ij} = \begin{Vmatrix} \varepsilon_{xx} & \varepsilon_{xy} \\ \varepsilon_{yx} & \varepsilon_{yy} \end{Vmatrix}, (\varepsilon_{xy} = \varepsilon_{yx}), \quad (3)$$

where components ε_{xx}, ε_{xy}, ε_{yy} are related with U_x and U_y movements by relationships

$$\varepsilon_{xx} = \frac{\partial}{\partial x}, \varepsilon_{yy} = \frac{\partial}{\partial y}, \quad \varepsilon_{xy} = -\left(\frac{\partial}{\partial y} + \frac{\partial}{\partial x} \right) \quad (4)$$

In a random moment of time *t* tensor ε_{ij} can be presented as a sum of tensors [1]

$$\varepsilon_{ij} = \varepsilon^e_{ij} + \varepsilon^p_{ij} + \varepsilon^c_{ij}, \quad (5)$$

where ε^e_{ij} is the tensor of elastic deformation; ε^p_{ij} is the tensor of non-elastic deformation of instantaneous ductility; ε^c_{ij} is the tensor of non-elastic creep deformation.

Relationship between tensor σ_i and tensor ε^e_{ij} is determined by Hooke's law, i.e. there are following dependencies taking into account temperature and microstructure changes 3φ in point *x*, *y* in a moment of time *t* in comparison with *t* = 0 has

$$\varepsilon^e_{ij} = \frac{\sigma_{ij} - \delta_{ij}\sigma}{2G} + \delta_{ij}[K\sigma + \varphi(t) - \varphi(0)], \quad (i, j = x, y), \quad (6)$$

where δ_{ij} is the single tensor or Kronecker symbol, i.e. $\delta_{ij} = 1$ at $i = j$ and $\delta_{ij} = 0$ at $i \neq j$; $\sigma = (\sigma_{xx} + (\sigma_{yy})/3$, $G = E/(2(1 + \nu))$ is the shear modulus; E is the normal elasticity modulus; ν is the Poisson's ratio; $K = (1 - 2\nu)/E$ is the volumetric compression modulus.

Relationship of stress tensor σ_i with instantaneous ductility deformations ε^p_{ij} in current commercial packages of computer software such as «Weldpredictions» is enunciated based on flow theory, associated with Mises yield criterion. i.e. relationship is registered between a tensor of plastic deformation increments $\Delta\varepsilon^p_{ij}$ and stress deviator $\sigma_{ij} - \delta_{ij}\sigma$ in form of

$$\Delta\varepsilon^p_{ij} = d\lambda(\sigma_{ij} - \delta_{ij}\sigma), \quad (i, j = x, y), \quad (7)$$

where a scalar function $d\lambda$ is determined by yield condition through yield surface

$$f = \sigma_i^2 - \sigma_{0.2}^2(T), \quad (8)$$

where

$$\sigma_i = \frac{1}{2}\sqrt{(\sigma_{xx} - \sigma_{yy})^2 + \sigma_{xx}{}^2 + \sigma_{yy}{}^2 + 6\sigma_{xy}^2}, \quad (9)$$

$\sigma_{0.2}(T)$ is the material yield in *x*, *y* point at temperature $T(t)$.

$$d\lambda = 0, \text{ if } f < 0 \text{ or } f = 0, \text{ but } df < 0; \quad d\lambda > 0, \text{ if } f = 0 \text{ and } df > 0; \quad \text{state } f > 0 \text{ is inadmissible.} \quad (10)$$

Tracing of the development of elastic-plastic deformations is carried out step-by-step, stating from moment $t = 0$ through time gap $\Delta\tau$, the same as tracing of the development of temperature field $T(x, y, t)$ in time is carried out in series through finite increments of time Δt.

Deformation tensor will acquire final increment during this tracing step.

$$\Delta\varepsilon_{ij} = \Delta\varepsilon^e_{ij} + \Delta\varepsilon^p_{ij} \quad (11)$$

or taking into account (6), (7)

$$\Delta\varepsilon_{ij} = \psi(\sigma_{ij} - \delta_{ij}\sigma) + \delta_{ij}K\sigma - b_{ij}, \quad (12)$$

where

$$\psi = \frac{1}{2G} + \Delta\lambda, \quad b_{ij} = \left(\frac{\sigma_{ij} - \delta_{ij}\sigma}{2G} \right)_{t-\Delta\tau} + \delta_{ij}[(K\sigma_{t-\Delta\tau} - \Delta\varphi)]. \quad (13)$$

Function ψ reflects a state of the material in point *x*, *y* in time moment t. It equals $1/2G$ (elastic behavior) or more than $1/2G$ elastic-plastic behavior. Yield condition (8) allows for developing ψ function iterative refinement. Value b_{ij} is known for tracing stage (time moment *t*), if solution at stage $(t - \Delta\tau)$ is known.

Dependence (12) at each iteration on ψ, i.e. when ψ is set, converts considered problem to a well known problem of thermoelasticity theory with additionally set deformations b_{ij}. Numerical methods based on finite-element method [8] are sufficiently well developed for such problems' solution. Such an algorithm type is used in software package «Weldpredictions». It made a basis for investigation of residual deformations depending on applied load as well as heat input (or welding mode).

Figure 1 shows the model for macrolevel (sample and scheme of its loading). The sample was divided on 8 sections, within the limits of which the deformation rate was constant. Kinetics of stress-strain state in the weld and heat-affect zone (HAZ) was calculated

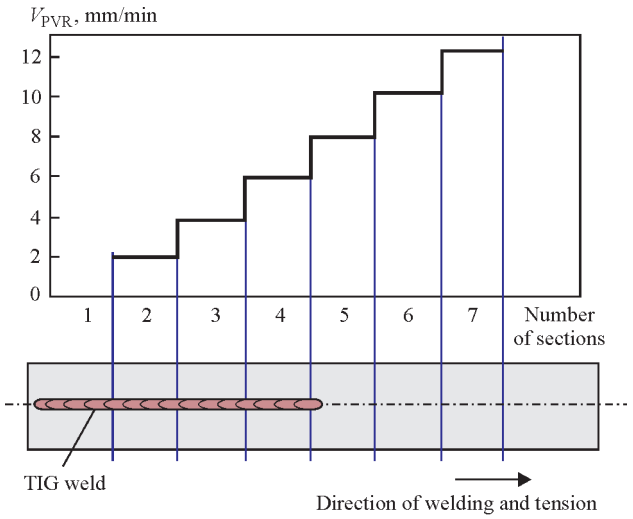

Figure 1. Sample and scheme of its loading

for each of sections (2–8) for macrolevel at 0.5 mm distance from fusion line in the places of appearance of ductility dip cracks under real testing conditions.

The model considers all heat and mechanical effects in the process of real PVR-Test of the welds produced with Ni–Cr–Fe wire depending on time. Physical properties of material, depending on temperature (Table), parameters of welding mode (I_w = 60 A, U_a = = 10.5 V, v_w = 6.5 m/h) and nature of mechanical loading and change of sample geometry were used. The process of testing was modeled for plane sample of 200×40×3 mm size. Size of finite element in calculations made 0.5×0.5×0.5 mm.

Comparative kinetics of change of temperature, stresses and deformations in HAZ for sections 2 and 4 is shown in Figures 2 and 3.

Tension plastic deformations rise in the weld and heat affected zone in heating stage at simultaneous tension of the sample. Plastic deformations reduce to zero when reaching the temperature maximum in the weld, further decrease of temperature provokes their re-increase. Somewhat another pattern is for HAZ.

Dependence of mechanical and thermo-physical properties on temperature for examined material

T, °C	$E\cdot10^{-5}$, MPa	σ_y, MPa	$\alpha\cdot10^6$, 1/°C	λ, J/(cm·s·°C)	$c\gamma$, J/(cm^3·°C)
20	2.06	350	14.1	0.120	0.450
100	2.03	280	14.1	0.135	0.470
200	1.95	250	14.3	0.154	0.500
300	1.87	240	14.5	0.173	0.530
400	1.85	230	14.8	0.191	0.550
500	1.77	225	15.2	0.210	0.580
600	1.67	215	15.7	0.229	0.600
700	1.58	200	16.2	0.248	0.630
800	1.52	190	16.6	0.266	0.660
900	1.45	175	17.0	0.285	0.680
1000	1.35	150	17.4	0.301	0.710
1100	1.25	125	17.8	0.316	0.740
1200	1.0	100	18.0	0.330	0.770

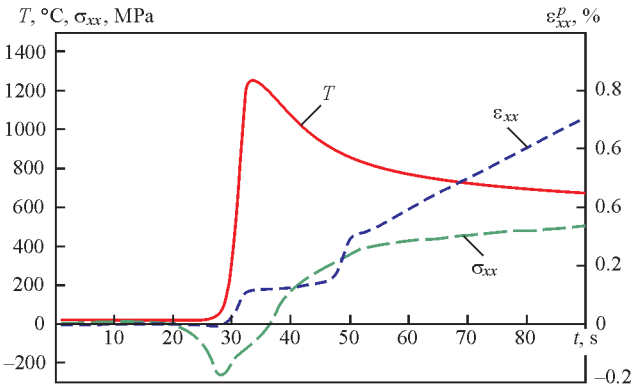

Figure 2. Kinetics of change of temperature, stresses and deformations in section 2

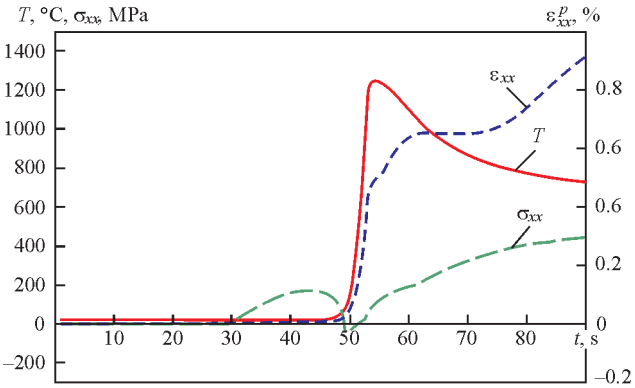

Figure 3. Kinetics of change of temperature, stresses and deformations in section 4

Since there is no metal melting in the HAZ, plastic deformations grow continuously. Rate of plastic deformation at tension rate 2 mm/min in section 2 during cooling makes 0.00119 %/°C that is significantly lower than plastic deformation rate (0.00539 %/°C) in section 4 at tension rate 4 mm/min. This determines higher susceptibility of material to crack formation in this section. Figure 4 shows kinetics of change of longitudinal plastic deformations in sections 2 and 4 as well as boundaries of brittleness temperature interval BTI 2.

Obtained results well agree with the experimental researches of crack resistance using PVR-Test method, when formation of ductility dip cracks under real

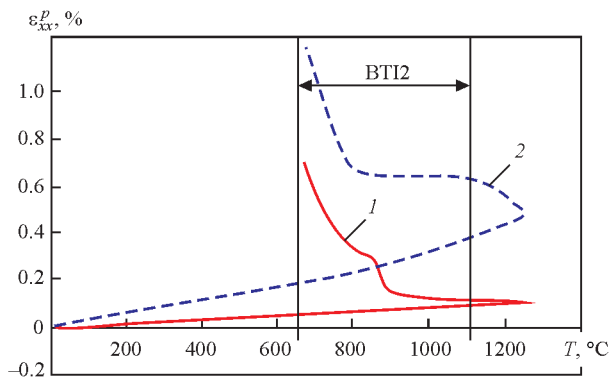

Figure 4. Kinetics of change of longitudinal plastic deformations on temperature in sections 2 (*1*) and 4 (*2*)

tests took place at forced tension rate of more than 3 mm/min.

Conclusions

1. Finite-element method was used for mathematical modelling of weldability on PVR-Test and computational data were received on distribution of temperature, stresses and strains in different zones of the welded joint.

2. Local deformations, appearing at high temperatures, were computed for a plane sample of nickel alloy of Ni–Cr–Fe alloying system and data were acquired relatively to positive increments of plastic deformations in the range of brittleness temperature interval. It is shown that the rate of plastic deformation for given modelling conditions varies from 0.00119 to 0.00539 %/°C. This will determine higher susceptibility to hot crack formation in BTI 2 in this section.

3. The results of numerical prediction of material susceptibility to hot crack formation well agree with the experimental data that allows using the model for evaluation of risks of crack appearance in different zones of the welded joint.

1. Boellinghaus, T., Lippold, J., Cross, C. (2016) *Cracking phenomena in welds*. Springer.
2. *ISO/TR 17641-3:2005*: Destructive tests on welds and metallic materials — hot cracking tests for weldments: Arc welding processes. Pt 3: Externally loaded tests.
3. Fink, C., Keil, D., Zinke, M. (2012) Evaluation of hot cracking susceptibility of Ni-based alloys by the PVR-Test. *Welding in the World*, 56(**7/8**), 37–43.
4. Vallant, R.,Cerjak, H. The influence of different Nb/C ratio in Ni-base weld metals type 70/20 and 70/15 on the hot cracking susceptibility. *IIW Doc. II-1535–04*.
5. Prokhorov, N.N. (1956) Problem of metal strength in welding during solidification. *Svarochn. Proizvodstvo*, **6**, 5–11.
6. Yushchenko, K.A., Savchenko, V.S., Chervyakov, N.O. et al. (2011) Comparative hot cracking evaluation of welded joints of alloy 690 using filler metals FM 52 and 52 MSS. *Welding in the World*, 55(**9/10**), 28–35.
7. Lindgren, L.-E. (2006) Numerical modeling of welding. *Computer Methods in Applied Mechanics and Engineering*, **195**, 6710–6736.
8. Makhnenko, V.I. (1976) *Calculation methods for investigation of kinetics of welding stresses and strains*. Kiev: Naukova Dumka.

Received 19.10.2016

doi.org/10.15407/tpwj2016.12.03

DIRECT NUMERICAL MODELLING OF FORMATION OF WELD METAL DENDRITE STRUCTURE WITH DISPERSE REFRACTORY INOCULANTS

D.Yu. ERMOLENKO, A.V. IGNATENKO and **V.V. GOLOVKO**
E.O. Paton Electric Welding Institute, NASU
11 Kazimir Malevich Str., 03680, Kiev, Ukraine. E-mail: office@paton.kiev.ua

Studied were the advantages of alloy feeding with the disperse refractory inoculants for regulation and optimizing the primary structure of high-strength low-alloy steel weld metal. The main assumptions and limitations of a model of weld metal solidification process, proposed in this work, were considered. The model of melt solidification was described in details taking into account effect of the introduced disperse refractory inoculants. A hypothesis was presented on mechanism of interaction of a refractory inoculant with moving solidification front, which was taken in computations. Effect of the different alloying elements on surface energy of phase interface was described. Boundary conditions of the proposed model, realized in form of author software, were described. The results are given of computational experiments showing the possibilities of regulation of parameters and morphology of the primary structure of high-strength low-alloy steel weld metal by means of melt feeding with the disperse refractory inoculants (by example of TiO_2 introduction). Presented is a comparison of experimental and computational results of change of the primary structure parameters. Developed mathematical model and software, written on its basis, are good for prediction of dimensional parameters and morphology of the weld metal primary structure considering refractory inoculants being fed in the weld pool. 17 Ref., 1 Table, 10 Figures.

Keywords: *dendrite structure, disperse refractory inoculants, solidification, high-strength low-alloy steels, morphology, mathematical modelling*

Continuous increase of the requirements to metal structure safety promotes for the necessity of mastering new steel grades with higher level of mechanical properties. In practice of metallurgical production a volume of high-strength low-alloy steels (HSLA) production continuously rises. The main tendencies in optimizing the properties of HSLA steels are reduction of content of alloying elements, increase of total number of microalloying elements, decrease of content of additives and residual elements promoting metal degradation, improvement of structural inhomogeneity, rise of mechanical properties level [1].

Alloy feeding with the refractory inoculants is a perspective method for optimizing the structure and properties of HSLA steels due to regulation, first of all, of structure parameters and, respectively, weld metal mechanical properties. It is known that grain size of the primary structure effects the nature of $\gamma \rightarrow \alpha$ transformations. If nucleation of α-phase in the disperse dendrite structure starts at grain boundary in the upper area of bainite transformation, then nucleation of ferrite inside the primary grains at boundaries with non-metallic inclusions at temperatures close to bainite transformation end [2] is typical for coarser dendrites.

Work [3] considers a series of models of primary structure development and their critical analysis is carried out from point of view of possibility of their application for simulation of weld metal solidification process taking into account effect of the disperse refractory inoculants. Present work proposes a model based on finite element method coupled with cellular automation method.

Main assumptions and limitations of the model of metal solidification process. Studied system includes the refractory inoculants distributed in a liquid phase and significantly effecting solidification process.

Metal solidification process considering effect of the refractory inoculants can be considered as a result of interaction of two competing processes, namely high-rate movement of solidification front, caused by local non-equilibrium of diffusion processes at phase interface, and effect of the inoculants on local surface tension at phase interface, which has significant effect on formation of the weld metal primary structure of HSLA steel [4].

Solution of this problem in present work is based on a model of local non-equilibrium solidification (freezing) [5], which was supplemented by a model of solidification front interaction with the refractory in-

oculants. The model taken as a basis is used for small as well as high rates of crystalline phase growth. Theoretical grounds of this model are made in work [6].

In two-dimensional medium the equations of model [5] describe a mass balance (1), evolution of solid and liquid phase interface and diffusion flow of additives (2, 3), growth of solid phase (4) and relationship of additive concentration in liquid and solid phases (5).

$$\frac{\partial}{\partial t}[(1-G)+C_L+kGC_L]+\frac{\partial J_x}{\partial x}+\frac{\partial J_y}{\partial y}=0, \quad (1)$$

$$\frac{\partial J_x}{\partial t}+J_x+\frac{1-G}{q}\frac{\partial C_L}{\partial x}=0, \quad (2)$$

$$\frac{\partial J_y}{\partial t}+J_y+\frac{1-G}{q}\frac{\partial C_L}{\partial y}=0, \quad (3)$$

$$\frac{\partial G}{\partial t}=\frac{\omega}{v}V, \quad (4)$$

$$C_S=kC_L. \quad (5)$$

where J_x and J_y are the projections of vector **J** of diffusion flow on coordinate axis; C_L and C_S are the concentration in liquid and solid phases, respectively; G is the fraction of solid phase in a cell [0–1]: t is the time; w is the area of phase interface in solidifying system; v is the volume of two-phase area; V is the rate of movement of intergrain boundary (interface of solid and liquid phases) along vector normal directed to liquid phase side; k is the coefficient of additive non-equilibrium distribution.

It is known that small freezing rate and low overcooling promote for disturbance of microscopically smooth phase interface, it becomes morphologically unstable according to scenario of authors of work [7]. This is a classical example of development of cell-dendrite structure type, which is regulated by diffusion mass transfer in the locally equilibrium conditions. Increase of overcooling can result in deviation of local thermal-dynamic equilibrium in the system as well as initiation of quick freezing [8].

Main assumptions of the used model:

1. Isothermal two-phase system with constant pressure is considered.

2. The system consists of chemically inert binary-alloy, which solidifies from overcooled liquid.

3. Freezing from liquid phase can be so fast that rate V of phase interface movement is compared on value with rate V_D of additive diffusion.

4. Convection in liquid phase and diffusion in solid solidification phase are neglected.

5. Refractory inoculants are present in the liquid phase volume.

6. It is accepted that the refractory inoculants are uniformly distributed in the weld pool volume with some probability φ ($0 \le \varphi \le 1$).

7. Refractory inoculants are stationary in solidification. All inoculants have similar size, comparable with size of cell of computational network (≈0.4 μm).

Under these assumptions the process of dendrite structure development is regulated by mass transfer and kinetics of phase boundary movement. In particular, from assumption 4 it is necessary to take into account a finiteness of rate of diffusion transfer of additive and deviation from local equilibrium at phase boundary [9]. Thus, the model, describing the system, considers a local non-equilibrium diffusion of additive and kinetics of movement of phase interface.

Model of metal solidification process. A calculation area (solidification zone) is initiated at the beginning of calculation. It consists of solid phase of specific morphology (it can be separate cybotactic groupings randomly distributed in liquid phase, single nuclei of solid phase, plane front with inhomogeneities or without them, or their combinations) and liquid phase with determined initial additive concentration. A level of cell solidification is determined by fraction of solid phase in cell G. Each cell of the system can be liquid ($G = 0$) or completely solidified ($G = 1$), or belong to solidification front ($0 < G < 1$), i.e. freeze in a present moment of time (Figure 1).

In order to determine an increment of fraction of solid phase G it is necessary to calculate rate V of phase interface. This should be done with the help of non-linear kinetic equation «rate-overcooling»

$$V=\beta(\Delta T-\Delta T_C(V)-\Delta T_N(V)-\Delta T_G, \quad (6)$$

where ΔT is the complete initial overcooling in the system; ΔT_C is the concentration overcooling caused by additive diffusion; ΔT_N is the overcooling caused by change of inclination of kinetic liquidus and determined by difference between equilibrium line of liquidus $T_A + m_e C_0$ and kinetic liquidus $T_A + m_C 0$; ΔT_G is the overcooling caused by curvature of phase interface (Gibbs–Thompson effect).

Contributions of overcoolings are determined in the equations:

$$\Delta T = T_A + m_e C_0 - T_0, \quad (7)$$

$$\Delta T_C = m(V)(C_0 - C_L), \quad (8)$$

$$\Delta T_N = (m_e - m(V))C_0, \quad (9)$$

$$\Delta T_G = -G(1 - 15\cos(4(\theta_1 - \theta_0)))K. \quad (10)$$

In the equations (6)–(10): β is the kinetic coefficient of crystal growth; T_A is the solidification (freezing) temperature of system main component; T_0 is the temperature in isothermal system; m_e is the tangent of inclination angle of liquidus equilibrium line; C_0 is the initial concentration of additive in the melt; $m(V)$ is the inclination of kinetic liquidus; G is the capillarity constant; K is the curvature of phase interface; θ_1 is the angle of orientation of vector-normal to phase

interface; θ_0 is the angle of orientation of the main crystallographic direction [10].

Capillarity constant G is determined as

$$G = \frac{\gamma}{\Delta S}, \quad \Delta S = \frac{Q_L}{T_A},$$

where γ is the surface tension; ΔS is change of entropy in solidification; Q_L is the solidification latent heat.

In metal solidification process the weld pool is always characterized with presence of some stochastic process at phase interface caused by probabilistic processes. In order to get the results comparable with the experimental data, let's enter a kinetic coefficient of crystal growth in form of [11]

$$\beta = 1 + \delta\eta(t, x, y), \tag{11}$$

where $\delta \geq 0$ is the amplitude of stochastic noise; $\eta(t, x, y)$ is the probabilistic function taking the values in [–1–1] interval for different points in (t, x, y)-space.

Serious effect on the results of computations of dendrites growth has artificial anisotropy, developed by computational mesh geometry [12]. In order to reduce this effect the computation of surface curvature considers an effect of not only the closest cells, but more distant neighbors. This work accounts effect of the cells being in a radius of three cells (Figure 2) with some weight coefficient. The weight coefficient depends on cell area, which is covered by radius circumference 3.5*h* (*h* is the size of one cell in the computational mesh), the center of which is in the center of cell being computed. Thus, the computation of surface curvature in each separate cell takes into account effect of 44 neighbor points. A matrix of the weight coefficients *M* is calculated one time and appears to be constant for all cells of the system. Numbers, shown in Figure, these are the values of weight coefficients of cell-neighbors.

Let's introduce a solidification vector $\vec{F}_S$ [10] for formalizing a computation of surface curvature. A value of this vector corresponds to sum of solid phase in radius circumference 3.5*h* around the cell considering weight coefficients of matrix *M*, determined above.

$$\left|\vec{F_S}\right| = \sum_{i,j=-3}^{3} G_{i,j} M_{i,j}. \tag{12}$$

Direction of vector corresponds to a line joining the mass center of all solid phase and center of studied cell. The coordinates of mass center relatively to studied cell in the Cartesian coordinates can be easily calculated on formulae:

$$\Delta x = \sum_{i,j=-3}^{3} iG_{i,j} M_{i,j}, \Delta y = \sum_{i,j=-3}^{3} iG_{i,j} M_{i,j}. \tag{13}$$

A vector of normal line of phase interface can be determined by formula

$$\vec{n} = \frac{\vec{F_S}}{\left|\vec{F_S}\right|}. \tag{14}$$

Thus, angle of orientation of vector-normal to phase interface θ_1 in formula (10) is computed by formula

$$\theta_I = \arctan\left(\frac{\Delta x}{\Delta y}\right). \tag{15}$$

Curvature of the surface in studied cell containing some fraction of solid phase *G* is computed following from semiempirical dependence:

$$K = \frac{A + BG - \left|\vec{F_S}\right|}{S} \frac{2}{h}, \tag{16}$$

where

$$S = \sum_{i,j=-3}^{3} M_{i,j} = 38.484, \quad A = \sum_{i=-3}^{-1} \sum_{j=-3}^{3} M_{i,j} = 15.754,$$

$$B = \sum_{j=-3}^{3} M_{0,j} = 6.976,$$

where *S*, *A*, *B* are the constants determined from the matrix of weight coefficients; *h* is the size of cell in the computational mesh.

Geometrically these constants are determined as different sections of the circle of 3.5*h* radius (Figure 3); *S* is the area of whole circle ($S = 2A + B = 3.5^2\pi$); *A* is the area of sector «*cde*», and *B* is the area of domain «*abcd*». It is easy to see that equation (16) takes the zero value of surface curvature coefficient *K* independent on solid phase fraction *G* in the studied cell at plane solidification front. When modulus of vector $\vec{F}_S$ is less than $A + BG$ sum, then the surface is convex, in the opposite case it is concave, that can be seen in Figure 3.

Formula (16) is the modification of a method of surface curvature determination proposed in work [13]. This method imposes limitations on size of the cells and radius of matrix of the weight coefficients, which should be sufficiently small in comparison with typical scales of modeled structure.

For computation of fraction of additive, which is pushed out by newly-formed solid phase into the melt, let's determine a coefficient of non-equilibrium distribution of additive, which depends on local solidification rate and being calculated using equation

$$k(V) = \begin{cases} \dfrac{(1 - V^2)k_e + Vr}{1 - V^2 + Vr}, & V < 1, \\ 1, V \geq 1, \end{cases} \quad r = \frac{V_D}{V_{DI}}, \tag{17}$$

where k_e is the equilibrium coefficient of distribution; V_D is the rate of additive diffusion in a liquid phase volume; V_{DI} is the rate of additive diffusion at phase interface.

Inclination *m(V)* of the kinetic liquidus for calculation of overcooling ΔT_N and ΔT_C is determined by

coefficient of non-equilibrium distribution $k(V)$ (17) and rate V

$$m(V) = \frac{m_e\left(1-k+\ln\left(\frac{k}{k_e}\right)+(1-k)^2 V\right)}{1-k_e}. \qquad (18)$$

Updating of a concentration field takes place for each cell of computational domain following from mass balance and diffusion flow of additive. Concentration of C_S additive in completely solid cells ($G = 1$) remains the same.

There is a surge of concentration at a diffusion wave front «*DF*» (leading edge of diffusion profile which moves with rate V_D) [5] in process of local non-equilibrium transfer of additive in the liquid phase volume. Detailed analysis of this effect can be found in work [11]. The boundary conditions at the diffusion wave front are set as boundary conditions of the first order and are as follows

$$J_{DF}^{-} = \exp\left(-\left(\frac{\xi}{4}\tau\right)^{1/2}\right)\left(C_F - C_0\right)\mathbf{n},$$

where J_{DF}^{-} is the outgoing flow of additive; $C_F - C_0$ is the concentration surge at a diffusion front; **n** is the vector of normal of diffusion front; ξ is the parameter of stability of calculation scheme; τ is the time step.

Effect of the refractory inoculants on solidification process. Analysis of series of experimental data [2, 4] allowed taking for computations a hypothesis assuming that the solidification front absorbs the inoculant and surface tension in zone of contact is changed at the moment of contact.

In order to consider the effect of refractory inoculants on solidification front movement it is necessary to compute a value of interphase tension between the inoculant and melt (σ_{12}) using table data [14].

$$\sigma_{12} = \sigma_1 + \sigma_2 - W_a,$$

where σ_{12} is the value of interphase tension between refractory inoculant and melt; σ_1 is the inoculant surface tension; σ_2 is the alloy surface tension; W_a is the adhesion work.

Surface tension of the melt is computed based on procedure proposed by S. Popel [15]:

$$\sigma_2 = \sigma_{Fe} - 2000 \lg \Sigma F_i x_i,$$

where σ_{Fe} is the surface tension of pure iron; F_i is the parameter characterizing capillary activity of alloying additive; x_i is the atomic fraction of i^{th} alloy component.

The boundary conditions are not set in common understanding (Figure 4). Initially there are completely solid cells in the bottom of computational domain, computation in which is not carried out. From the right and from the left the computational domain forms a «cylinder» by means of development of virtual data, to which data from the cells being closest to the boundary of computational domain are copied. It is done for emulation of position of computational domain in the weld pool, where development of the primary structure in it can also be effected by growth of dendrites in metal adjacent volumes. From above the computational area is limited by a layer of cells, computation in which is not carried out. This develops the layer, which does not prevent propagation of diffusion wave that physically corresponds to weld pool large dimensions.

The model described above made a basis for development of a program for tracing the movement of phase interface in solidification of weld metal of HSLA steels in time depending on initial conditions (initial solidification rate, initial morphology of solid phase, inclination angle of a vector of the most intensive heat rejection to solidification surface) and physical parameters of alloy (solidification temperature of alloy main component, growth kinetic coefficient, tangent of inclination angle of liquidus equilibrium line, equilibrium coefficient of additive distribution, coefficient of additive diffusion, solidification latent heat, rate of additive diffusion in volume and on phase interface, stochastic noise amplitude).

Based on developed software a series of computational experiments was carried out, the results of which are given below.

Evaluation of melt composition effect on solidification process. Composition of weld metal of HSLA steel (wt.%): 0.049 C; 0.298 Si; 1.39 Mn; 0.023 S; 0.015 P; 0.15 Cr; 2.26 Ni; 0.25 Mo; 0.039 Al; 0.008 Ti was taken as a basis for computational experiments. Initial rate of solidification was accepted $0.27V_D$. Physical parameters of alloy are given in the Table. Figure 5 shows difference in size and morphology of dendrites, which were developed for similar period of time, without considering the effect of alloying elements on alloy surface tension (Figure 5, *a*) and taking into account the effect alloying elements (Figure 5, *b*).

Results of computational experiments of effect of refractory inoculants introduction on dendrite metal structure. Titanium dioxide (TiO_2) was taken as introduced inoculant for the computations. It has the following parameters of surface interaction with iron melt, namely melting temperature (T_m) 1834 °C; surface tension of liquid phase (σ_1) 1780 mJ/m^2; limiting wetting angle (θ) 0 degree; adhesion work (W_a) 3560 mJ/m^2. A parameter of refractory inoculants distribution in the weld pool metal φ was taken equal 0, 0.1, 0.2 and 0.3. The results of computations showing evolution of the dendrite structure in time with different density of inoculants distribution in the weld pool metal are given in Figures 6–9, respectively.

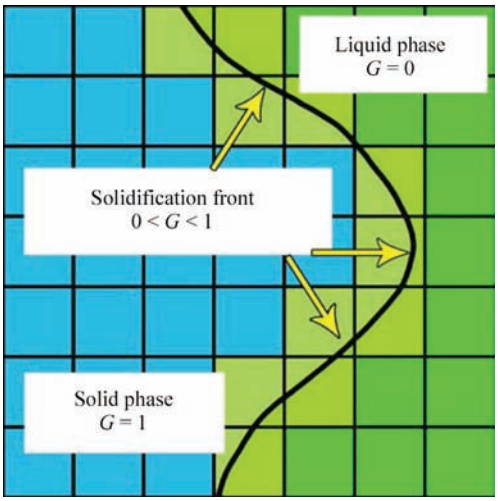

Figure 1. Value of fraction of solid phase G for liquid and solid phases and solidification front

Thus, a branched solidification structure with wide branches of dendrites (up to 100 μm) can be observed in absence (Figure 6) of the refractory inoculants in the weld pool.

The weld pool feeding with the refractory inoculants, affecting the surface tension between solid phase and melt, promoted for a change of dendrite structure from branched one to completely columnar morphology (Figures 7–9). Such a significant change of nature of the weld metal primary structure is only caused by the processes taking place on a contact surface of refractory inoculant with growing dendrite.

In this case TiO_2 is well wetted by iron melt that promoted for increase of local solidification rate in a contact zone of growing dendrite with inoculant. This occurs due to rise of overcooling value in the contact zone (Gibbs–Thompson, ΔT_G effect). Increase of rate of dendrite growth due to Gibbs–Thomson effect results in rise of concentration overcooling (ΔT_C) due to pushing out a large amount of additive before the

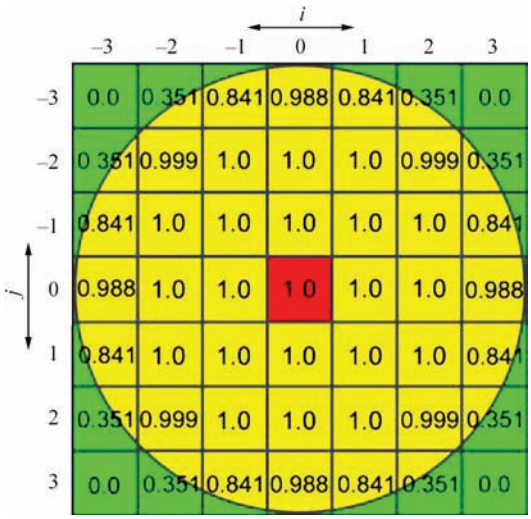

Figure 2. Matrix of weight coefficients for determination of surface curvature [10]

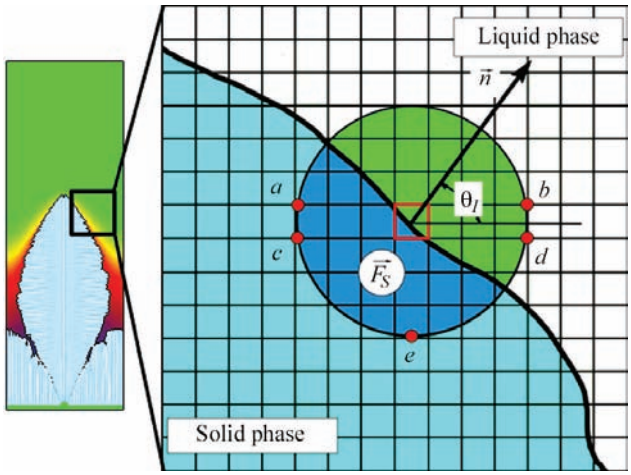

Figure 3. Determination of solidification vector and computation of surface curvature [16]

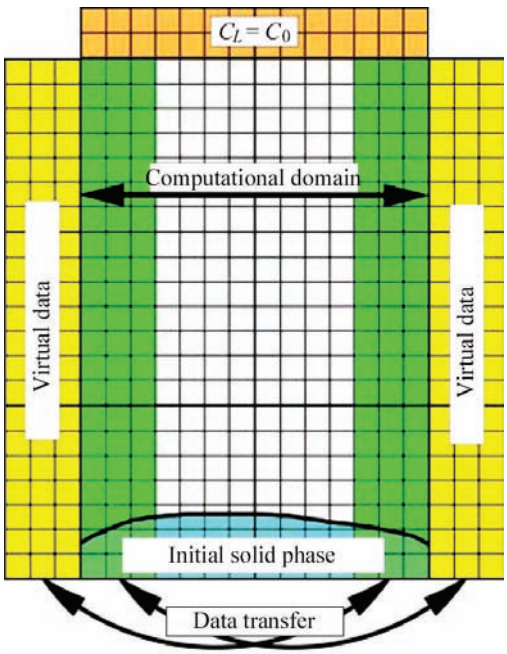

Figure 4. Rules at computational domain boundaries [10]

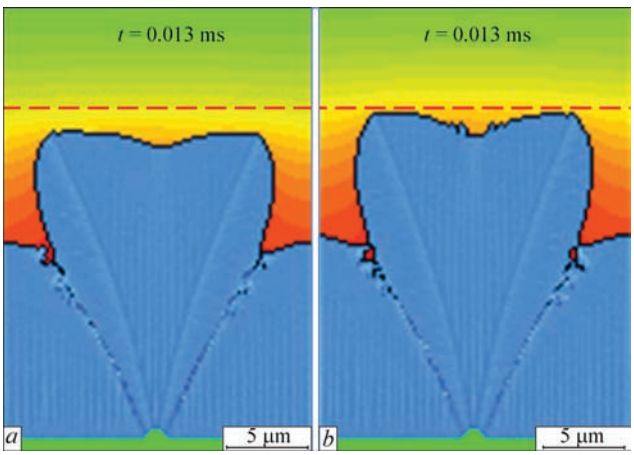

Figure 5. Results of computations of solidification start: *a* — without effect of alloying elements; *b* — with alloying elements effect

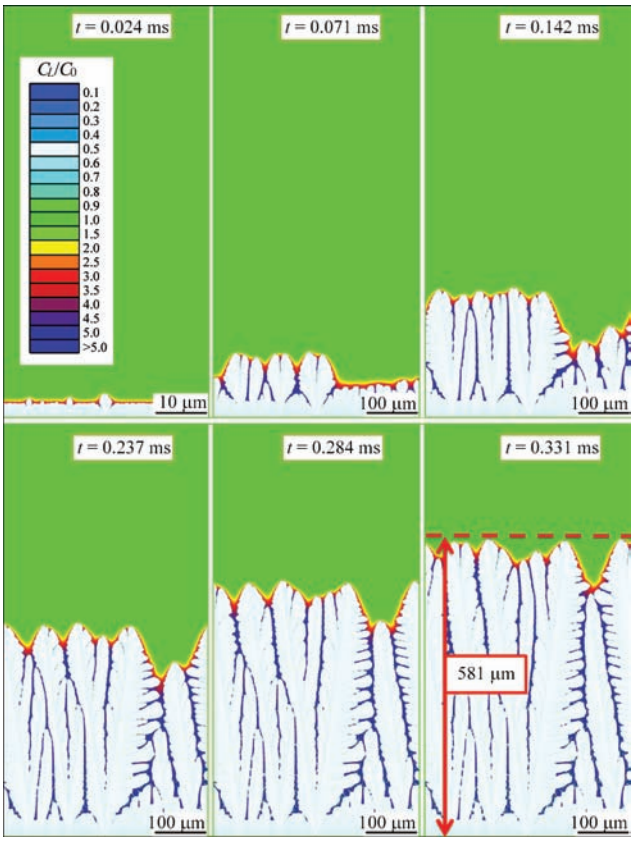

Figure 6. Evolution of dendrite structure in time considering refractory inoculants (φ = 0)

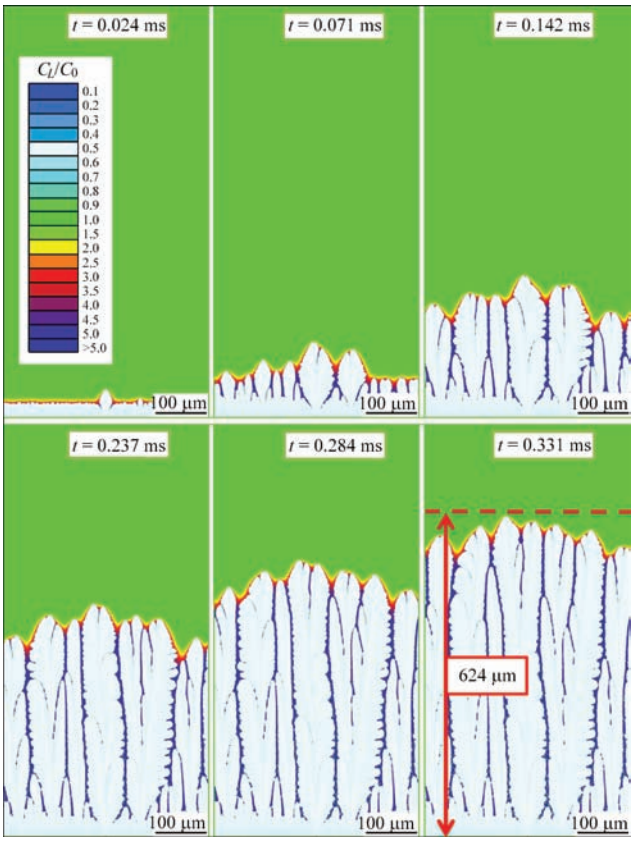

Figure 8. Evolution of dendrite structure in time considering refractory inoculants (φ = 0.2)

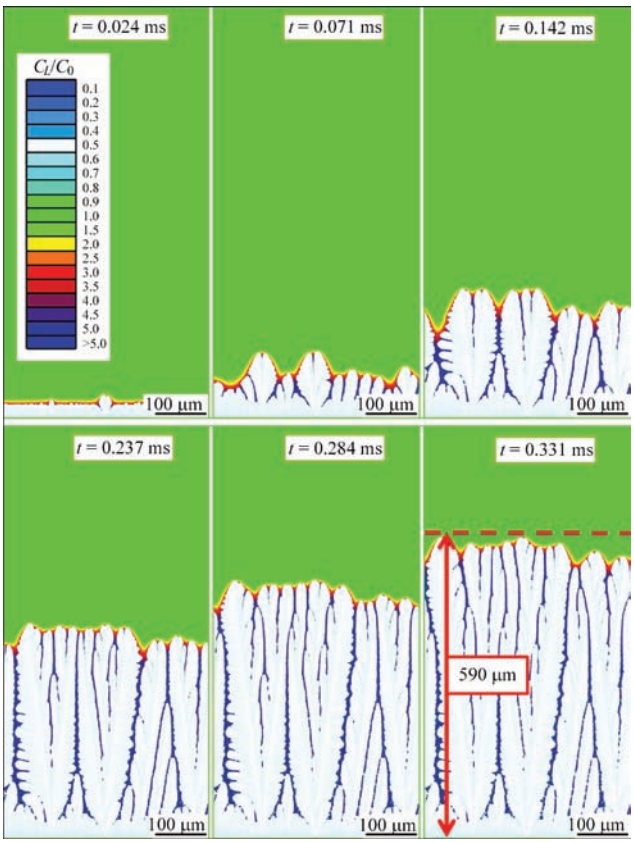

Figure 7. Evolution of dendrite structure in time considering refractory inoculants (φ = 0.1)

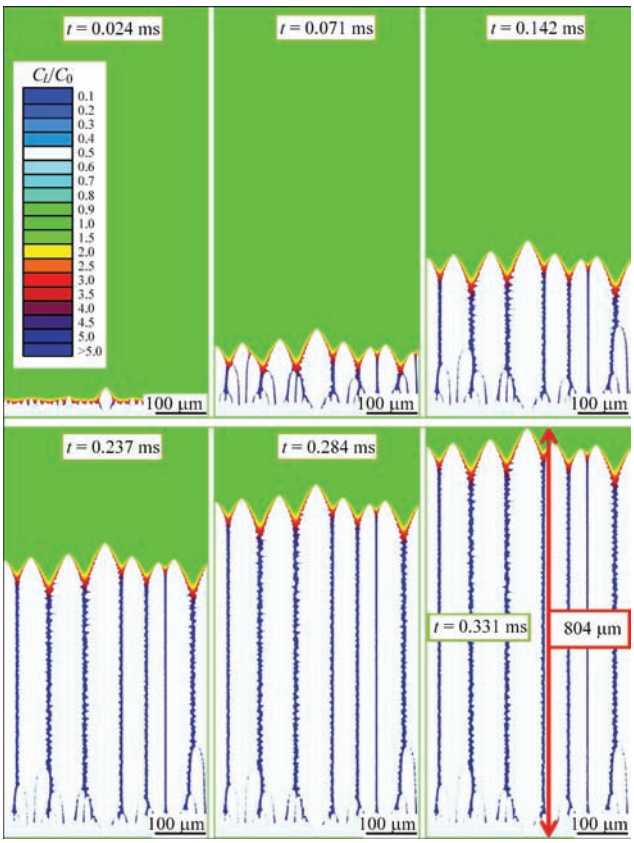

Figure 9. Evolution of dendrite structure in time considering refractory inoculants (φ = 0.3)

Values of physical parameters taken in computation

Physical parameters	Designations	Unit of measurement	Value
Temperature of main component freezing	T_A	K	1809
Kinetic coefficient of growth	β	m/(s·K)	0.4
Tangent of inclination angle of liquidus equilibrium line	m_e	K/wt.%	–80
Distribution equilibrium coefficient	k_e	–	0.1
Coefficient of additive diffusion	D	m^2/s	$6 \cdot 10^{-8}$
Solidification latent heat	Q_L	J/m^3	10^9
Diffusion rate in volume	V_D	m/s	17
Diffusion rate at phase interface	V_{DI}	m/s	17
Amplitude of stochastic noise	δ	–	0.07

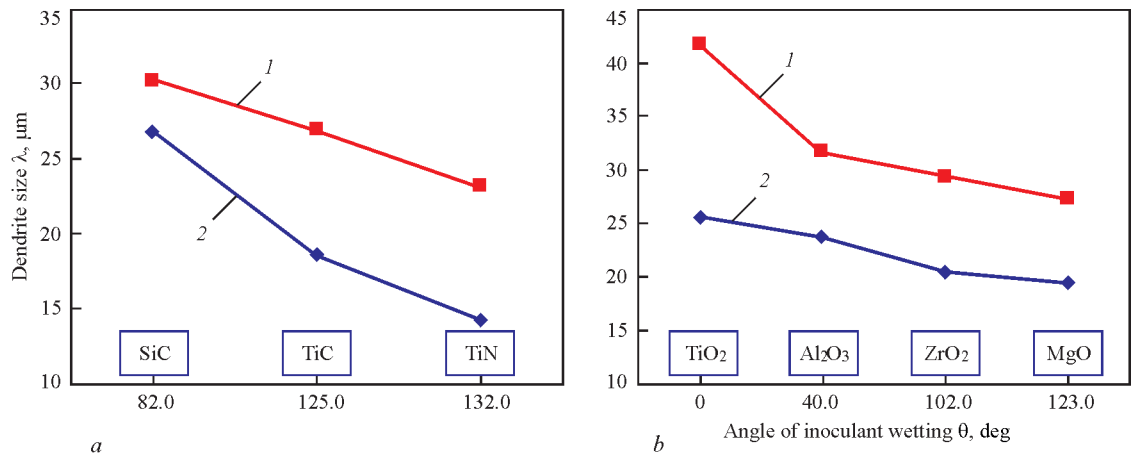

Figure 10. Comparison of experimental results of measurement and computational data of parameters of metal primary structure of specimens in the first (*a*) and second (*b*) series of experiments: *1* — λ_{1exp}; *2* — λ_{1comp}

solidification front. Also, change of growth rate at the end of dendrite promotes for further deviation of the process from equilibrium and rise of overcooling due to deviation from liquidus equilibrium line (ΔT_N).

Hypothetical description of nature of development of the physical processes, imbedded in the proposed solidification model, allows simulating quality changes of the weld metal dendrite structure depending on number and properties of introduced inoculants. If refractory inoculants are absent, the solidification front in the weld pool moves for 581 μm during 0.331 ms (Figure 6), and at their uniform distribution with φ = 0.3 probability this makes 802 μm (Figure 9) all other things being equal (including initial solidification rate). It is necessary to note significant change of morphology of the dendrite structure from much branched, formed because of competitive growth of separate crystals, to completely columnar dendrites. Reduction of wetting angle in the local points of contact of growing dendrite with metal melt can provide significant qualitative change of the dendrite structure, that, in turn effect further solid phase transformations in metal and as a result final microstructure and mechanical properties of HSLA steel weld metal.

Figure 10 *a*, *b* presents a comparison of dimensions of the dendrite primary structure, received in computational and experimental way [2, 17] for the specimens of the first and second series, respectively. An average error of data, obtained by means of computational experiment, makes around 25 % and increases with rise of wetting angle of the refractory inoculant by weld pool metal. Such a difference in received results can be related with selection of parameters of distribution of the refractory inoculants in the weld pool metal φ equal 0.3. It apparently does not correspond to the conditions of carried experiment researches. This factor should be taken into account in further investigations and it is necessary to study in more details the effect of distribution parameter on development of the weld metal primary structure. Also, the error was introduced by inaccurate composition and model limitations.

Conclusions

The model, based on finite element method coupled with cellular automation method, well suits simulation of solidification process of weld pool metal taking into account the effect of the refractory inoculants. It is related with the fact that the main model of crystalline structure development can be easily completed by additional rules and laws of interaction of moving

solidification front with inclusions introduced in the weld metal volume. Also, an advantage of such approach is the possibility of tracing of any parameters of cellular automation discrete cells (concentration of additive, overcooling value, coefficient of surface curvature etc.) in time.

Computational experiments, carried with the help of developed software, showed the possibility of regulation of parameters and morphology of metal primary structure by means of melt feeding with the refractory disperse inoculants. Developed mathematical model and software, written on its basis, are good for prediction of dimensional parameters and morphology of weld metal primary structure considering refractory inoculants introduced in the weld pool.

1. Sandeep, J., Chhibber, R., Mehta, N.P. (2012) Issues in welding of HSLA steels. *Advanced Materials Research*, **365**, 44–49.
2. Golovko, V.V., Pokhodnya, I.K. (2013) Effect of non-metallic inclusions on formation of structure of the weld metal in high-strength low-alloy steels. *The Paton Welding J*., **6**, 2–10.
3. Ermolenko, D.Yu., Golovko, V.V. (2014) Numerical modeling and prediction of weld microstructure in high-strength steel welding (Review). *Ibid*., **3**, 2–10.
4. Golovko, V.V., Stepanyuk, S.N., Ermolenko, D.Yu. (2015) Effect of titanium-containing inoculants on structure and properties of weld metal of high-strength low-alloy steels. *Ibid*., **2**, 14–18.
5. Galenko, P.K., Krivilev, M.D. (2000) Isothermal growth of crystals in undercooled binary alloys. *Matematicheskoe Modelirovanie*, 12(**11**), 17–37.
6. Galenko, P., Danilov, D. (1997) Local nonequilibrium effect on rapid dendritic growth in binary alloy melt. *Physics Letters A*, 235(**3**), 271–280.
7. Mullins, W.W., Sekerka, R.F. (1964) Stability of the planar interface during crystallization of a dilute binary alloy. *J. Applied Physics*, **35**, 444–459.
8. Kurz, W., Fisher, D.J. (1992) Fundamentals of solidification. *Transact. Tech. Publications Ltd*.
9. Galenko,P., Sobolev, S. (1997) Local nonequilibrium effect on undercooling in rapid solidification of alloys. *Physical Review E*, 55(**1**), 343–352.
10. Pavlyk, V. (2004) *Modeling and direct numerical simulation of dendritic structures under solidification conditions during fusion welding*. Aachen: Shaker Verlag GmbH.
11. Galenko, P.K., Krivilev, M.D. (2000) Finite-difference scheme for modeling of crystalline structure formation in undercooled binary alloys. *Matematicheskoe Modelirovanie*, 12(**12**), 11–13.
12. Guillemot, G., Gandin, C.-A., Combeau, H. (2006) Modeling of macrosegregation and solidification grain structures with a coupled cellular automaton-finite element model. ISIJ *Int.*, 46(**6**), 880–895.
13. Sasikumar, R., Sreenivasan, R. (1994) 2-dimensional simulation of dendrite morphology. *Acta Metallurgica et Materialia*, 7(**2**), 2381–2386.
14. Panasyuk, A.D., Fomenko, V.S., Glebova, G.G. (1986) *Resistance of non-metallic materials in melts*. Kiev: Naukova Dumka.
15. Popel, S.I. (1971) *Theory of metallurgical processes*. Moscow: VINITI.
16. Diltey, U., Pavlik, V., Raihel, T. (1997) Computer modeling of formation of weld metal microstructure in fusion welding. *Avtomatich. Svarka*, **3**, 3–9.
17. Golovko, V.V., Stepanyuk, S.N., Ermolenko, D.Yu. (2014) Technology of welding of high-strength low-alloy steels by introduction of titanium-containing inoculants. In: *Nanodimensional Systems and Nanomaterials*: Research in Ukraine. Monography. Ed. by A.G. Naumovets. Kiev: Akademperiodika.

Received 26.10.2016

doi.org/10.15407/tpwj2016.12.04

WELDABILITY OF HIGH-STRENGTH MICROALLOYED STEEL S460M

V.D. POZNYAKOV, S.L. ZHDANOV, A.V. ZAVDOVEEV, A.A. MAKSIMENKO and **T.G. SOLOMIJCHUK**
E.O. Paton Electric Welding Institute, NASU
11 Kazimir Malevich Str., 03680, Kiev, Ukraine. E-mail: office@paton.kiev.ua

The structural steels of strength class S350 and higher are widely used in manufacture of metal structures of different purpose. Their application allows significant reducing the total metal consumption of structures as compared to the products of steels of grades St.3 and 09G2S. In the present work the influence of welding thermal cycles on the properties and structure of HAZ metal, resistance of joints to cold crack formation is considered. The selection of welding consumables for steels of strength class S490 was justified and the change of mechanical properties of welded joints was analyzed. It was revealed that with increase in the rate of cooling the HAZ metal of model specimens-simulators, the strength characteristics increase, and the ductile ones decrease. Thus, the values of impact toughness are sharply reduced at the cooling rate of 3 °C/s. It is possible to increase greatly the resistance to cold crack formation in technological samples of steel S460M at the increased content of diffusion hydrogen in the deposited metal by decreasing the value of residual stresses in welded joints to the level not exceeding $0.5\sigma_y$ of steel (≤235 MPa). 13 Ref., 1 Table, 9 Figures.

Keywords: *high-strength steel, welding thermal cycle, cooling rate, mechanical properties, cold cracks, diffusion hydrogen, brittle fracture*

The development of modern industry, building industry and power engineering specifies new requirements to metal structures in reducing the metal consumption and increasing their reliability [1–4]. Such effect can be achieved by applying new high-strength steels with the yield strength of higher than 390 MPa. The structural steels of strength class S350 and higher are applied in bridge construction, construction of tall buildings, wind power engineering for construction of supports of windmills, as well as in manufacture of metal structures of railway freight transport [1, 5]. The application of high-strength rolled metal allows reducing the total metal consumption of structures to 80 % as compared to the products of steels of grades St.3 and 09G2S [6].

To develop steels of improved strength in the modern production, two approaches are mainly used. The first one consists in application of alloying elements increasing the strength characteristics. But this method leads to a significant increase in the cost of manufactured rolled metal. The alternative of alloying is the thermal deformational hardening of metal or controllable rolling with the subsequent heat treatment. Such steels include high-strength low-alloyed steel S460M (strength class S490), microalloyed with niobium and vanadium. According to the data of the standard EN 10025-4 the steel has the following mechanical properties: $\sigma_y > 460$ MPa, $\sigma_t = 540$–720 MPa, $\delta_5 > 18$ %, $KCV_{-40} > 27$ J/cm^2. Such characteristics are provided by a finely dispersed structure obtained after controllable rolling.

In the manufacture of structures of low-alloyed steels of such strength class the problem of study of their weldability becomes urgent [7]. It is known that in the process of welding the metal of heat affected zone (HAZ) undergoes structural transformations which lead to changes in mechanical properties [8]. In this connection in the present paper the influence of welding thermal cycles (WTC) on the properties and structure of HAZ metal, resistance to cold crack formation are considered. The welding consumables for steel S460M of strength class S490 were proposed, the mechanical properties of welded joints and their resistance to brittle fracture were investigated.

The procedure of investigations. For experiments the structural steel S460M of 16 mm thickness of the following composition was selected, wt.%: 0.15 C; 0.23 Si, 1.3 Mn; 0.09 Cr; 0.019 Ni; 0.01 V; 0.05 Nb; 0.025 Al; 0.007 N_2; 0.013 S; 0.017 P. The mechanical properties of the investigated steel S460M are the following: $\sigma_y = 480$ MPa; $\sigma_t = 600$ MPa; $\delta_5 = 27$ %; $\psi = 58$ %.

As the criteria of WTC the metal cooling rate in the temperature range of 600–500 °C ($w_{6/5}$) was accepted. According to the results of investigations the cooling rates were determined at which the decrease in the values of strength, ductility, and impact toughness of HAZ metal occurs as compared to the

requirements specified to welded joints. The investigations were carried out using the model specimens of the size 120×12×12 mm, which were heat treated in accordance with the thermal cycles of welding in the installation MSR-75 [9]. The heat treatment process consisted in the following. At first, the specimens were heated using current, passing through them, to the temperatures of 1200–1300 °C, which are characteristic for the area of overheating the HAZ welded joints. The heating rate of specimens was 150–170 °C/s, which corresponds to heating conditions in the metal of heat affected zone in arc welding processes. At this temperature, the specimens were held for about two seconds and then they were subjected to a forced cooling. For testing on static tension the steel specimens were mechanically manufactured (type II) according to GOST 6996–96 (3 specimens for each cooling rate). The tests were carried out in accordance with GOST 6996–66 at room temperature. For tests on impact toughness the specimens of the type XI were manufactured, which were tested at the temperatures of 20, –20 and –40 °C.

The investigation of susceptibility of steel S460M to delayed fracture was performed using the method Implant in the specialized installation, designed at the E.O. Paton Electric Welding Institute of the NAS of Ukraine [10]. The cooling rate of HAZ metal was changed due to different initial temperature of plates, which, depending on technological variant of welding, ranged from 20 to 90 °C. For this purpose, preheating was used. Such approach allowed changing the cooling rate of welded joints $w_{6/5}$ in the range of 21–14 °C/s. The content of diffusion hydrogen in the deposited metal (evaluated by the method of pencil samples using the mixture of glycerine and distilled water in the ratio of 1:4 as a sealing liquid) was changed using electrodes with different humidity of coatings. For this purpose they were wetted and calcinated at different temperatures. The static loading of specimens at the speed of 10 MPa/s was started after their cooling to the temperature of 150–100 °C, and as the value of resistance of welded joints to cold crack formation the critical stresses σ_{cr} were accepted, at which the specimen was not fractured within 24 hours.

As far as one of the main factors influencing the resistance of welded joints to cold crack formation, is the level of residual stresses, the investigations were carried out using butt technological samples with a regulated hardness. This allowed regulating only stress state of technological samples and evaluating its influence on stability of joints against cold cracks formation without changing the hydrogen and structural factors influencing the formation of cold cracks in welded joints.

To carry out investigations in the work the technological sample was selected representing a massive plate of the size of 400×400 mm and the thickness of 40–60 mm, on which two plates are installed and welded-on around the whole perimeter with a leg of 12 mm, of which a reference welded joint is formed. In the V-shaped butt joint of steel S460M the presence of 1.5–2.0 mm gap and blunting of 3.0–4.0 mm are provided to ensure a technological lack of penetration, which is a stress concentrator and initiates the crack formation. The level of hardness was determined by the width of plates, of which the reference butt joint is composed. According to the methods of investigations the welding of butt joints of the plates of 50, 100 and 150 mm width, and of 16 mm thick was performed. The total width of the joints in this case was 100, 200 and 300 mm.

The investigations of the past years [11] which were performed on multilayer joints, indicate that in the process of formation of welded joints, the significant transverse shortening of weld and HAZ metal along the whole length of specimen occurs. The most intensive shortening was observed in a central part of the weld after producing the root beads. According to these data, the highest value of displacements was observed in the hard specimens of 300 mm width ($\Delta L \approx 0.45$ mm). In the narrower samples of 200 and 100 mm width the running of plastic deformation processes is complicated, and therefore the maximum values of cross shortening in them are lower: $\Delta L \approx 0.4$ mm and 0.33 mm, respectively. It contributes to formation of a higher level of residual welding stresses in the specimens with the maximum rigidity of fixing (fixing base $B = 100$ mm). With increase in fixing base B from 100 to 300 mm, the level of residual stresses in the weld metal of joints decreases from 0.8–0.9 to 0.4–0.5 of yield strength of weld metal. The manual arc welding of joints of steel S460M was performed using electrodes UONI-13/55 and FOX EV-50 of 4.0 mm diameter at the mode: I_w = 160–170 A; U_a = 24–25 V; v_w = 8.5–9.0 m/h. For the mechanized welding of joints of this steel the solid wires St-08G2S and G3Sil and the flux-cored wire of grade Megafil 821R of 1.2 mm diameter were applied. The welding was performed in the mixture of gases 82 % Ar + 18 % CO_2 at the modes: I_w = 170–190 A; U_a = = 26–28 V; v_w = 11.5–12 m/h using the solid wire and at I_w = 220–240 A; U_a = 28–30 V; v_w = 14–15 m/h using flux-cored wire.

To determine the values of the critical stress intensity factor K_{1C} and the crack opening displacement δ_c the specimens of rectangular cross-section of the size

10×20×90 mm with a notch of 7 mm length and fatigue crack of 3 mm length were applied. These specimens were tested at three-point bending in the temperature range from 20 to –40 °C. Using the criteria of fracture mechanics [12] the evaluation of resistance to brittle fracture of welded joints of steel S460M was carried out depending on the applied welding consumables and methods. The tip of fatigue crack in one specimens was located in the weld metal, and in the other one — in the HAZ metal. For comparison, the specimens were manufactured of steel S460M base metal.

Obtained results and discussion. Effect of welding thermal cycle on structure and properties. In the present work the structure and mechanical properties of thermomechanically hardened steel S460M (strength class S440), manufactured according to DSTU EN 10025-4:2007 at the Mariupol Metallurgical Plant were studied. Due to thermomechanical rolling in the temperature range of 900–700 °C with the controllable cooling the ferrite-pearlite banded structure with the hardness *HV*-195 (Figure 1) is formed in steel S460M.

The mark of grain corresponds to No. 10 according to GOST 5639–82, and banding mark — to the number 5 on the scale 3 of GOST 5640–68. The contamination with non-metallic inclusions, such as silicates, aluminum silicates, sulfides and oxysulfides, corresponds to the mark No.1 in accordance with GOST 1778–70.

The values of impact toughness of steel S460M greatly exceed the standard values of $KCV_{-40} \geq$ $\geq$ 34 J/cm^2, even at the test temperature of –60 °C (KCV_{-60} = 76 J/cm^2).

In their turn, the dependencies characterizing the changes of values of strength and ductility in the simulated HAZ metal of steel S460M under the influence of WTC, are shown in Figure 2, *a*, *b*. The results of investigations evidence, that with the change in cooling rate in the temperature range of 600–500 °C ($w_{6/5}$) from 3 to 25 °C/s the values of strength of HAZ metal increase as compared to the initial state, namely σ_y from 490 to 810 MPa and σ_t from 600 to 1000 MPa. At the same time, the ductile properties of the simulated HAZ metal are deteriorated as compared to the initial state. Especially this refers the values of elongation, which are reduced by 2.5–3.0 times, at the same time the values of relative reduction in area are decreased by 15–20 %.

In the tests of specimens with a sharp V-notch on impact bending it was revealed that the impact toughness of HAZ metal of steel S460M decreases in relation to the base metal (Figure 2, *c*). The most significant decrease in *KCV* values by 4–9 times is

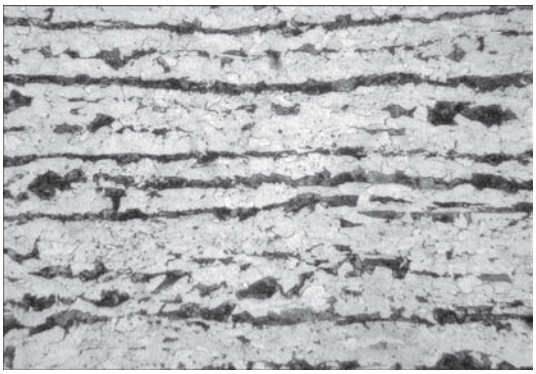

Figure 1. Microstructure (×500) of steel S460M

observed in specimens, which cooled down at the rate $w_{6/5}$ = 3 °C/s (from 111 to 33 J/cm^2 at the test temperature of 20 °C, from 109 to 15 J/cm^2 at the temperature of –20 °C and from 95 to 10 J/cm^2 at the temperature of –40 °C). With increase in cooling rate to 10 °C/s, they are increased to the values of KCV_{-40} = 27 J/cm^2, and then slightly decrease and at $w_{6/5}$ = 25 °C/s they are: KCV_{20} = 50 J/cm^2 , KCV_{-20} = 30 J/cm^2 and KCV_{-40} = 20 J/cm^2 (for comparison of the values of impact toughness of steel S460M tests at the test temperatures ranging from 20 to –40 °C are in the range of 95–110 J/cm^2).

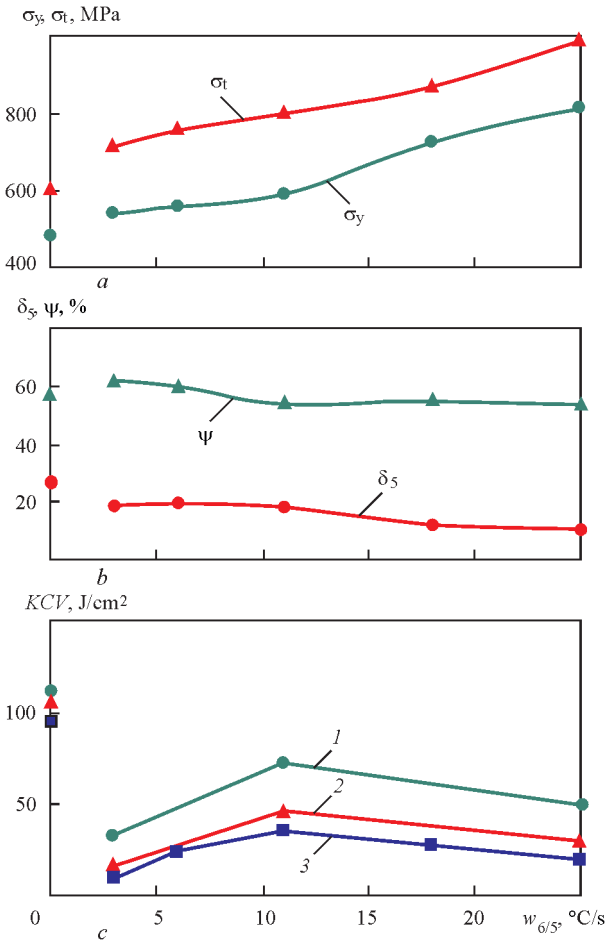

Figure 2. Influence of cooling rate on strength (*a*), ductility (*b*) and impact toughness at the test temperature: *1* — 20; *2* — –20; *3* — –40 °C (*c*) of simulated HAZ metal of steel S460M

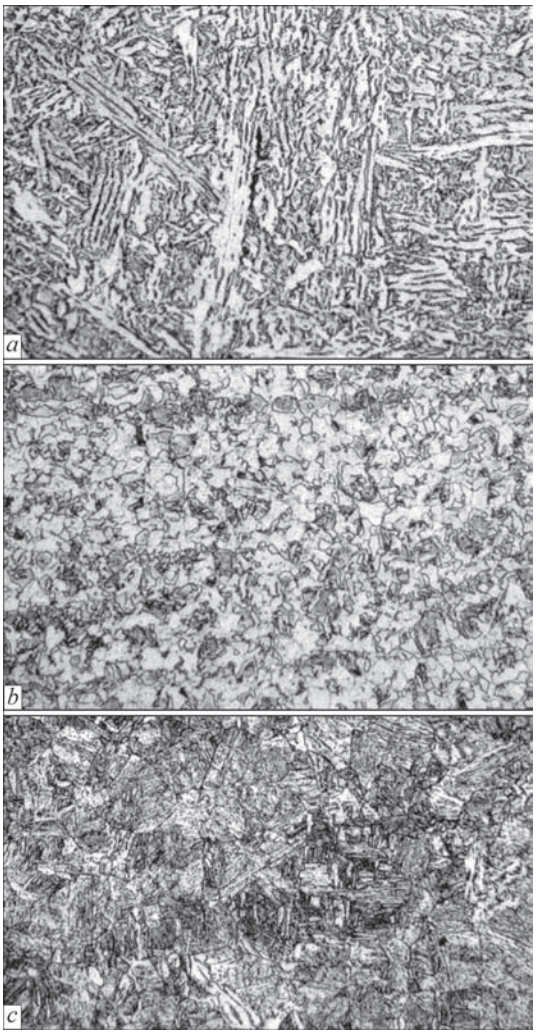

Figure 3. Microstructure (×500) of HAZ metal of model specimens of steel S460M: *a* — $w_{6/5}$ = 3; *b* — 10; *c* — 25 °C/s

Such changes in mechanical properties of HAZ metal of steel S460M are caused by different structural transformations in the range of investigated cooling rates. This is evidenced by the results of metallographic examinations.

It was found by the metallographic examinations that in the overheating area in the HAZ metal of steel S460M at the cooling rate $w_{6/5}$ = 3 °C/s the structure was formed consisting of different morphological forms of ferrite and a small amount of pearlite (Figure 3, *a*). The hardness of such metal amounts to *HV*1-2400 MPa and the banding of structure, which was observed in it before the treatment by a thermal cycle, disappears completely.

At the increase in $w_{6/5}$ to 10 °C/s the equiaxial ferrite-pearlite fine-dispersed structure with the areas of bainite component is formed. The grain size in accordance with GOST 5639–82 corresponds to the mark 9 on the scale 1, and the hardness almost does not change, although the values of strength grow approximately by 100 MPa.

At the further increase in cooling rate to $w_{6/5}$ = = 25 °C/s in the simulated HAZ metal the structure is formed, consisting of mixture of upper and lower bainite and a small amount of martensite and ferrite. Due to that the hardness of metal is increased to *HV*1-2800–2960 MPa, which in its turn leads to growth of values of its static strength and decrease in ductile properties.

Resistance of welded joints to cold crack formation. It is known that the following factors have a decisive influence on cold crack formation: hardening structures in the HAZ and weld metal, hydrogen in these areas of welded joint and the stresses of the I type caused by the welding process and rigidity of joints fixing.

During welding in the HAZ metal of low-carbon heat strengthened steels the structures are formed, the ductility of which sharply decreases with increase in hydrogen content. The hydrogen is released in the imperfections of metal structure (pores, cracks along the grain boundaries, etc.) and causes arising of high local stresses. At the mutual effect of stresses caused by the welding process, structural transformations and hydrogen in the HAZ metal, the cold cracks can occur.

The simplest solution to the problem of reducing of diffusion hydrogen concentration in the weld metal is the use of low-hydrogen welding consumables, namely, electrodes with a basic coating for manual arc welding and flux-cored wires of a basic type for mechanized welding in shielding gases.

Regarding the possibility of removing diffusion hydrogen from welded joints, it is necessary to note the effectiveness of applying preheating or performing this procedure after welding. If the purpose of preheating is decrease in cooling rate and, at the same time, increase in cooling period in the temperature range of 800–500 °C, then the preheating after welding delays the cooling rate of HAZ metal in the temperature range of 300–100 °C, which allows removing diffusion hydrogen from welded joints to the greater extent.

It was found that at low concentrations of diffusion hydrogen in the deposited metal (Figure 4), and namely at $[H]_{diff}$ = 1.6 ml/100 g, even during welding without preheating ($w_{6/5}$ = 21 °C/s) the steel S460M is not subjected to a delayed fracture. This is evidenced by the fact that within 24 h after loading the specimens, the cracks were not formed in them even in the case when the level of stresses was approaching the yield strength of HAZ metal of steel.

With increase in the content of diffusion hydrogen in the deposited metal from 1.6 to 3.8 ml/100 g, the risk of cold crack formation in the HAZ metal of welded joints increases. To improve the resistance of

welded joints to cold crack formation is possible by using preheating. Thus, at $[H]_{diff}$ = 3.8 ml/100 g, the preheating T_{ph} to the temperature of 60 °C allows increasing the level of critical stresses to 350 MPa, and at T_{ph} = 90 °C — to σ_{cr} = 390 MPa.

At the limited content of diffusion hydrogen in the deposited metal the steel S460M does not reveal susceptibility to a delayed fracture. Accordingly, the welded joints of these steels under the given conditions should have a good resistance to cold crack formation. As the results of testing technological samples (Table) show, during welding without preheating in the joints of steel S460M regardless of rigidity of their fixture, it is possible to eliminate the probability of cold crack formation, under the conditions when the content of diffusion hydrogen in the deposited metal does not exceed 1.6–1.7 ml/100 g at Q_w = = 11–13 kJ/cm and 3.0 ml/100 g at Q_w = 15–16 kJ/cm and higher. This is well correlated with the results of tests by the Implant method.

The cracks in the technological samples of steel S460M of width B = 100 mm were observed in the cases when welding was performed without preheating ($w_{6/5}$ = 21 °C/s) and the content of diffusion hydrogen in the deposited metal was 5.3 ml/100 g. In the technological samples with the fixing base of 100 mm the crack which passed in the welded joint along the entire length and escaped to the surface of a root weld, began its formation already within 2 hours after the welding completion. This was evidenced by the signals of acoustic emission which were fixed using IKD-128 device [13]. Within 4 hours the crack was visually seen on the weld surface.

It is possible to improve significantly the resistance to cold crack formation in the technological samples of steel S460M at the increased content of diffusion

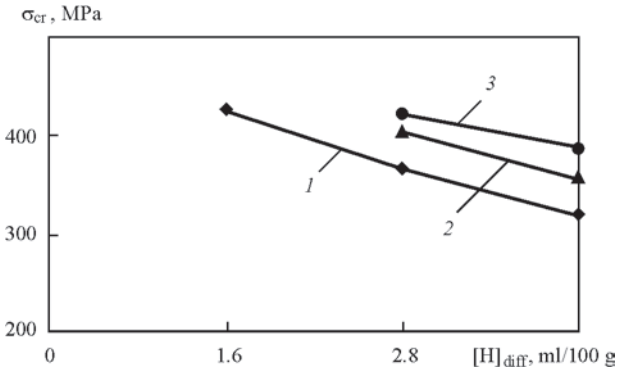

Figure 4. Influence of diffusion hydrogen on resistance to a delayed fracture of HAZ metal of steel S460M: *1* — without preheating; *2* — T_{ph} = 60; *3* — 90 °C

hydrogen in the deposited metal by decreasing the value of residual stresses in welded joints to the level not exceeding 0.5σ_y of steel (≤ 235 MPa). Namely, such a level of stresses is formed in the weld metal of joints of steel S460M produced using electrodes UONI 13/55 at the fixing base of 200 mm (see Table).

Structure and mechanical properties of steel S460M welded joints. The analysis of test results shows that according to the values of static strength and ductility those welds correspond to the requirements of steel S460M ($\sigma_y \geq$ 460 MPa, $\sigma_t \geq$ 540–720 MPa, $\delta_5 \geq$ 17 %) according to EN 10025-4:2007, which were produced using electrodes FOX EV 50, solid wire G3Sil and flux-cored wire of grade Megafil 821R.

Somewhat lower by 5–13 % than the standard indicators is the value of yield stresses of weld metal of steel S460M welded joints produced using electrodes UONI-13/55 and the wire Sv-08G2S, which are, respectively, 440 and 400 MPa. At the same time, the values of tensile strength ($\sigma_t \approx$ ~556 MPa) and elongation (δ_5 = 31 %) exceed their minimum standard values for steel.

Results of investigation of technological samples «hard welding» of steel S460M

Width *B*, mm	Welding consumables	Welding modes				T_h, °C	$[H]_{diff}$, ml/100 g	Presence of cracks, %		
		I_w, A	U_a, V	v_w, m/h	Q_w, kJ/cm			Root	Middle	Surface
100	Electrodes UONI-13/55 of 4 mm diameter	150–170	24–26	8–10	12.5–11.0	20	5.3	100	100	100
200	Electrodes UONI-13/55 of 4 mm diameter	150–170	24–26	8–10	12.5–11.0	20	5.3	0	0	0
100	Electrodes UONI-13/55 of 4 mm diameter	150–170	24–26	8–10	12.5–11.0	60	5.3	0	0	0
100	Wire Sv-08G2S of 1.2 mm diameter in CO_2	180–200	28–30	13–14	13.0–11.0	20	1.0	0	0	0
100	Wire Sv-08G2S of 1.2 mm diameter in CO_2	220–240	30–32	6–7	33.0–28.4	20	1.0	0	0	0
100	Wire Megafil 821R of 1.2 mm diameter in CO_2	240–260	28–30	17–18	15.8–14.8	20	3.0	0	0	0

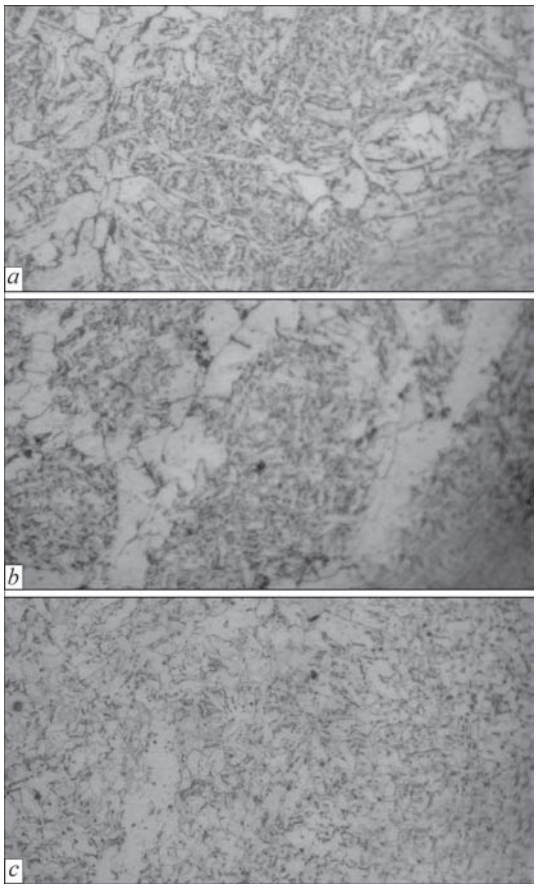

Figure 5. Microstructure (×400) of metal of steel S460M welded joints produced using UONI-13/55 (*a*), solid wire Sv-08G2S (*b*) and flux-cored wire Megafil 821R (*c*)

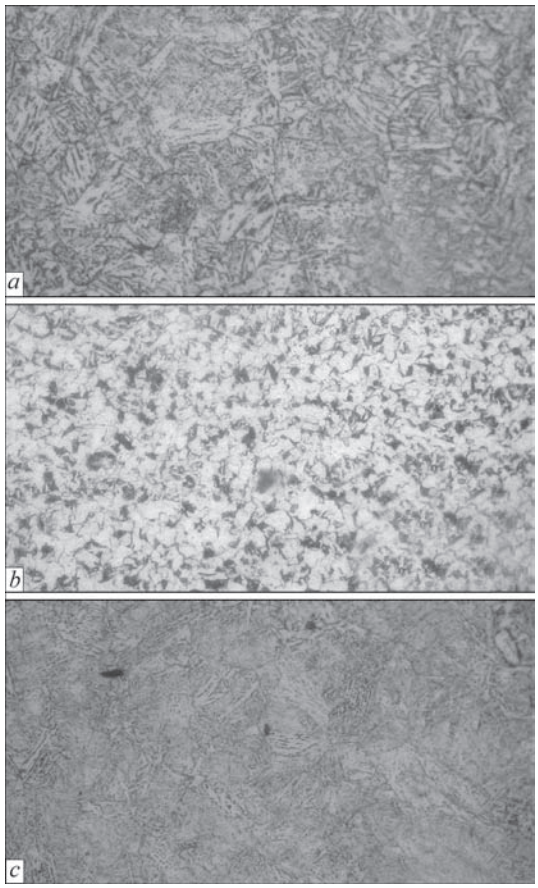

Figure 6. Microstructure (×400) of HAZ metal in the area of overheating of steel S460M welded joints produced using UONI-13/55 (*a*), solid wire Sv-08G2S (*b*) and flux-cored wire Megafil 821R (*c*)

The high values of yield strength and tensile strength relative to the welds, produced using electrodes UONI-13/55 and the wire Sv-08G2S belong to the metal deposited using electrodes FOX EV-50, and also in gas mixture using solid wire G3Sil and flux-cored wire of grade Megafil 821R, respectively. However, although the values of elongation in mechanized welding are lower than the similar values for the metal, deposited using covered electrodes, they exceed the standard values specified to the base metal.

There is the fact which attracts attention that the values of strength and ductility of weld metal produced using electrodes UONI-13/55 and solid wire Sv-08G2S, are sufficiently close. This is evidenced by the results of metallographic investigations. They showed that the structure of such welds (Figure 5, *a*, *b*) is finely dispersed and consists mainly of polygonal ferrite with negligible pearlite inclusions on the boundaries of ferrite grains with the hardness *HV*-191–200. But in welding using flux-cored wire Megafil 821R the structure of weld metal is composed primarily of structurally free ferrite with a low content of coarse acicular ferrite (Figure 5). The hardness in the given case amounts to *HV*-210, which results in increasing values of strength and decrease in plastic properties.

The structure of metal in the area of overheating the HAZ of welded joints of steel S460M is identified as a coarse ferrite-pearlite with approximately equal ratio of ferrite and pearlite components and the hardness *HV*-205–221 (Figure 6, *a–c*).

According to the results of tests of specimens with a sharp notch, it was revealed, that all the mentioned steel-welding consumable combinations are capable to provide impact toughness of both the weld and HAZ metal of welded joints of steel S460M at the level of Euronorm requirements, namely $KCV_{-40} \geq$ $\geq$ 27 J/cm^2 (Figure 7).

Resistance of steel S460M welded joints to brittle fracture. The brittle fracture occurs in welded joints in the zones of small volume of metal where plastic deformations are localized. The zones of fracture can be the metal, near which there are such defects as cracks, lacks of fusion, pores, slag inclusions, undercuts. These defects (especially tiny ones) can not always be detected by the methods of non-destructive testing such as ultrasonic and magnetic flaw detection, radiography, etc. During static and cyclic loading of welded structures these defects can initiate propagation of cracks in the metal, which during

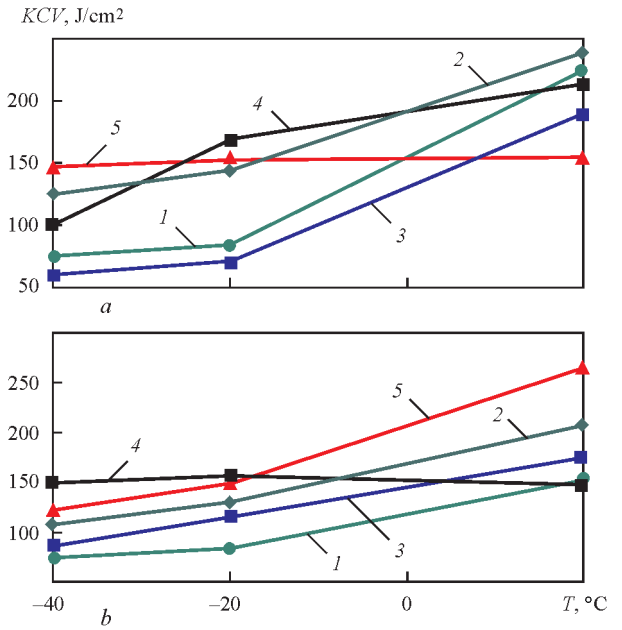

Figure 7. Impact toughness of weld metal (*a*) and HAZ metal (*b*) of steel S460M welded joints produced using electrodes UONI-13/55 (*1*) and FOX EV-50 (*2*); solid wire Sv-08G2S (*3*), G3Sil (*4*) and flux-cored wire Megafil 821R (*5*)

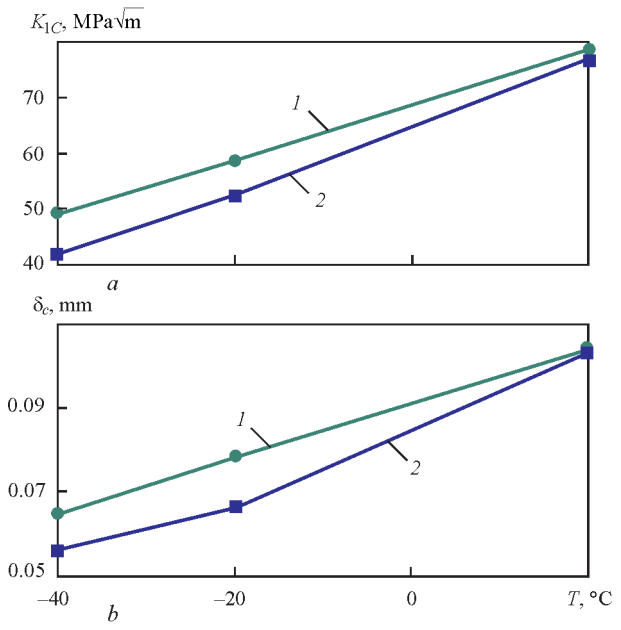

Figure 8. Dependence of values of critical stress intensity factor K_{1C} (*a*) and crack opening displacement δ_c (*b*) on the test temperature for weld metal of steel S460M welded joints made using flux-cored wire Megafil 821R (*1*) and electrodes UONI-13/55 (*2*)

operation (especially under the conditions of sub-zero temperatures) cause their fracture.

According to the methods of fracture mechanics the critical stress intensity factor K_{1C} is used for evaluation of sensitivity of metal to stress concentration under the conditions of plane deformation at static loading (more often bending). At the increase in values K_{1C} the sensitivity of metal to stress concentration is reduced. The second criterion of fracture mechanics is the crack opening displacement δ_c, which is a deformation criterion and is used for evaluation of resistance of metal to the start of crack movement. With its help the evaluation of metal resistance to brittle fracture is carried out under the conditions of large plastic deformation, when the crack in its tip reaches critical values δ_c and begins a rapid propagation, using the energy released at its further growth [11].

It was revealed by the carried out investigations that for the weld metal, produced using electrodes UONI-13/55 at the test temperature of –40, –20 and 20 °C, the average values K_{1C} are respectively equal to 42.1; 52.2 and 77.2 MPa√m, and for the metal of weld, produced using flux-cored wire of grade Megafil 821R under the similar test temperatures, the average values K_{1C} are respectively equal to 49.1; 58.5 and 78.6 MPa√m, i.e. they are increased by 14.3; 10.8 and 1.8 % (Figure 8).

For HAZ metal of welded joints, produced using electrodes UONI 13/55, at the test temperature of –40, –20 and 20 °C the average values K_{1C} are, respectively. equal to 41.4, 52.3 and 73.2 MPa√m, and for HAZ metal of welded joints, produced using flux-cored wire of grade Megafil 821R, they amount to 47.6; 52.9 and 76.4 MPa√m, which is also increased on average by 13.1; 1.2 and 4.2 % (Figure 9). At the same time, for the base metal the average values of the stress intensity factor K_{1C} amount to 49.7; 59.2 and 82.5 MPa√m at the test temperature of –40, –20 and 20 °C and they are by 11–15 % higher than the values of this factor for the metal of welded joints.

The average values δ_c for weld metal in manual welding using electrodes UONI-13/55 (test temperatures –40, –20 and 20 °C) are, respectively, equal to

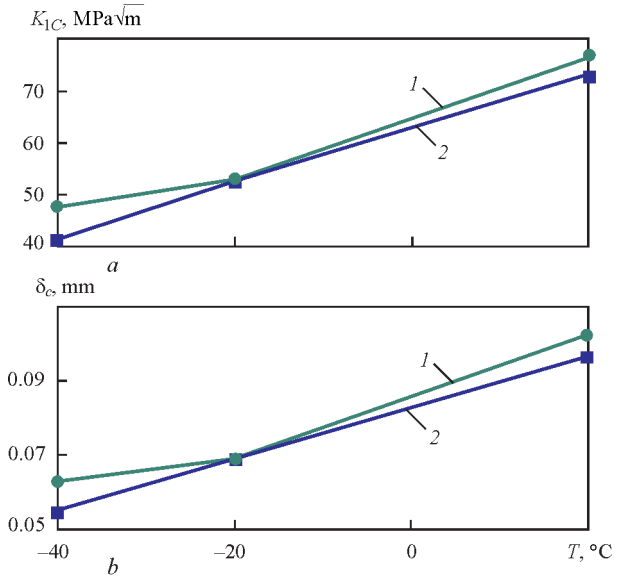

Figure 9. Dependence of values of critical stress intensity factor K_{1C} (*a*) and crack opening displacement δ_c (*b*) on the test temperature for HAZ metal of steel S460M welded joints made using flux-cored wire Megafil 821R (*1*) and electrodes UONI-13/55 (*2*)

0.056; 0.066 and 0.103 mm, and for the weld metal, produced using flux-cored wire of grade Megafil 821R at the similar temperature conditions of the tests, they amount, respectively, to 0.065; 0.078 and 0.104 mm. The same tendency is typical also for HAZ metal of welded joints. In welding using electrodes UONI-13/55, the value δ_c for test temperatures –40, –20 and 20 °C is, respectively, 0.055; 0.069 and 0.097 mm, and for HAZ metal, produced using flux-cored wire of grade Megafil 821R, they are, respectively, equal to 0.063; 0.069 and 0.103 mm (Figure 9). The value δ_c for the base metal, the same as the values K_{1C}, is higher than in the metal of welded joints and, respectively, equal to 0.066, 0.078 and 0.12 mm. It should be noted that the ratio of values δ_c for the weld and HAZ metal of welded joints of steel S460M for different welding consumables are similar to the ratios of values K_{1C}.

The common factor is that in mechanized welding using flux-cored wire Megafil 821R in the gas mixture 82 % Ar + 18 % CO_2 the metal of welded joints of steel S460M has a higher resistance to brittle fracture, than in manual arc welding using electrodes UONI-13/55. These data are well correlated with the results of investigations of resistance to brittle fracture of welded joints similar in chemical composition to the steel S355J2.

Conclusions

1. It was found that in the range of cooling rates $7 \le w_{6/5} \le 15$ °C/s of HAZ metal of model specimens of steel S460M the values of static strength, ductility and impact toughness are preserved at the level of values of base metal.

2. It was found that at low concentrations of diffusion hydrogen in the deposited metal, namely at $[H]_{diff} = 1.6$ ml/100g, even in welding without preheating the steel S460M is not prone to a delayed fracture.

3. It is possible to significantly improve the resistance to cold crack formation in the technological samples of steel S460M at the increased content of diffusion hydrogen in the deposited metal by reducing the value of residual stresses in welded joints to the level, not exceeding $0.5\sigma_y$ of steel (≤ 235 MPa) or by applying the preheating to 60 °C.

4. It was shown that in mechanized welding using flux-cored wire Megafil 821R in the gas mixture 82 % Ar + 18 % CO_2 the metal of welded joints of steel S460M has a higher resistance to brittle fracture, than that in manual arc welding using electrodes UONI-13/55.

1. Ufuah, E. (2013) Elevated temperature mechanical properties of butt welded connections made with high-strength steel grades S355 and S460M. In: *Proc. of Int. Conf. on Design, Fabrication and Economy of Metal Structures* (Miskolc, Hungary, April 24–26, 2013), 407–412.
2. Nazarov, A., Yakushev, E., Shabalov, I. et al. (2014) Comparison of weldability of high-strength pipe steels microalloyed with niobium, niobium and vanadium. *Metallurgist*, 7(**9/10**), 911–917.
3. (1993) *Welded building structures*. Vol. 1: Basis of structural design. Ed. by L.M. Lobanov. Kiev: Naukova Dumka.
4. Tylkin, M.A., Bolshakov, V.I., Odessky, P.D. (1983) *Structure and properties of construction steel*. Moscow: Metallurgiya.
5. Odessky, P.D., Molodtsov, A.F., Morozov, Yu.D. (2011) New efficient low-alloy steels for building metal structures. *Montazhnye & Spetsialnye Raboty v Stroitelstve*, **5**, 20–25.
6. Bilyk, A.S., Kurashev, R.V., Gorbatenko, V.V. et al. (2013) Application of thermomechanically strengthened sheet products in welded metal structures. *Promyslove Budivnytstvo ta Inzh. Sporudy*, **4**, 1–4.
7. *Ragu* Nathan, S., Balasubramanian, V., Malarvizhi, S. (2015) Effect of welding processes on mechanical and microstructural characteristics of high strength low alloy naval grade steel joints. *Defence Technology*, **11**, 308–317.
8. Poznyakov, V.D., Zhdanov, S.L., Maksimenko, A.A. (2012) Structure and properties of welded joints of steel S390 (S355 J2). *The Paton Welding J.*, **8**, 6–10.
9. Sarzhevsky, V.A., Sazonov, V.Ya. (1981) Unit for simulation of welding thermal cycles on the base of machine MSR-75. *Avtomatich. Svarka*, **5**, 69–70.
10. Hrivnak, I. (1984) *Weldability of steels*. Ed. by E.L. Makarov. Moscow: Mashinostroenie.
11. Mikhoduj, L.I., Poznyakov, V.D., Yushchenko, A.K. (2000) Resistance of 12KhN2MFDRA steel welded joints to a delayed fracture. *The Paton Welding J.*, **11**, 4–10.
12. Hall, U., Kukharova, Kh., Zut, V. (1978) *Brittle fracture of welded structures*. Ed. by I.V. Kudryavtsev et al. Moscow: Mashinostroienie.
13. Musiyachenko, V.F., Kasatkin, B.S., Zhdanov, S.L. et al. (1981) Examination of conditions of formation and propagation of cold cracks in high-strength steel welded joints by acoustic emission method. *Avtomatich. Svarka*, **7**, 5–7.

Received 21.06.2016

doi.org/10.15407/tpwj2016.12.05

EVALUATION OF HIGH TEMPERATURE RESISTANCE OF THREE-LAYER HONEYCOMB PANEL PRODUCED FROM YuIPM-1200 ALLOY BY VACUUM DIFFUSION WELDING

I.A. GUSAROVA[1], **M. PARKO**[2], **A.M. POTAPOV**[1], **Yu.V. FALCHENKO**[3], **L.V. PETRUSHINETS**[3], **T.V. MELNICHENKO**[3] and **V.E. FEDORCHUK**[3]

[1]SC «M.K. Yangel Design Bureau «Yuzhnoje»
3 Krivorozhskaya Str., 49008, Dniepr, Ukraine. E-mail: infor@yuzhnoye.com
[2]TECNALIA, Parque Tecnolygico de San Sebastian Mikeletegi Pasealekua
2 E-20009 Donostia-San Sebastian-Gipuzkoa, Spain. E-mail: maria.parco@tecnalia.com
[3]E.O. Paton Electric Welding Institute, NASU
11 Kazimir Malevich Str., 03680, Kiev, Ukraine. E-mail: office@paton.kiev.ua

Development of thermal protection systems is one of the important engineering problems that should be solved at development of reusable space vehicles. Metal panels of thermal protection systems should consist of separate tiles with individual fastening to load-carrying structure of space vehicle, with surface density of not more than 10 kg/m^2, capable of withstanding multiple long flights and providing temperature lowering from 1100 ºC on the outer wall to 200 ºC on the inner wall. The work shows the results on development of the technology of vacuum diffusion welding of a three-layer honeycomb panel from experimental powder alloy YuIPM-1200. Technological samples of three-layer honeycomb panel were made from this alloy, and their testing was performed in the working temperature range. 7 Ref., 11 Figures.

Keywords: *thermal protection systems; metal three-layer panel, powder high-temperature alloy, vacuum diffusion welding, thermal cycling tests*

Development of thermal protection systems with outer metal three-layer panel for reusable space vehicles has been conducted in the USA and Europe starting from the middle of the XXth century. So far, however, there is no information about their development for the windward hull of reusable space vehicles, preserving their performance at service loads for the required number of launches [1]. Development of such thermal protection will allow creation of a reliable reusable space vehicle (RSV) and reducing the cost of taking payloads to orbit.

In Ukraine (SC «DB «Yuzhnoje») developed a removable multilayer thermal protection structure (TPS) with outer metal three-layer panel, consisting of separate tiles with individual fastening to vehicle load-carrying structure, of not more than 10 kg/m^2 density, capable of withstanding multiple long flights and providing temperature lowering from 1100 ºC on the outer wall to 200 ºC on the inner wall [2]. Schematic of TPS with metal outer three-layer panel with U-shaped butt joint and plate thermal insulation is shown in Figure 1. Metal outer three-layer panel with plane dimensions of 300×300 mm consists of upper skin 0.5 mm thick, honeycomb core and lower skin 0.1 mm thick.

Special high-temperature powder alloy YuIPM-1200 based on Ni-Cr was developed for fabrication of outer metal structure. The alloy has the required level of emissivity and is resistant to oxidizing medium at superhigh temperatures that allows eliminating special coatings [3].

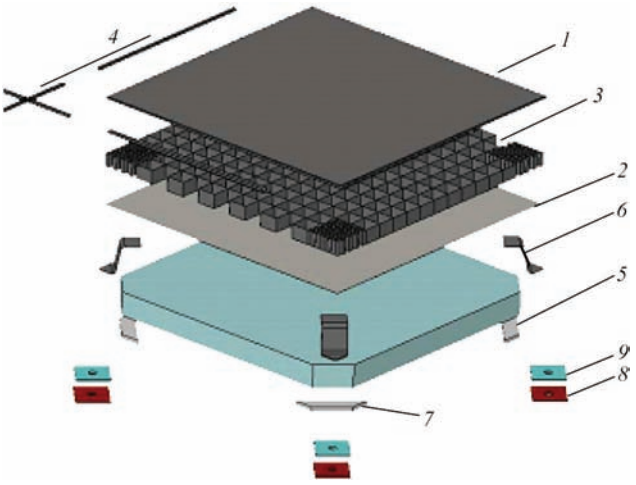

Figure 1. General view of TPS tile: *1* — panel upper skin; *2* — panel lower skin; *3* — honeycomb core; *4* — U-shaped stampings; *5* — thermal insulation; *6* — Z-shaped metal posts of fastening system; *7* — felt substrate; *8* — damping gasket from heat-resistant rubber; *9* — thermostat

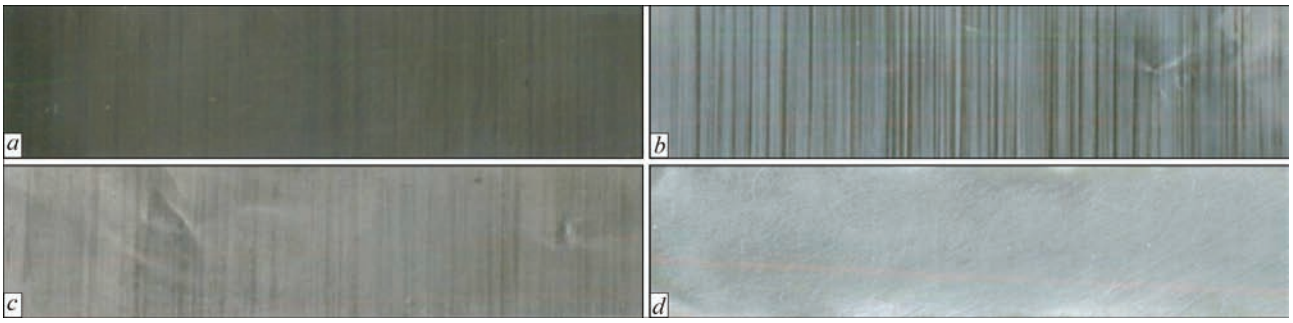

Figure 2. Appearance of the surface of foil from Ni–Cr high-temperature alloy YuIMP-1200; *a* — appearance of foil in as-delivered state; *b* — chemical etching in the following solution: 500 ml HNO_3, 250 ml H_2SO_4, 10 g NaCl; *c* — chemical etching in the solution of 750 ml HCl, 250 ml HNO_3; *d* — mechanical cleaning with sandpaper with R1000 grain size

As the developed high-temperature powder alloy YuIPM-1200 based on Ni–Cr has practically no analogs, development of the technology of manufacturing three-layer panel with honeycomb core and making its engineering mock-up is of interest.

As available equipment allows welding parts of up to 200 mm size, the objective of this work was manufacturing the engineering mock-up of metal three-layer panel from YuIPM-1200 alloy of 150×150 mm size and conducting experimental studies of TPS mock-up performance at thermal cycling in the working temperature range.

Technological process of manufacturing three-layer panel mock-up includes the following operations [4]:

- skin manufacturing;
- manufacturing blanks for honeycomb core;
- forming profiled strips from the blanks;
- welding the honeycomb core;
- manufacturing three-layer panels.

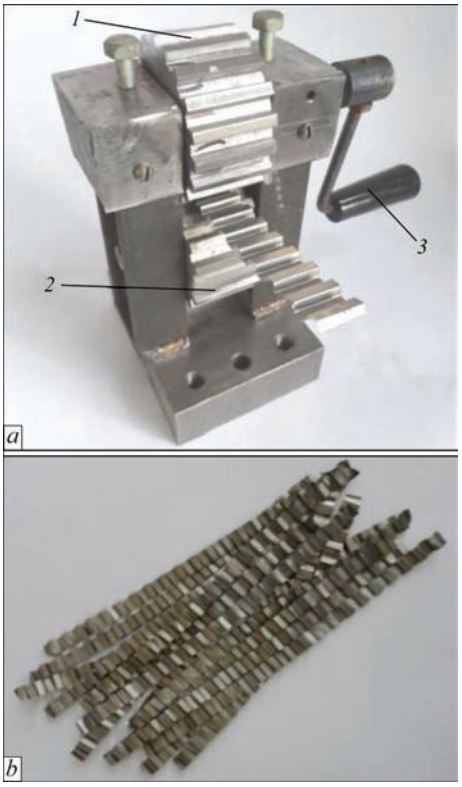

Figure 3. Device for strip forming (*a*) and profiled strip (*b*) (for description of *1–3* see the text)

Manufacturing skins and foil for honeycomb core of required thickness was conducted by rolling by specially developed technology in SPC «Rubin».

In the initial as-rolled state the surface of foil from YuIPM-1200 alloy is covered by a dense oxide film (Figure 2, *a*). The possibility of application of chemical or mechanical cleaning for its removal was considered.

The following chemical solutions were used to remove the oxide film from foil surface: 500 ml HNO_3 + 50 ml H_2SO_4 + 10 g NaCl or 750 ml HCl + 250 ml HNO_3 [5]. Analysis of the state of foil surface after chemical etching showed that its complete cleaning does not take place (Figure 2, *b*, *c*).

Mechanical cleaning of foil using fine grain sandpaper R1000 allows producing a cleaner surface, compared to treatment in chemical solutions (Figure 2, *d*). Foil cleaning with sandpaper allows eliminating defects found on its surface, which were due to unevenness of the surface of rolls used in its manufacture. Foil surface does not have any contamination or discoloration. Further on, removal of oxide film from foil surface was conducted by the method of mechanical cleaning. After cleaning, the foil was rinsed in water to remove fine dust particles and dried in air for 20–30 min at the temperature of 30–40 ºC. Foil cutting up to ensure the required accuracy of sample length and absence of tears or burrs was conducted in keeping with GOST 618–73.

Method of rolling in profiled rollers which allows producing corrugated strips with a high precision, became widely applied for manufacturing honeycomb structures [6]. In this connection, a special device was designed and manufactured to form profiled strip of honeycomb core (Figure 3, *a*).

The device consists of two gears *1* and *2* with teeth parameters corresponding to honeycomb cell size. Driving wheel *1* is mounted on one axle with handle *3*,

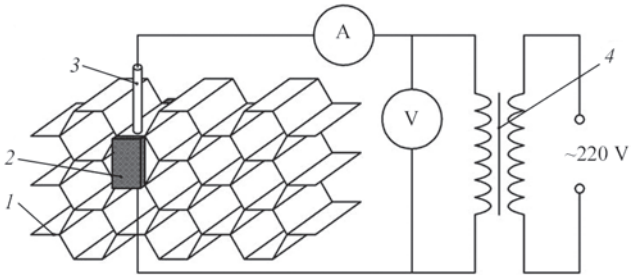

Figure 4. Schematic of a device for welding honeycomb core from Ni–Cr alloy: *1* — profiled strips; *2* — graphite electrode; *3* — copper electrode; *4* — transformer

setting the device into motion. Appearance of formed strip of honeycomb core is given in Figure 3, *b*.

As shown by investigations, foil from YuIPM-1200 alloy in as-delivered condition has considerable work hardening, due to its rolling. At manufacture of honeycomb core strip cracking occurred in a number of cases in the points of foil bending, which was caused by a change of material properties through work-hardening.

It is known [7] that application of heat treatment in the temperature range of 0.35–0.40 of the alloy melting temperature allows its ductility to be increased.

It is also established than vacuum annealing for 20–30 min at the temperature of 780–800 ºC is sufficient to relieve work-hardening of the studied alloy. After this heat treatment alloy ductility increases, that allows preventing cracks at forming of honeycomb core cells.

Spot welding was used to produce honeycomb core from profiled strips (Figure 4). Profiled strip surfaces were degreased in alcohol before their assembly into blocks. Strips *1* were mounted on graphite electrode *2*, which was made proceeding from overall dimensions of honeycomb cells (Figure 4). After compression of metal sections to be welded, current was passed through electrode *3*. Optimum parameters of the process for this foil thickness are current

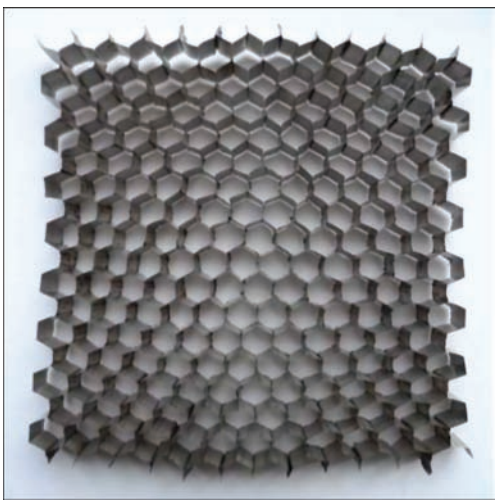

Figure 5. Honeycomb core made from foil of YuIPM-1200 alloy

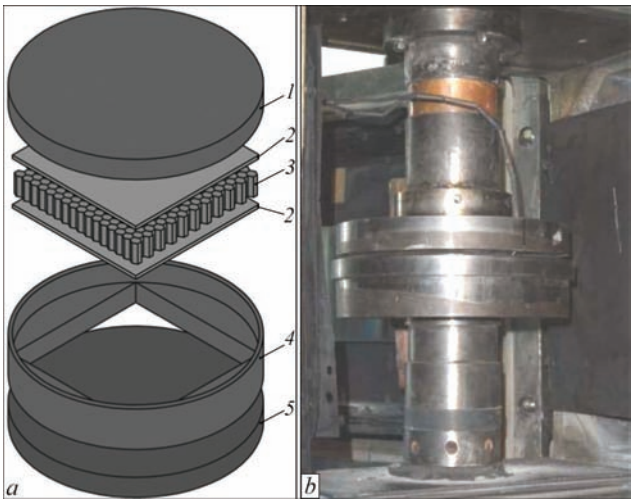

Figure 6. Schematic of fixture for welding three-layer honeycomb panels (*a*) and working chamber with the fixture mounted in it (*b*): *1* — upper flange; *2* — skin; *3* — honeycomb; *4* — limiting sleeve; *5* — lower flange

I = 300 mA, voltage U = 5 V at 2 mm diameter of copper electrode. Appearance of honeycomb core package of 150×150 mm size from YuIPM-1200 alloy based on Ni–Cr is shown in Figure 5.

It is experimentally established that the best conditions for welding YuIPM-1200 alloy are provided by

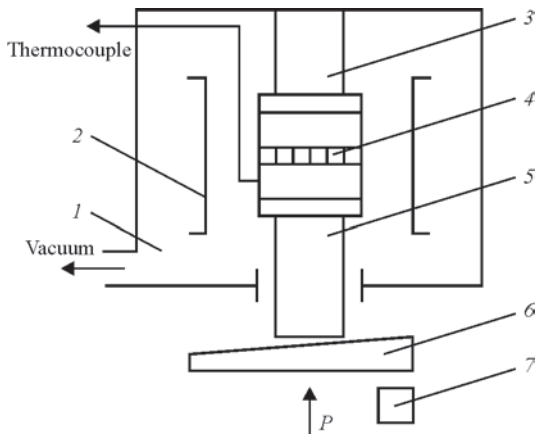

Figure 7. Schematic of working chamber with fixture: *1* — working chamber; *2* — molybdenum heater; *3* — upper rod; *4* — three-layer panel mounted in limiting sleeve; *5* — lower rod; *6* — wedge; *7* — press

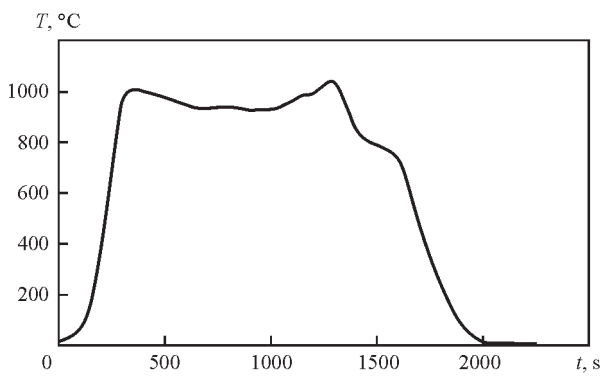

Figure 8. Dependence of temperature on TPS outer surface on time

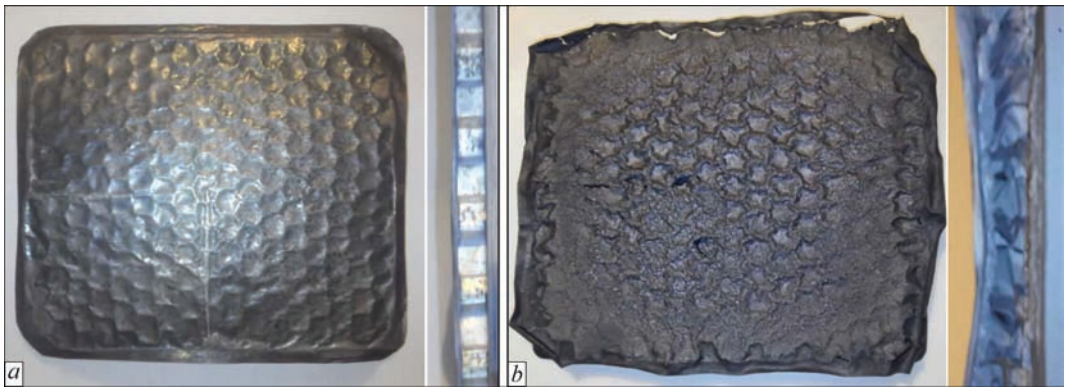

Figure 9. Appearance of three-layer panel before (*a*) and after testing (*b*)

application of upper electrode from copper and lower electrode from graphite that eliminates undesirable adhesion of foil surface to the electrodes. Welding was followed by grinding of end faces of the honeycomb core.

Vacuum diffusion welding was used for joining the honeycomb core and skins into a three-layer structure. Welding was conducted in a specially designed and manufactured fixture (Figure 6). In terms of design, the device (fixture) for three-layer panel welding consists of the lower and upper flanges and limiting sleeve (Figure 6, *a*). During welding, flanges ensure pressing of skins to honeycomb core over the entire area of contact, and limiting sleeve allows equalizing the temperature field in the item being welded. Figure 6, *b* shows the appearance of the fixture for welding a three-layer honeycomb panel in the vacuum chamber of diffusion welding unit.

Figure 7 shows the schematic of working chamber of diffusion welding unit with the fixture installed in it. The possibility of placing a thermocouple in the fixture was envisaged for welding temperature control. Pressure was applied to the part being welded from the press through wedge *6* and lower rod *5*. Pressure magnitude was evaluated by a dynamometer.

Heating of the fixture with three-layer honeycomb panel mounted in it, was conducted at the rate of 25–30 ºC/min, and after reaching the welding temperature, pressure was applied to it. Soaking at welding temperature was conducted for 25–30 min. After that the applied pressure level was lowered to zero, and cooling to room temperature was performed under vacuum.

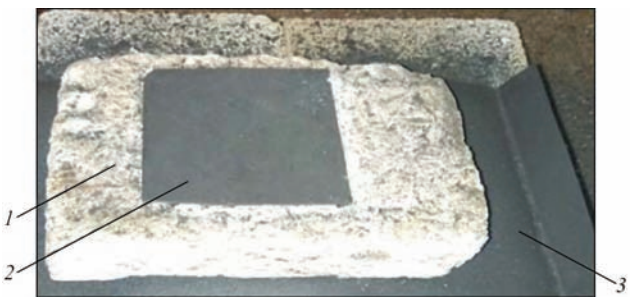

Figure 10. Sample in thermal insulation cell: *1* — thermal insulation cell; *2* — outer skin of three-layer metal TPS; *3* — tray for loading into the furnace

Thus, engineering samples of three-layer honeycomb panel mock-up of 150×150 mm size were produced, which were used for experimental studies. Thickness of upper skin of three-layer honeycomb panel was 0.5 mm, that of lower skin was 0.1 mm, honeycomb core was made from foil 0.03 mm thick.

Temperature modes of heating and cooling of the studied samples were selected proceeding from theoretical temperature curve on the structure surface during RSV descent (Figure 8).

Maximum working temperatures on the surface of a three-layer honeycomb panel are equal to 1100 ºC. To improve structure reliability, a 10 % margin of high-temperature strength is incorporated into their design. Therefore, the first stage was optimization of test procedure and determination of structure performance at one-time exposure to the temperature of 1200 ºC.

Testing an engineering sample of three-layer panel was conducted, using «SNOL» laboratory furnace. Before the start of testing, the furnace was heated up to the temperature of 1210 ºC, which was followed by placing the sample into the furnace with lower skin 0.1 mm thick facing upwards, and upper skin 0.5 mm thick resting on the furnace lower wall. Soaking of three-layer panel mock-up in the furnace for 20 min, at the temperature of 1200 ºC was performed. Then, the sample was removed and cooled to the temperature in the premises. Cooling time was 3 min.

Appearance of the studied sample before and after testing is given in Figure 9. Upper skin 0.5 mm thick preserved its intactness. Skin 0.1 mm thick deformed during cooling in the points of welding to the honeycombs, and through-thickness cracks formed in it in several places. After complete cooling of the mock-up to temperature in the premises, 0.1 mm thick skin became brittle, honeycomb faces lost their stability and strength in the transverse direction.

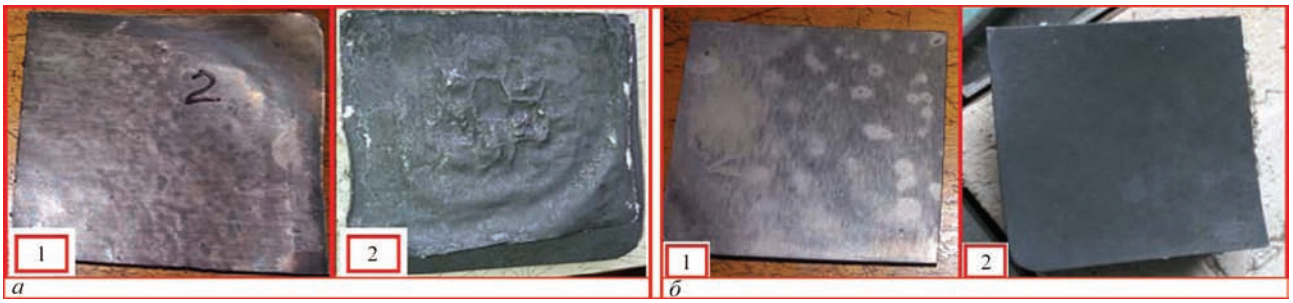

Figure 11. Appearance of mock-up lower (*a*) and upper (*b*) skins before thermal cycling (*1*) and after 11 thermal cycles (*2*)

As thin-layered elements of the structure of 0.03 mm (honeycombs) and 0.1 mm (lower skin) thickness fail under the impact of 1200 ºC for 20 min, thermal cycling of the next sample was conducted in the standard temperature range of 20–1100 ºC. To model standard service conditions the sample was placed into a special thermal protection cell from ceramic fibre, which ensured end face insulation from the impact of direct heat flows, and also modeled TPS inner thermal insulation located under the panel lower skin (Figure 10). Number of thermal cycles at testing was determined by structure integrity at visual examination of three-layer outer panel mock-up after each thermal cycle.

Before the start of testing the furnace was heated to the temperature of 1150 ºC. After that the sample was placed into the furnace and was soaked for 20 min at the temperature of 1100 ºC. The sample was taken out together with thermal insulation cell and cooled to the temperature in the premises (15 ºC) in 11 min, that corresponds to the time of cooling of the vehicle outer surface, obtained at theoretical calculations (Figure 8).

After the first thermal cycle, a protective oxide film of dark-grey colour formed on sample surface. The honeycombs deformed.

After the fifth thermal cycle, the lower skin of three-layer metal thermal protection 0.1 mm thick deformed. Residual deformations remained after cooling. After 11th thermal cycle through-thickness defects 5 mm long along honeycomb faces were found in the point of joining with the honeycomb core (Figure 11, *a*). Panel upper skin 0.5 mm thick did not show any visible changes of shape or dimensions (Figure 11, *b*).

Thus, thermal cycling of a mock-up of three-layer outer panel of thermal protection structure from YuIPM-1200 alloy in the working temperature range showed that the structural elements 0.5 mm thick preserve their serviceability for 11 thermal cycles in the set mode. Thinner elements of the structure deform and fail after thermal cycling.

To ensure normal functioning of the structure at standard heat flows, it is necessary to increase the thickness of structural elements (more than 0.1 mm) and adjust the parameters of welding the three-layer structures.

Work was performed under project LightTPS FP7 # 607162.

1. Tumino, G. (2002) European development and qualification status and challenges in hot structures and thermal protection systems for space transportation concepts. In: *Proc. of 4th Europ. Workshop on Hot Structures and Thermal Protection Systems for Space Vehicles* (Palermo, Italy, 26–29 Nov. 2002). Paris: Europ. Space Agency, 2003, 39–43.
2. Potapov, A.M., Shevtsov, E.I., Tikhy, V.G. et al. *Multilayer thermal protection system of reusable space vehicle*. Pat. 91891 Ukraine. Int. Cl. B64G 1/58, B64C 1/38, B64C 3/36. Fil. 25.11.2013. Publ. 25.07.2014.
3. Skorokhod, V.V., Solntsev, V.P., Frolov, G.A. et al. *Method of producing of heat-resistant nickel-chrome based alloy*. Pat. 108096 Ukraine. Int. Cl. C22C 19/05, B22F 3/16, B22F 3/12, B22F/00. Fil. 09.10.2012. Publ. 27.01.2014.
4. Bitzer, T.N. (1997) *Honeycomb technology. Materials, design, manufacturing, applications and testing*. New York: Chapman & Hall.
5. Baranova, L.V., Demina, E.L. (1986) *Metallographic etching of metals and alloys*: Refer. Book. Moscow: Metallurgiya.
6. *Qiuming* Zhang, Xiaodong He. (2009) Microstructural evolution and mechanical properties of a nickel-based honeycomb sandwich. *Materials Characterization*, 60(**3**), 178–182.
7. Gorelik, S.S. (1978) *Resolidification of metals and alloys*. Moscow: Metallurgiya.

Received 06.10.2016

doi.org/10.15407/tpwj2016.12.06

MATHEMATICAL MODEL OF WELDING CIRCUIT IN ROBOTIC CONSUMABLE ELECTRODE ARC WELDING

G.A. TSYBULKIN
E.O. Paton Electric Welding Institute, NASU
11 Kazimir Malevich Str., 03680, Kiev, Ukraine. E-mail: office@paton.kiev.ua

In the article the mathematical model of dynamic processes, running in the welding circuit during robotic gas-shielded arc welding using consumable electrode, is investigated The welding circuit is considered as a self-stabilizing system with a feedback by the electrode melting rate. Unlike the known mathematical models, in the investigated model the dependence of the electrode melting rate on actual values of welding current and arc voltage is taken into account. The basic aim of the article is the study of reaction of welding circuit on external disturbances arising in the process of arc welding. In the frames of the developed model the criteria for asymptotic stability were established, which in addition to the already known criteria impose certain limits on the parameters of arc welding mode itself, which is important from the practical point of view. Using the computer modeling a good correlation of this model with the real processes, running in welding circuit, was illustrated. 14 Ref., 4 Figures.

Keywords: *robotic arc welding, consumable electrode, welding circuit, mathematical model, stability of welding processes*

To develop the effective algorithms for adaptive control of robotic consumable electrode arc welding, it is necessary to dispose, if possible, an accurate and, at the same time, rather simple mathematical model of dynamic processes, running in welding circuit. As one of such models the following system of equations is used [1, 2]:

$$\left.\begin{aligned} (L_1+L_2)\frac{di}{dt}+(R_1+R_2)i &= u_x - u_a(i,l),\\ u_a(i,l) &= u_0+El+S_a i,\\ l &= H-h,\\ h &= h_0+\int_0^t (v_e-v_m)dt,\\ v_m &= Mi. \end{aligned}\right\} \qquad (1)$$

In these equations and in Figure 1 $i = i(t)$ is the welding current; L_1, R_1, u_x, u_s is the inductance, internal resistance, open-circuit voltage and the voltage at the output terminals of the welding power source (WPC), respectively; L_2 is the inductance of the circuit formed by connecting wires; R_2 is the total resistance of electrode stickout, connecting wires, sliding contact in the torch nozzle and a part of the workpiece being welded; $u_a = u_a(l, i)$ is the arc voltage; u_0 is the sum of near-electrode voltage drops; $l = l(t)$ is the arc length; $E = \partial u_a/\partial l$ is the intensity of electric field in the arc column; $S_a = \partial u_a/\partial i$ is the tangent of the inclination angle of static volt-ampere characteristic of the arc in the vicinity of the working point of welding; H = const is the distance between the end of the current-carrying nozzle and a free surface of welding pool; h_0, $h = h(t)$ is the initial and actual values of electrode stickout; v_e = const, $v_m = v_m(t)$ are the speeds of feed and melting of electrode, respectively; $M = \partial v_m/\partial i$ is the steepness of current characteristic of electrode melting; t is the actual time.

The mathematical model (1) is successfully used in solving the problems of geometric adaptation, i.e. adaptation of welding automatic machine or robot to unexpected deviations of a welding tool from the axial line of joint being welded directly in the process of arc welding [2–4]. Meanwhile, it still remains unclear how effective the use of this model will be in solving other types of problems, in particular, the problem of adaptive control of arc welding modes themselves. The matter is that the dependence of the electrode melting rate $v_m(t)$ on the actual value of arc voltage $u_a(t)$ is not taken into account in the model (1). The main argument in favor of such simplification was the fact that the distance H between the end of the torch and the workpiece being welded during robotic arc welding is maintained constant unlike in the manual arc welding. It was considered that in this case the voltage $u_a(t)$ also negligibly changes and, thus, has a low influence on melting rate of the electrode. Therefore, the calculated average value u_a was actually included into the generalized parameter M = const, namely which appeared in the last equation of the system (1). We should note that instead of the equality $v_m = Mi$ sometimes (at high welding currents) the ratio $v_m = Mi + Nhi^2$ is used, where N = const [3–6]. But also in this ratio the actual value of arc voltage $u_a(t)$ is not taken into account.

The electrode melting rate $v_m(t)$, as is known [7, 8], is proportional to the electrical power supplied to the arc gap, i.e. proportional to the product $u_a(t)$ by $i(t)$. On the other hand, due to the famous effect of arc self-regulation, the speed $v_m(t)$ in the steady mode is equal to the electrode feed speed v_e, i.e. $v_m(t) = v_e$ = = const. Therefore, any changes of $u_a(t)$ will certainly result in the corresponding changes in $i(t)$. Taking this into account, let us specify the mathematical model (1) introducing the more correct ratio instead of the approximate equality $v_m = Mi$

$$v_m = Ku_a i. \qquad (2)$$

In this ratio the constant coefficient K includes electrical, thermophysical and geometric characteristics of consumable electrode. It can be easily calculated or experimentally determined if these characteristics are known. Furthermore, using the coefficient K it is simply enough to consider that part of electrical power which is directly consumed for melting the electrode.

Excluding the variables u_a, h, v_m from the new system of equations (i.e., from the system (1) taking into account the equality (2)), let us reduce it to two differential equations relative to the variables i and l:

$$\left.\begin{aligned} L\frac{di}{dt} &= -R_w i - El + u_x - u_0, \\ \frac{dl}{dt} &= K(u_0 i + Eli + S_a i^2) - v_e, \end{aligned}\right\} \quad (3)$$

where

$$L = L_1 + L_2,\ R_w + R_1 + R_2 + S_a. \quad (4)$$

It is easy to see, that the system of equations (3) is non-linear. It is important to check the conditions under which the dynamic processes described by these equations will bear a stable nature.

Conditions for welding process stability. Let us find the relations between the parameters of welding circuit and arc welding mode, guaranteeing steady (stationary) modes. For this purpose, let us introduce the constant values i_∞ and l_∞ in the equations (3) instead of the variables i and l. As a result, we obtain the following equations

$$\left.\begin{aligned} -R_w i_\infty - El_\infty + u_x - u_0 &= 0, \\ K(u_0 i_\infty + El_\infty i_\infty + S_a i_\infty^2) - v_e &= 0, \end{aligned}\right\} \quad (5)$$

from which we find:

$$l_\infty = \frac{u_x - u_0}{E} - \frac{R_w}{E} i_\infty, \quad (6)$$

$$R_+ i_\infty^2 - u_x i_\infty + \frac{v_e}{K} = 0, \quad (7)$$

where

$$R_+ = R_w + S_a = R_1 + R_2. \quad (8)$$

It is easy to check that fulfilling the condition

$$v_e < \frac{Ku_x^2}{4R_+} \quad (9)$$

the roots of the quadratic equation (7) are real and positive. Hence, if the inequality (9) is true and the limit $0 < l(t) < l_k$ is provided, where l_k is the critical value of arc length, at which its break occurs, then stationary modes of arc welding do certainly exist.

Let us replace the variables i and l in the differential equations (3) by the sums $i = i_\infty + \xi$ and $l = l_\infty + \lambda$ where ξ and λ are the deviations of actual values of welding current i and arc length l from the corresponding established values $i_\infty = \lim_{t\to\infty} i(t)$ and $l_\infty = \lim_{t\to\infty} l(t)$. Restricting by the terms containing variables ξ and λ in the first degree and taking into account the equations (5), we shall obtain the system of differential equations of the first approximation:

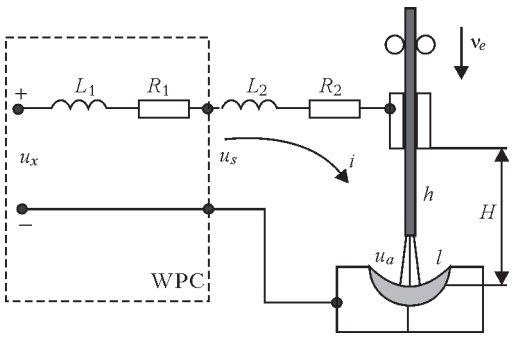

Figure 1. Scheme of welding circuit

$$\left.\begin{aligned} L\frac{d\xi}{dt} &= -R_w \xi - E\lambda\ , \\ \frac{d\lambda}{dt} &= K[u_x - (R_w - 2S_a)i_\infty)]\xi + KEi_\infty \lambda. \end{aligned}\right\}$$

Excluding the variable λ from this system, we shall come to the only differential equation with respect to ξ:

$$L\frac{d^2\xi}{dt^2} + (R_w - KELi_\infty)\frac{d\xi}{dt} + KE(u_x - 2R_+ i_\infty)\xi = 0. \quad (10)$$

Thus, the problem concerning the stability of arc welding mode is reduced to investigation of stability of zero (trivial) solution $\xi = 0$.

It is known [9] that for stability of the process, described by an ordinary differential equation of second order, it is necessary and sufficient that all its coefficients were positive (Stodola criterion). Hence, the variable $\xi = i - i_\infty$ in the equation (10) at $t \to \infty$ will tend to zero, if the following inequalities are correct:

$$R_w > 0,\ R_w - KELi_\infty > 0,\ u_x - 2R_+ i_\infty > 0. \quad (11)$$

The first inequality in (11) means that the algebraic sum $R_w = R_1 + R_2 + S_a$ should be positive. It is a known criterion of Kaufman–Nikitin [10–14]. In fact, the resistance R_1, included into this sum, is the absolute value of the angular coefficient of the volt-ampere characteristic of WPC. Hence, $R_1 = |-\partial u_s/\partial i| > 0$. The angular coefficient $S_a = \partial u_a/\partial i$, as is known [7, 8], can be both positive and negative. If $S_a \geq 0$, then $R_w > 0$ also. Whereas if $S_a < 0$, then to fulfill the condition $R_w > 0$, it is necessary that according to (4) and (8) we obtained the inequality

$$R_+ - |S_a| > 0. \quad (12)$$

The second and the third conditions in (11) impose limits on the inductance L and on the relation between the parameters of arc welding mode u_x and i_∞. Let us write these conditions in the following way:

$$L < \frac{R_w}{KEi_\infty},\ \ \frac{u_x}{i_\infty} > 2R_+. \quad (13)$$

Thus, in order that the process, described by the equation of the first approximation (10), was asymptotically stable, it is necessary and sufficient that the following conditions (9), (12), (13) were fulfilled. If the mentioned conditions are fulfilled and the disturbing effects are sufficiently low, then, according to the known Lyapunov theorem [9], the process, described by the initial non-linear equations (3) was also asymptotically stable.

Reaction of welding circuit on external effects. The welding circuit including electric arc, consumable electrode supplied in the welding process at a certain speed v_e and the welding power source WPC, from the point of view of the theory of automatic control represents, as is known [2, 7], a closed system with the internal negative feedback by the electrode melting rate. Thanks to this feedback, the system itself (without special devices) performs stabilization of the electrode melting rate v_m at the level of the preset electrode feed speed v_e.

It is used to judge about the stabilizing properties of welding circuit, including quickness and accuracy of practicing the input actions, by its reaction to these influences. Studying the reaction of the mathematical model (3) on the similar effects, it is possible to evaluate the degree of its conformity (adequacy) to the real processes running in welding circuit, and, in particular, to compare the models (3) and (1).

For such kind of verification of the model (3) let us carry out the simulation experiment on the computer. Let us suppose that it is necessary to perform shielded-gas arc welding using consumable electrode with the diameter equal to 1 mm. The welding current $i_\infty \approx 150$ A, and the arc length $l_\infty \approx 4$ mm. The values of welding circuit parameters are the following: $L = 4\cdot10^{-4}$ H, $R_1 = 0.025$ Ohm, $R_2 = 0.01$ Ohm, $H = 17$ mm, $u_0 = 16$ V, $E = 2$ V/mm, $S_a = 0.005$ V/A, $K = 0.012$ mm/(A·V·s).

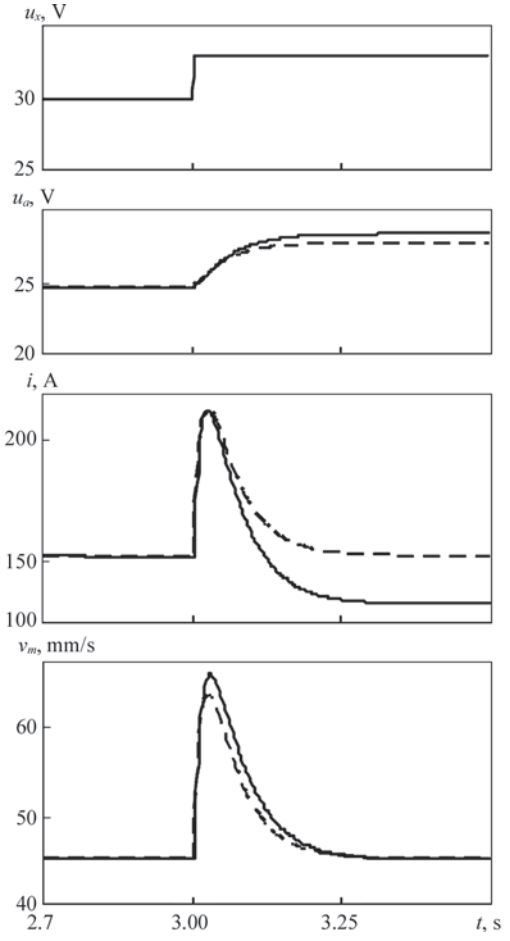

Figure 2. Reaction of welding circuit on disturbance $\Delta u_x = 3$ V

The voltage u_x can be calculated using the equation (6): $u_x = El_\infty + u_0 + R_w i_\infty = 2\cdot4 + 16 + 0.04\cdot150 = 30$ V. Let us determine the electrode feed speed v_e from the equation (7): $v_e = Ki_\infty(u_x - R_+ i_\infty) = 0.012\cdot150\cdot(30 - 0.035\cdot150) \approx 45$ mm/s.

Substituting these values to the expressions (8), (12) and (13)

$$v_e < \frac{0,012\cdot30^2}{4\cdot0.035} \approx 77 \text{ mm/s},$$

$$R_+ - |S_a| = 0.035 - 0.005 - 0.030 > 0,$$

$$L < \frac{0.04}{0.012\cdot2\cdot150} \approx 1\cdot10^{-2} \text{ H},$$

$$\frac{30}{150} > 2\cdot0.035 \rightarrow 0.2 > 0,07$$

we are convinced that the conditions for stability of the arc welding mode selected by us, are performed with a «margin».

As the typical disturbing effects we use the step changes (jumps) of open-circuit voltage Δu_x and the electrode feed speed Δv_e:

$$u_x(t) = \begin{cases} u_x, & t < t_*, \\ u_x + \Delta u_x, & t \ge t_*, \end{cases}$$

$$v_e(t) = \begin{cases} v_e, & t < t_*, \\ v_e + \Delta v_e, & t \ge t_*. \end{cases}$$

Here t_* is the moment of arising relevant effects.

The experiment results are presented in Figures 2 and 3. In these Figures, the solid lines depict the processes described by the specified mathematical model (3), and the dashed lines depict the processes described by the initial model (1).

The diagrams, presented in Figure 2, reflect the reaction of welding circuit on the voltage jump $\Delta u_x = 3$ V. In this figure it is clearly seen, that at the moment of jump (at $t_* = 3$ s) the welding current $i(t)$ and the electrode melting rate v_m are almost instantly increased (the rate of increasing $i(t)$ and $v_m(t)$ is as higher, the lower is the ratio L/R_+). Whereas the arc voltage $u_a(t)$ is increased considerably slower, and as slower, the higher is the electric welding time constant $T_w \approx R_w/[KE\,(u_x - 2R_+ i_\infty]$. The estimated value $T_w \approx 0.085$ s. Then, the current $i(t)$ and rate $v_m(t)$ also decrease slowly. At the end of transition process (after the time $\tau \approx 3T_w$), the variables $i(t)$ and $u_a(t)$ accept new values, moreover, $u_a(t)$ becomes higher and $i(t)$ lower as compared to their values Δu_x before disturbance. Whereas the rate of melting $v_m(t)$ is preset as equal to the electrode feed speed v_e.

The diagrams, presented in Figure 3 reflect the reaction of the same variables $u_a(t)$, $i(t)$ and $v_m(t)$ on the jump of electrode feed speed $\Delta v_e = 5$ mm/s. Here the situation is quite different. First of all, the change of all the variables occurs slowly (at the rate determined by the parameter T_w). At the end of the transition processes the new values of all the variables, including also $v_m(t)$ are established corresponding to the new electrode feed speed $v_e + \Delta v_e$.

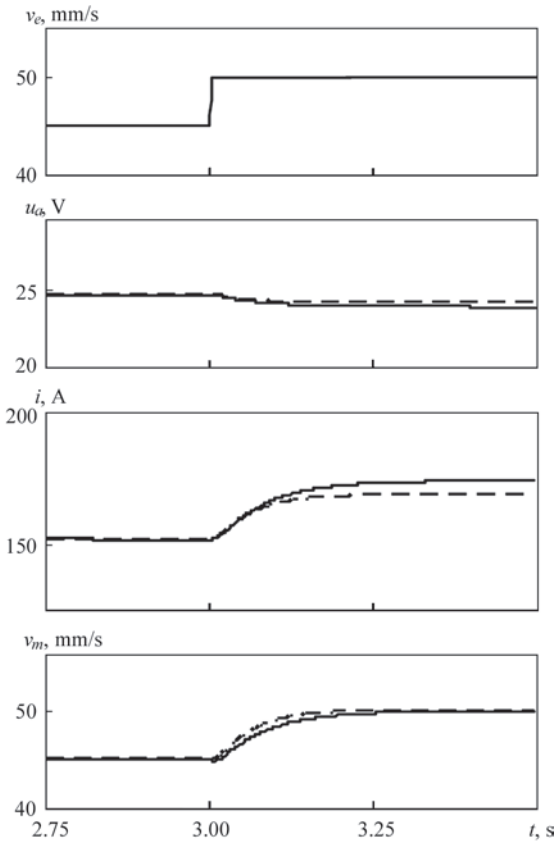

Figure 3. Reaction of welding circuit on disturbance Δv_e = 5 mm/s

A significant difference in the quickness of reaction of welding circuit to disturbances Δu_x and Δv_e is easy to understand, if to follow the propagation paths of these disturbances from the points of their application to the points of measuring variables $i(t)$, $u_a(t)$, $v_m(t)$ (see schematic block diagram in Figure 4). Here it is appropriate to note that this difference is often overlooked, but meanwhile, its taking into account in the development of different methods of pulsed arc welding can turn to be decisive.

By comparing the transition processes depicted in Figures 2 and 3 in solid and dashed lines, we find that the reactions of welding current $i(t)$ one and on the same disturbance Δu_x vary significantly. Namely this fact indicates that in the mathematical model (3), unlike in the model (1), the dependence of the electrode melting rate $v_m(t)$ not only on the actual value of welding current $i(t)$, but also on the actual value of arc voltage $u_a(t)$ is taken into account

In conclusion, we shall note that the results of the simulation experiment are well correlated with the experimental data presented in [7, 14] and demonstrate a fairly good compliance of the mathematical model (3) with the real dynamic processes, running in the welding circuit during arc consumable electrode welding.

Conclusions

1. The mathematical model (3), as compared to the model (1), reflects the essential aspects of dynamic processes more precisely. Consequently, it provides an opportunity to extract also the more precise information about these processes, which is necessary both at the profound study of the considered processes, as well as in solving tasks of adaptive control of these processes.

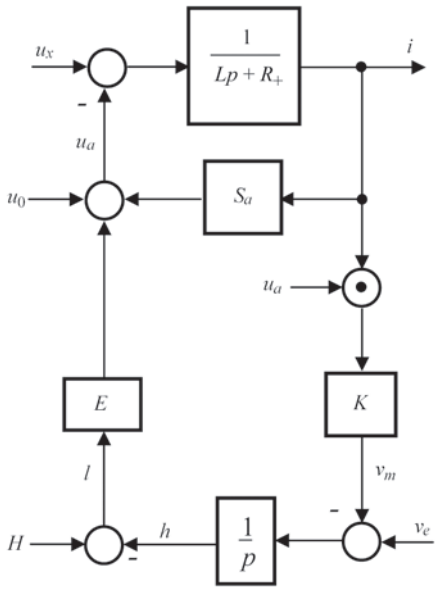

Figure 4. Schematic block diagram of welding circuit

2. The criteria of stability (9), (12) and (13), established on the basis of the mathematical model (3), in addition to the already known criteria, impose certain limits on the parameters of welding arc mode, which is particularly valuable in practice.

1. Pan, J. (2003) *Arc welding control*. Woodhead Publishing Ltd.
2. Tsybulkin, G.A. (2014) *Adaptive control in arc welding*. Kiev: Stal.
3. Sugitani, Y. (2000) Making best use of the arc sensor. *J. of JWS*, 69(**2**), 46–50.
4. Ushio, M. (1991) Sensors in arc welding. *Transact. of JWRI*, 20(**2**), 157–163.
5. Sudnik, V.A., Ivanov, A.V. (1998) Mathematical model of heat source in metal-arc shielding-gas welding. Pt 1. Normal process. *Svarochn. Proizvodstvo*, **9**, 3–9.
6. Korinets, I.F. (1995) Mathematical model of electrode wire melting in arc welding. *Avtomatich. Svarka*, **10**, 39–43.
7. Paton, B.E., Lebedev, V.K. (1966) *Electric equipment for arc and slag welding*. Moscow: Mashinostroenie.
8. Leskov, G.I. (1970) *Electric welding arc*. Moscow: Mashinostroenie.
9. Barbashin, E.A. (1967) *Introduction in stability theory*. Moscow: Nauka.
10. Finkelnburg, V., Mekker, G. (1961) *Electric arcs and thermal plasma*. Moscow: Inostr. Literatura.
11. Nikitin, V.P. (1934) *Electric machines and transformers for arc welding*. Moscow; Leningrad: Energoizdat.
12. Tsybulkin, G.A. (2008) On the influence of small parameters on MIG/MAG welding stability. *The Paton Welding J.*, **8**, 22–25.
13. Dyurgerov, N.G., Sagirov, Kh.N. (2009) Stability of system of arc self-adjustment in mechanized and automatic welding. *Svarochn. Proizvodstvo*, **2**, 13–14.
14. (1986) *Automation of welding processes*. Ed. by V.K. Lebedev et al. Kyiv: Vyshcha Shkola.

Received 06.09.2016

oi.org/10.15407/tpwj2016.12.07

BENCH RESEARCH OF HIGH-FREQUENCY ELECTRIC WELDING OF BIOLOGICAL TISSUES*

G.S. MARINSKY[1], **A.V. CHERNETS**[1], **V.A. TKACHENKO**[1], **D.A. GRABOVSKY**[1], **S.E. PODPRYATOV**[1, 2], **E.G. LOPATKINA**[1], **S.S. PODPRYATOV**[2], **S.V. TKACHENKO**[1] and **S.G. GICHKA**[3]

[1] E.O. Paton Electric Welding Institute, NASU
11 Kazimir Malevich Str., 03680, Kiev, Ukraine. E-mail: office@paton.kiev.ua
[2]Kiev City Center of Electric Welding Surgery
121 Kharkov Highway, 02091, Kiev, Ukraine. E-mail: sepodpryatov@yahoo.com
[3]Kiev City Clinical Hospital #1
121 Kharkov Highway, 02091, Kiev, Ukraine

The paper gives a description of an all-purpose laboratory complex for investigations of biological tissue behaviour at application of high-frequency currents to them under the conditions, corresponding to welding live tissues by different algorithms. This complex allows studying the influence of various design features of the instruments and welding process parameters on the behaviour and structural changes of biological tissues. This equipment is optimal to conduct optimization of new technological procedures, parameters and software, oriented towards specific surgical procedures. Given as an example are the results of experiments on welding the walls of pig stomach and small intestine at pulsed and continuous feeding of 440 kHz voltage under the conditions corresponding to electric welding of biological tissues. 10 Ref., 10 Figures.

Keywords: *high-frequency welding, biological tissues, all-purpose testing bench, welding algorithms, biological tissue structures*

Further development of technology and equipment for high-frequency welding of biological tissues, which is becoming ever wider applied in medical practice [1–7], is inseparably linked to comprehensive studies of the influence of various process parameters on behaviour and structural changes of these tissues, which form the welded joint at high-frequency (HF) current passing through them.

To conduct this research series, the authors developed a specialized complex (Figure 1), which allows studying under laboratory conditions at minimum cost the regularities of HF current passage, depending on biological tissue type, as well as behaviour of various types of tissues at HF current passage through them by the most diverse algorithms. This complex allows studying the influence of various design features and process parameters, such as, for instance, material, shape, dimensions and weight of electrodes, specific pressure at variable energy parameters of the welding process, etc., on behaviour and structural changes of biological tissues. This equipment is optimum for refining new technological procedures, parameters and

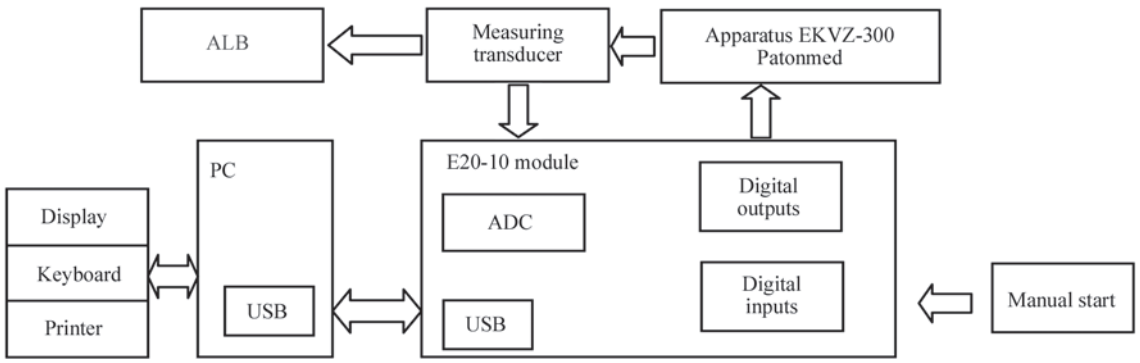

Figure 1. Functional block-diagram of research complex

*The following staff of PWI participated in the work: V.A. Vasilchenko, Yu.Z. Buryak, V.K. Serdyuk, A.M. Aleksandrov, P.G. Semenov.

Figure 2. Appearance of all-purpose laboratory bench at operation with flat and circular electrodes

program products, oriented to specific surgical procedures.

Other research can also be performed, such as studying the impact of HF current on hydration of various types of biological tissues, and nature of tissue heating at HF current passing through them by various algorithms.

The basic element of this complex is an all-purpose laboratory bench (ALB), where the object of study (biological tissue samples) is placed (Figure 2). Bench design allows using electrodes of different configurations at adjustable and preset pressure on the tissue.

A feature of ALB is availability of replaceable electrodes (Figure 3) that provides extreme flexibility at performance of experiments on selection of design, geometry, materials and coatings during development and manufacture of electrosurgical instruments. It is known that pressure on the tissue is one of the most important process parameters in live tissue welding. In this research complex electrode pressure on the tissue, which is adjustable, preset and reproducible from experiment to experiment, is provided by a system of levers and standard loads within 0–160 N.

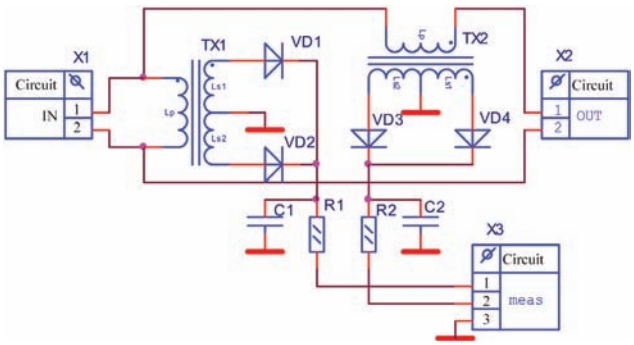

Figure 4. Elementary diagram of measuring transducer

Power source is EKVZ-300 apparatus for live tissue welding, adapted to the conditions of laboratory experiments. Its design allows issuing signals by the most diverse algorithms [8–10]. Current from the power source passes through measuring transducer module (Figure 4) which provides galvanic decoupling of power and measuring circuits. Signals of HF voltage and current are first scaled, rectified and then pass through apparatus filtering by low-frequency filter with specified parameters (the diagram shows a simplified filter). Filter setting depends on apparatus working frequency.

E20-10 module is a module of high-speed analog-digital converter with USB 2.0 interface of L-Card Company. It provides dynamic recording of current and voltage values during HF impact on live tissues. It is possible to set sampling rate and dynamic range of measured analog values, using special programs. An optimum value of the number of measurements per second is selected to achieve a compromise between the validity of the obtained data and data file size. Sampling frequency can be increased at recording of short processes. Equipment allows measurements to be performed with the frequency of up to 5 MHz. A value of about 1000 measurements per second (1 KHz) was used in laboratory studies.

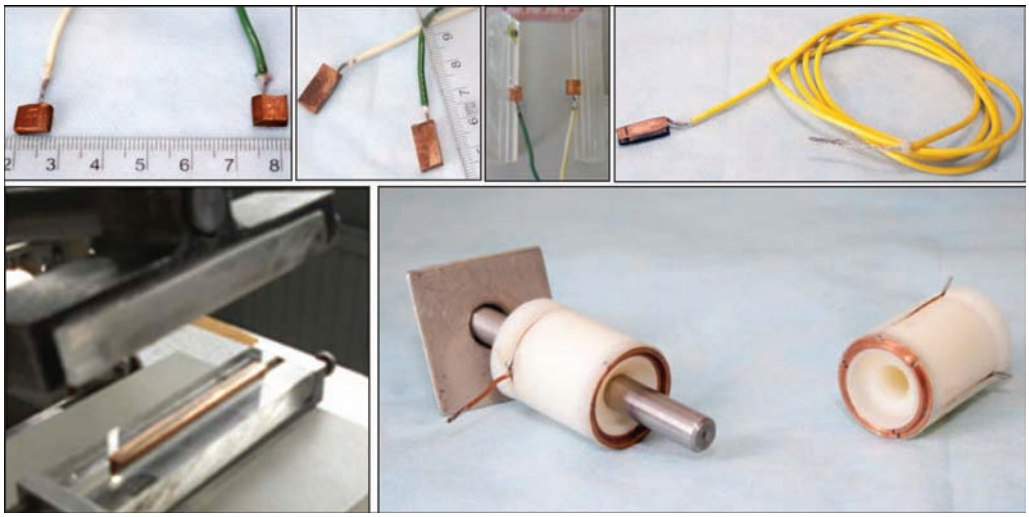

Figure 3. Electrodes of different design applied in ALB

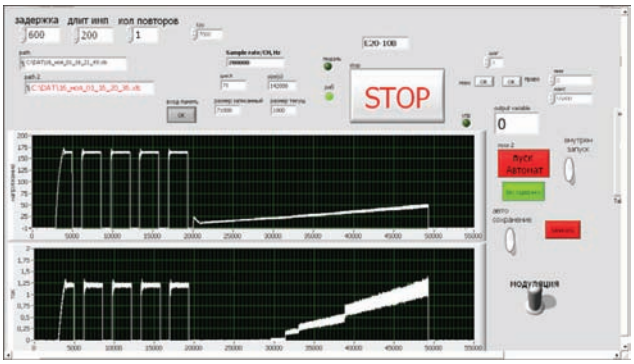

Figure 5. Appearance of the screen of recording and control program

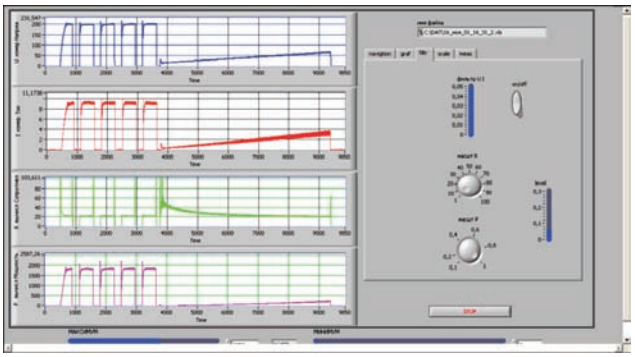

Figure 6. Appearance of the screen of data processing program

Digital output module is installed in one case with ADC (E20-10), but functionally, it has a different purpose. This module is used to form service signals of coagulator control, signals to source switching relays, etc. Digital output module allows, if required, starting the process in the manual mode. The device (ADC E20-10) is connected to the computer via USB cable and uses standard Windows drivers.

Electrical parameters of the process were recorded by an analog-digital converter L-Card E20-10, personal computer and laboratory oscillograph Tektronix TDS 3014C. Software consists of two independent parts: program of recording and program of processing the obtained data. Programs are written in graphic programming language LabVIEW. It allows using dataflow programming, in which the execution sequence is determined by data flow. The program is based on virtual instruments supplied by L-Card Company, together with the library for ADC E20-10 and similar modules. Recording program allows maximum automation of research process, thus reducing the influence of the human factor on the results. The program, in particular, fulfills service functions. Recording module uses a special program to form a time delay before the experiment start. Controls and indicators are located on virtual instrument front panel (Figure 5). There is the capability of assigning a large number of parameters. The following pulse parameters are adjusted: pulse duration, pause duration, number of repeats, there is the capability of additionally extending recording time, setting recording mode, adjusting parameters of preliminary visualization of the process. In some cases, external start is required (from a pedal or a button on the instrument). In the automatic mode there is the capability of activating the countdown to experiment start with sound signal and time display. During recoding the data are stored in the buffer. This buffer is used at process visualization. Here, the parameters of data displaying can be assigned (Figure 6). Software module of results processing provides the required graphs or tables for the required values with their storage in the form of .jpg and .xls type files. There is the capability of selection of the required scale and performance of program processing of the signal.

This complex was used to conduct more than 2500 studies on tissues of different type, in which optimum parameters and algorithms of operation in manual and automatic modes were determined, temperature of electrodes and tissue in the zone of electric current impact and variations of thickness of tissue with different structure at all the process stages were recorded. Results of these studies were further on used in preparation of recommendations and performance of actual surgical operations with application of the technology of live tissue welding both under laboratory and clinical conditions.

Results of experiments on welding the walls of pig stomach and small intestine are given below as an illustration. Influence of pulsed and continuous feed of voltage under the conditions corresponding to electric welding of biological tissues was studied. During the experiments, samples of the above tissues were placed between flat copper electrodes, compressed with specific pressure preset in the range from 2 up to 6 N/mm^2, and specific voltage in the range of 60–180 V at current frequency of 440 kHz and pulse duration of 0.1–0.5 s was applied. After completion of experiments, tissue samples were sent to the morphological studies.

Conducted experiments showed that the impact of a single pulse of set duration and voltage value causes minor denaturation of collagen fibers subserously located on stomach walls, as well as partial damage of gastric mucosa. This is accompanied by development of slight swelling and expansion of connective septum of stomach wall muscle membrane (staining using hematoxylin-eosin was applied in all the cases) (Figure 7, *a*).

Coagulative necrosis of individual smooth muscle cells and fibroblasts was found in the muscle membrane, but contours of cells and their nuclei remained undamaged (Figure 7, *b*).

Impact of two pulses of voltage, the same as in the first experiment, caused not partial, but complete destruction of the mucosa. Not just individual, but all the collagen and smooth muscular fibers in the point of electrode application also changed by the type of coagulative necrosis. Deformation of muscular fiber bundles across electrode plane and destruction of smooth muscular fibers was also noted in some points (Figure 8, *a*).

After application of nine voltage pulses formation of tight joints of collagen and smooth muscular fibers, having cell nuclei contours, was noted (Figure 8, *b*).

After application of twenty voltage pulses a tight joint of stomach walls was formed as a result of coagulative necrosis of bundles of smooth muscular fibers and collagen fibers (Figure 8, *c*). Contours of cell nuclei are revealed in part of bundles smooth muscular fibers. In the thickness of the tissue contours of cell nuclei are found between the remnants of smooth muscular fibers. At this stage of electric welding the seam does not yet become uniform.

Further increase of the number of pulses up to 35 showed that in this case already a uniform, strong, thin electric welding seam was produced, which was formed by collagen and smooth muscular fibers (Figure 8, *d*).

Investigations showed the possibility of producing a uniform electric welding seam under the experimental conditions after application of twenty voltage pulses and further constant application of HF voltage for a fixed time. Here, the bundles of smooth muscular fibers in the seam are completely destroyed and coalesce with coagulated collagen fibers (Figure 9). Morphological signs of peripheral impact of electric welding current passage cover not more than 1 mm distance from the boundary of electrode application under experimental conditions (Figure 10).

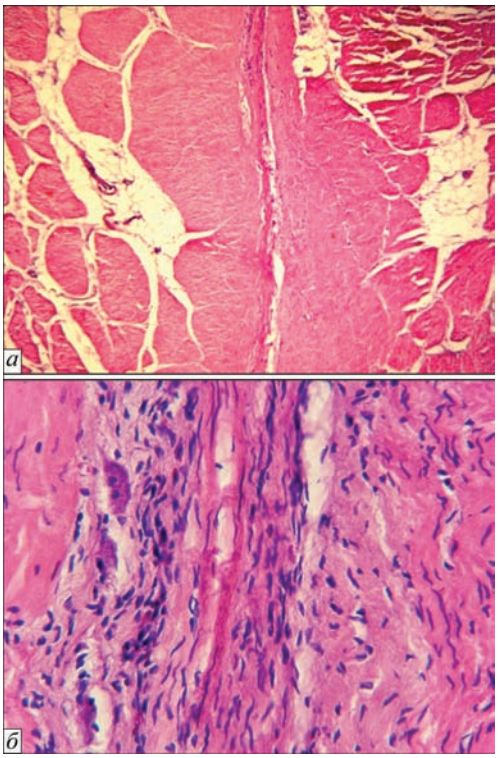

Figure 7. Structure of muscle membrane of stomach walls in the zone of application of isolated HF pulse: *a* — ×100; *b* — ×400

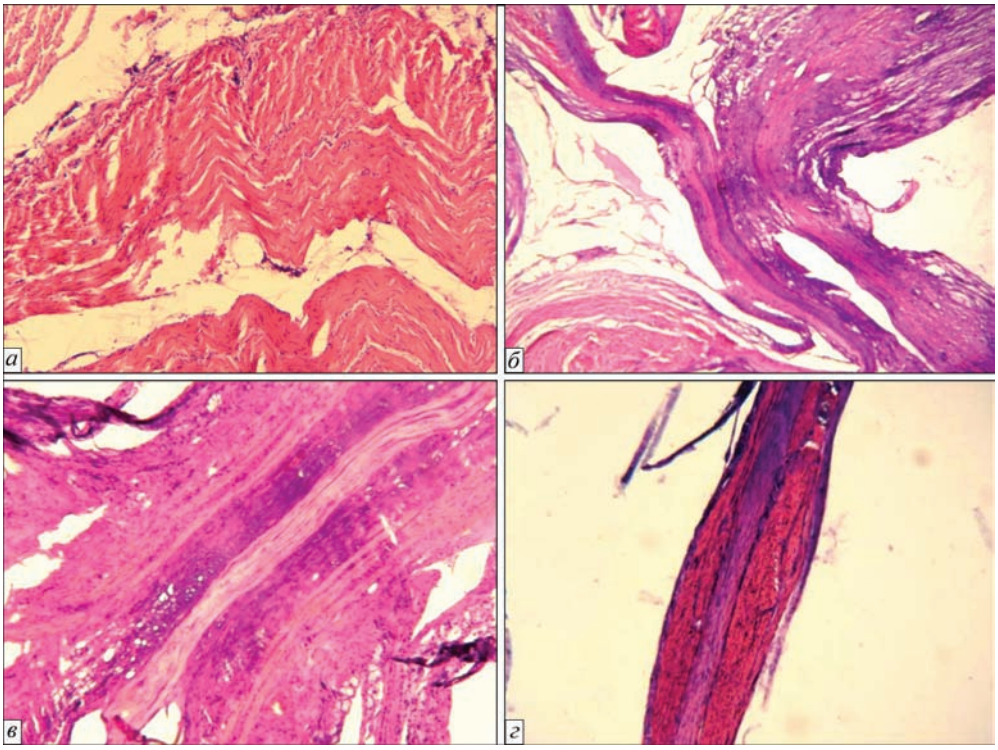

Figure 8. Structure of muscle membrane of stomach walls in the zone of application of two (*a*), nine (*b*); twenty (*c*); thirty five (*d*) HF pulses: *a*, *b* — ×100; *c* — ×400; *d* — ×40

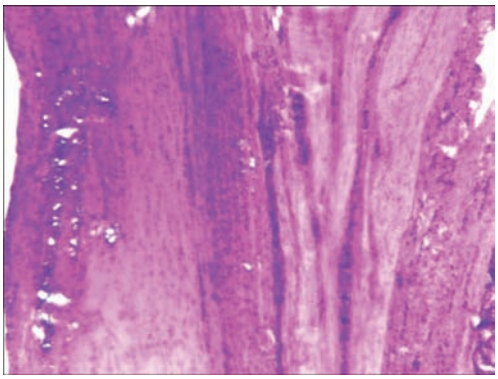

Figure 9. Uniform electric welding seam of two stomach walls after the impact of twenty HF pulses with subsequent application of HF voltage (×400)

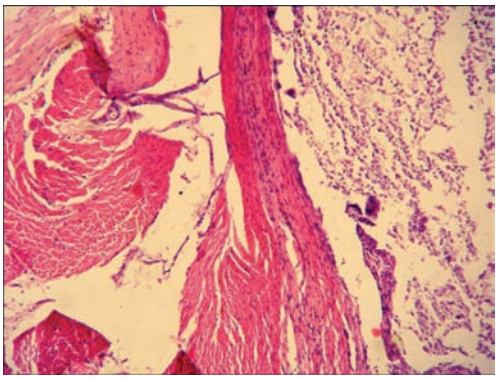

Figure 10. Indications of peripheral impact of electric welding voltage (×100)

Conducted studies confirmed that under the impact of a series of HF voltage pulses applied by a certain algorithm, a tight joint of biological tissues is formed – their electric welding seam. Necrosis areas are absent inside the seam. Such a seam is a new structure, which develops under the impact of electric current under optimum conditions that is exactly the purpose of electric welding.

Conclusions

1. Proposed all-purpose research complex allows quickly performing under laboratory conditions at minimum cost, studies of behaviour of biological tissues of various types under the impact of HF current on them at all the stages of the welding process.

2. Described research complex allows studying the influence of such design and process parameters, as electrode design and material, their compression forces, algorithms and modes of voltage application to the tissue on structural changes and process of welding of biological tissues. This complex allows determination of optimum modes and algorithms of welding various tissues both in the manual and automatic modes.

3. Results of performed studies can be recommended as basic ones at selection of process parameters during performance of surgical operations with application of the technology of live tissue welding both under laboratory and clinical conditions.

1. (2009) *Tissue-saving high-frequency electric welding surgery.* In: Atlas. Ed. by B.E. Paton and O.I. Ivanova. Kiev: IAW.
2. (2013) Theory. Practice. Prospects. In: *Proc. of 8th Sci.-Pract. Conf. on Welding and Heat Treatment of Live Tissues*. Ed. by G.S. Marinsky. Kiev: PWI.
3. (2014) Theory. Practice. Prospects. In: *Proc. of 9th Sci.-Pract. Conf. on Welding and Heat Treatment of Live Tissues*. Ed. by G.S. Marinsky. Kiev: PWI.
4. (2015) Theory. Practice. Prospects. In: *Proc. of 10th Sci.-Pract. Conf. on Welding and Heat Treatment of Live Tissues*. Ed. by G.S. Marinsky. Kiev: PWI.
5. Bondar, G.V. (2011) Widening of indications for application of electric welding complex of soft tissues in oncosurgery. In: *Proc. of 6th Int. Seminar on Welding of Soft Live Tissues. State-of-the-Art and Prospects of Development* (Kiev, Ukraine, 2–3 December 2011). Kiev: PWI.
6. Makarov, A.V., Getman, V.G., Myasnikov, D.V. et al. (2006) Welding of pulmonary tissue – as a method of non-resection intervention because of spontaneous pneumothorax. *Klinichna Khirurgiya*, **7**, 40–42.
7. Podpryatov, S.E., Gychka, S.G., Podpryatov, S.S. et al. (2008) Healing of interintestinal anastomoses and closing arteries by electric welding. *Ibid*., **11/12**, 64.
8. Paton, B.E., Marinsky, G.S., Podpryatov, S.E. et al. *High-frequency welding electrocoagulator EKVZ-300*. Pat. 72577U Ukraine. Int. Cl. A 61 B 18/12. Fil. 24.01.2012. Publ. 27.08.2012.
9. Paton, B.E., Krivtsun, I.V., Marinsky, G.E. et al. (2013) Welding, cutting and heat treatment of live tissues. *The Paton Welding J*., **10/11**, 142–153.
10. Paton, B.E., Tkachenko, V.A., Marinsky, G.S. et al. *Method of joining of biological human and animal tissues using high-frequency current*. Pat. 106513 Ukraine. Fil. 26.07.2012. Publ. 10.09.2014.

Received 03.11.2016

doi.org/10.15407/tpwj2016.12.08

EVALUATION OF STATIC STRENGTH OF WELDED DISK OF SMOKE EXHAUSTER IMPELLER

A.V. MOLTASOV[1], **P.N. TKACH**[1], **A.Ya. GOGOLEV**[2], **A.A. AVDYUSHKIN**[2] and **S.I. MOTRUNICH**[1]
[1]E.O. Paton Electric Welding Institute, NASU
11 Kazimir Malevich Str., 03680, Kiev, Ukraine. E-mail: office@paton.kiev.ua
[2]«Soyuzenergomash» LLC
8 Gavanskaya Str., 49127, Dnepr, Ukraine. E-mail:recept_prmz@souzenergo.com

A checking calculation of static strength was carried out for welded structure of a disk of smoke exhauster impeller under service loading. The impeller consists of the disk and welded to it cylinder shell with twenty blades uniformly located along its perimeter. Stressed state, being realized in the disk during operation, is caused by effect of inertia appearing as a result of impeller rotation with a constant angular velocity. The stress components were determined by solving a boundary problem of quasi-static elasticity theory. Setting of the boundary conditions required to determine stress on a disk outer profile, promoted by centrifugal forces, developed by blades. A corresponding formula was proposed for this taking into account mass-centering characteristics of the blade. It is determined that the maximum radial stress of the stamped disks of 48 and 44 mm thickness acts in a hub and makes 28 and 29.5 MPa, respectively. The maximum circumferential stresses at that are more than two times lower than the radial ones. The main difference between welded and stamped disks is a presence of stress concentrators, caused by geometry inhomogeneity of structure in zone of welded joints. Stressed state in the zone of stress concentration was described using an engineering method based on broken-sections hypothesis. The results of calculations of a stress concentration factor by proposed method well agree with the results, received by a finite element method. Taking into account stress concentration in the welded disks of 48 and 44 mm thickness the maximum radial stress acts in the place of ring to shell conjugation and makes 35.8 and 37.5 MPa, respectively. These values exceed stresses in the hub for corresponding stamped disks more than by 20 %, however it is 5 times lower than the yield strength of disk material. It can be state due to this that static strength is provided for both studied welded structures of the disk. 14 Ref., 12 Figures.

Keywords: *smoke exhauster impeller, welded disk, service loads, checking calculation, stressed state, stress concentration, broken-sections hypothesis*

Ensuring a continuous operation of heat power plants (HPP) is an important strategic direction for Ukrainian power engineering under modern economic conditions. Stable operation can be provided only under timely planned preventive repairs (PPR), which include replacement of the parts and assemblies of power installations. At that it is a significant dependence of domestic enterprises on the foreign components for these installations, to which the impellers of HPP smoke exhausters are referred. In order to reduce import dependence and preserve PPR terms it is necessary to develop domestic design being as good as imported on strength, technological effectiveness and service properties. At that it should be reasonable from economic point of view. The imported analogue applies an impeller design with stamped disks of 1940 mm diameter. Manufacture of the stamps of such a diameter is not reasonable from economic point of view. Therefore, «Soyuzenergomash» LLC developed the variants of disk welded structure, two of which (Figure 1) were delivered to the E.O. Paton Electric Welding Institute for evaluation of their working capacity. Grounding one of the variants requires determination of stress-strain state (SSS) of the disks taking into account stress concentration caused by their geometry in welds zone.

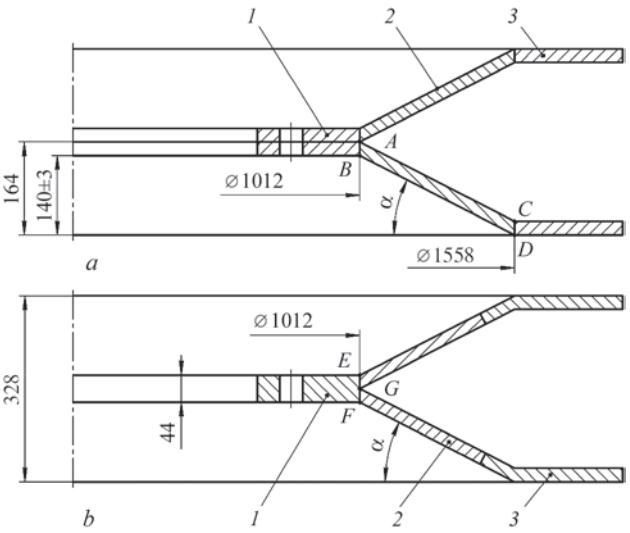

Figure 1. The first (*a*) and second (*b*) variants of performance of welded disk of smoke exhauster impeller: *1* — ring; *2* — shell; *3* — edge

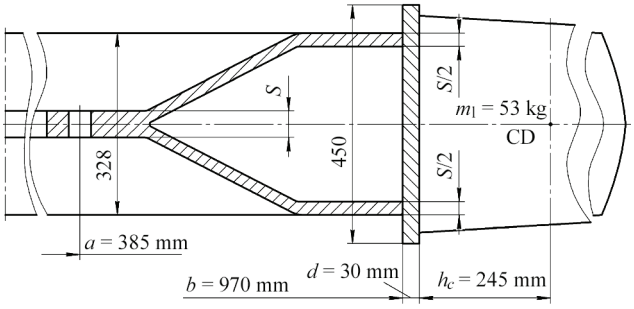

Figure 2. Impeller calculation scheme considering blades

At *a* distance the impeller disk is rigidly fixed by means of bolted joint and at distance *b* it contains a welded cylinder shell with twenty blades, uniformly located along its perimeter (Figure 2).

During operation the smoke exhauster impeller rotates at a constant angular velocity

$$\omega = \frac{\pi n}{30}, \tag{1}$$

where *n* is the impeller rotation frequency, rev/min.

Rotation in a blade root section promotes for appearance of centrifugal force [1]

$$P_c = mr_c\omega^2, \tag{2}$$

where *m* is the blade mass; r_c is the distance from rotation axis to blade mass center, determined by formula

$$r_c = b + d + h_c, \tag{3}$$

where *d* is the thickness of cylinder shell; h_c is the blade mass center, which for truncated pyramid (Figure 3) is determined by formula [2]

$$h_c = \frac{H}{4}\frac{F_1 + 2\sqrt{F_1F_2} + 3F_2}{F_1 + \sqrt{F_1F_2} + F_2}. \tag{4}$$

If it is assumed that the centrifugal forces, developed by the blades, are uniformly distributed over the impeller surface (Figure 4), then stress on its outer radius considering (2) can be determined from formula

$$p_c = \frac{zmr_c\omega^2}{2\pi bs}, \tag{5}$$

where *z* is the number of blades; *s* is the disk thickness.

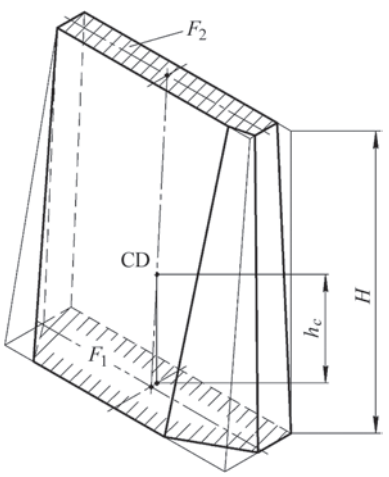

Figure 3. Blade model for mass center determination

Regardless the developed geometry, thickness of the disk *s* in radial section is constant along the radius. Due to small *s*/*b* relationship in the considered case a plane stressed state is formed in the impeller and stresses can be considered constant on thickness [3].

This problem can be solved as a quasi-static problem of elasticity theory, if according to d'Alembert's principle the impeller is stopped and corresponding volume forces are applied to it [4].

Solution of the problem about rotating disks is well known in scientific-and-technical literature [5, 6], therefore, without mentioning mathematical computations, we bring an expression for radial movement *u* as well as radial σ_r and circumferential σ_θ stresses, appearing in the disk.

$$u = \frac{1-\mu^2}{E}\left(C_1 r + C_2\frac{1}{r} - \frac{\rho\omega^2}{8}r^3\right), \tag{6}$$

$$\begin{cases} \sigma_r = (1+\mu)C_1 - (1-\mu)C_2\dfrac{1}{r^2} - (3+\mu)\dfrac{\rho\omega^2}{8}r^2; \\ \sigma_\theta = (1+\mu)C_1 + (1-\mu)C_2\dfrac{1}{r^2} - (1+3\mu)\dfrac{\rho\omega^2}{8}r^2, \end{cases} \tag{7}$$

where μ is the coefficient of lateral deformation; ρ is the density of disk and blade material; C_1, C_2 are the constants of integration, determined from boundary conditions on the inner and outer edge.

Since the impeller is rigidly fixed on inner radius and no movements there are possible $u = 0$ at $r = a$. Radial stresses p_c, developed by blade centrifugal forces, act on outer radius, therefore, $\sigma_r = p_c$ at $r = b$. A system of equations is received by inserting the boundary conditions in equation (6) and the first from equations (7). Its solution provides us with

$$C_1 = \frac{p_c b^2 + \frac{\rho\omega^2}{8}\left[(3+\mu)b^4 + (1-\mu)a^4\right]}{(1+\mu)b^2 + (1-\mu)a^2};$$

$$C_2 = -a^2b^2\frac{p_c + \frac{\rho\omega^2}{8}\left[(3+\mu)b^2 - (1+\mu)a^2\right]}{(1+\mu)b^2 + (1-\mu)a^2}.$$

Knowing an area of larger and smaller blade roots F_1 = 16440 mm^2 and F_2 = 6333 mm^2, respectively, and its height H = 578 mm, let's determining using formula (4) a distance from the root section to blade mass center h_c = 245 mm.

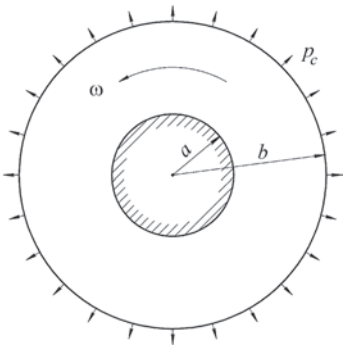

Figure 4. Scheme of loading of smoke exhauster impeller

Considering that outer diameter of the disk b = 970 mm, and thickness of the cylinder shell d = 30 mm, it is possible to determine the distance from rotation axis to blade mass center r_c = 1245 mm.

At set number of blades z = 20 and rotation velocity of the disk n = 500 rev/min, assuming that a calculated mass of one blade is m = 53 kg and after preliminary calculation by formula (1) ω = 52.3 rad/s, let's determine using formula (5) a value of radial stress, acting on disk outer profile:

- for the first variant (at s = 48 mm) p_c = 13.6 MPa;
- for the second variant (at s = 44 mm) p_c = 14.8 MPa.

The curves of radial and circumferential stresses along the radius (Figure 5) are plotted by formula (7) knowing disk inner diameter a = 385 mm, and taking material density for steel disk ρ = 7800 kg/m^3 and coefficient of lateral deformation μ = 0.3.

It follows from stress distribution that the largest stress acts in radial direction in the place of impeller to hub fixing and makes for the first and second variants 28 and 29.5 MPa, respectively. At that, the value of maximum radial stress in both cases is more than two times exceeds the value of maximum circumferential stress.

Since residual welding stresses were removed by means of respective heat treatment, the most significant difference of the disk welded structure from stamped variant is appearance in the weld zones of stress concentration, promoted by transfer from one part being joined to another, and value of acting radial stress will be determined by formula

$$\sigma_r = \alpha_\sigma \sigma_r^{nom}, \tag{8}$$

where σ_r^{nom} is the radial stress without concentration, determined by first formula (7); α_σ is the stress concentration factor (SCF).

For the first variant let's consider concentration of stresses in a zone of joining shell *2* to ring *1* (points *A* and *B*) and in zone of joining shell *2* to edge *3* (points *C* and *D*) (see Figure 1, *a*). For the second variant the concentration should be taken into account only for a weld joining shell *2* to ring *1* (points *E* and *F*) (see Figure 1, *b*), since weld reinforcement, joining shell *2* to edge *3*, is removed. The weld zone (point *G*) provides for smooth transfer between structure elements being joined (see Figure 1, *b*), therefore, it can be taken out from consideration, since stress concentration factor is rapidly reduced with curvature decrease [7].

An engineering method, based on broken sections hypothesis [8, 9], is used for investigation of stressed state in the zone of stress concentration. It guarantees high accuracy for different types of welded joints at various variants of loading [10, 11].

Pass a plane-broken section *ABCDGH* (Figure 6). The end areas of section *AB* and *GH* are normal to profile, length of these areas a_0 characterizes the depth of concentrator action

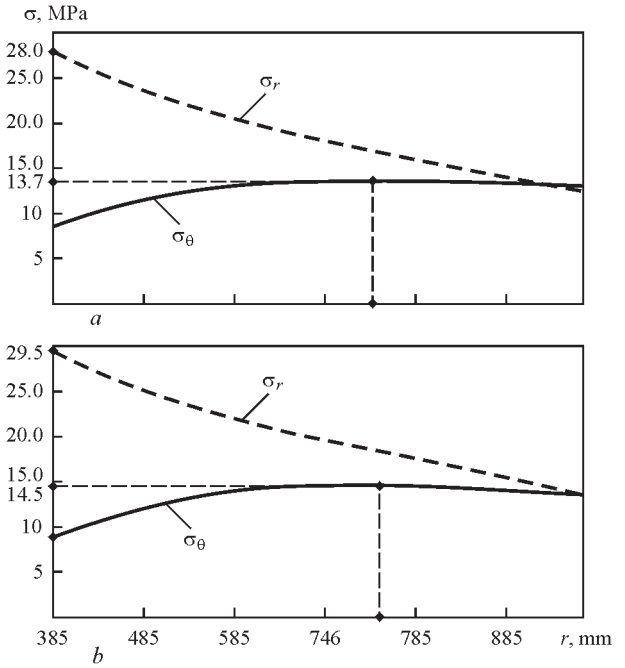

Figure 5. Distribution of radial σ_r and circumferential σ_θ stresses on radial coordinate in disk of the first (*a*) and second (*b*) variants

$$a_0 = 2\sqrt{tR}, \tag{9}$$

where t is the height of curving.

The middle areas of section *BC* and *DG*, which are regulated by hypothesis of plane sections, are passed perpendicular to applied load.

Pass the second plane-broken-section $A_1B_1C_1D_1G_1H_1$ through point A_1, located at small distance from point *A*. It is assumed by convention that $A_1B_1C_1D_1G_1H_1$ section remains stable in deformation, and the section *ABCDGH* takes a position marked by dashed line. At that *KF* fiber, situated at distance u from the axis and located normal to area *AB*, receives *KN* elongation.

Relative elongation of *KF* fiber

$$\varepsilon_u = \frac{KN}{KF} = \frac{KL\cos\beta}{(R + s/2 - u)\Delta\beta}.$$

Normal stress in this fiber according to Hooke's law

$$\sigma_u = \frac{KL\cos\beta}{(R + s/2 - u)\Delta\beta} E. \tag{10}$$

Now let's consider fiber *QS*, situated at a distance v from the axis and located normal to *BC* area. As a result of deformation this fiber will have *ST* elongation and normal stress will appear in it

$$\sigma = \frac{ST}{QS} E = \frac{KL}{(R + a)\Delta\beta\cos\beta} E \tag{11}$$

Equilibrium condition is as follows

$$ps = 2\int_{s/2-a_0}^{s/2} \sigma_u du\cos\beta + 2\int_{y_C}^{y_B} \sigma_v dv, \tag{12}$$

where

$$y_B = \frac{s}{2} + R(1 - \cos\beta) - a_0\cos\beta;$$

$$y_C = \left(\frac{s}{2} + R\right)(1 - \cos\beta).$$

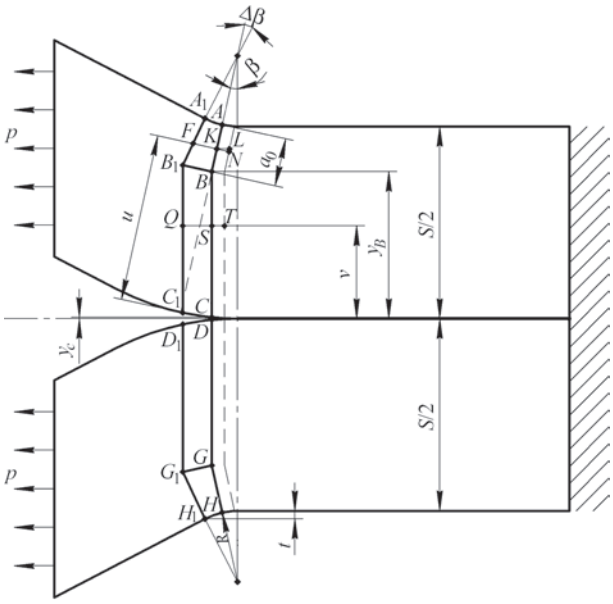

Figure 6. Construction of plane-broken sections in stress concentration zone

The next is received after integration by inserting σ_u from (10) and σ_v from (11) in the equilibrium condition (12)

$$\frac{KLE}{\Delta\beta} = \frac{ps}{2k}, \tag{13}$$

where k is the geometry characteristic of section

$$k = \ln\left(1+\frac{a_0}{R}\right)\cos^2\beta + \frac{s/2-a_0}{R+a_0}.$$

Inserting expression (13) in the dependencies (10) and (11) the expressions for stresses in areas *AB* and *GH* are obtained

$$\sigma_u = \frac{ps\cos\beta}{2k(R+s/2-u)} \tag{14}$$

and in areas *BC* and *DG*

$$\sigma_v = \frac{ps}{2k(R+a_0)\cos\beta} \tag{15}$$

respectively.

Analysis of expressions (14) and (15) shows that stress is constant on thickness in areas *BC* and *DG* and varies only from section to section. In areas *AB* and *GH* stress is changed on hyperbolic law and reaches the maximum on a surface in points *A* and *H*, i.e. at u = s/2

$$\sigma_u^A = \frac{ps\cos\beta}{2kR},$$

respectively *SCF* is determined by formula

$$\alpha_\sigma = \frac{\sigma_u^A}{p} = \frac{s\cos\beta}{2R\left[\ln\left(1+\frac{a_0}{R}\right)\cos^2\beta + \frac{s/2-a_0}{R+a_0}\right]}. \tag{16}$$

In calculation of *SCF* for the second variant of impeller design in (12) it is necessary to assume $y_C = 0$, then

$$\alpha_\sigma = \frac{s\cos\beta}{2R\left[\ln\left(1+\frac{a_0}{R}\right)\cos^2\beta + \frac{s/2+R(1-\cos\beta)-a_0\cos\beta}{(R+a_0)\cos\beta}\right]}. \tag{17}$$

Investigation of functions (16) and (17) on procedure [12] showed that α_σ monotonously decrease at rise of β in the interval

$$\beta \in [0;\alpha],$$

where

$$\alpha = \arccos\left(1-\frac{t}{R}\right), \tag{18}$$

therefore, it can be stated, that for two variants the *SCF* structure has the maximum value at $\beta = 0$.

As it was mentioned earlier the main geometry parameter affecting *SCF* value is a curvature, therefore it is necessary to determine conjugation radius R in the weld zones (points *B* and *C* for the first variant and points *E* and *F* for the second).

Butt weld S25 is used in assembly of the disk on variant I in accordance with GOST 5264–80, which provides for double groove preparation with γ = 25±2° and gap δ = 0–3 mm at 24 mm metal thickness. Shell angle in relation to rotation plane can be determined from relationship of sizes, marked on drawing (Figure 1, *a*). Since one of the sizes is set with tolerance, then angle α will be varied in 26.65–27.65° range. It is expected that conjugation radius R will be minimum , i.e. corresponding to the largest SCF value at maximum values of angle α. Since in practice the limiting values of sizes are unlikely, α close to the maximum angle 27.5° is taken.

Since the weld will be made at inclined relative position of the parts (Figure 7, *a*), then reinforcement removal with smooth transfer can be performed on conjugation radiuses in points *B* and *C*. Actual parameters of groove preparation will effect their value, moreover the smallest conjugation radiuses are received in choosing the dimensions on low limiting deviation γ = 23°, δ = 0.

The conjugation radiuses r_B and r_C can be determined from known relationship between the radius and chord at known central angle [2]

$$r_{B(C)} = \frac{a_{B(C)}}{2\sin\frac{\alpha}{2}} = \frac{S}{2}\left(\mathrm{tg}\gamma\mathrm{ctg}\frac{\alpha}{2}-1\right). \tag{19}$$

It is obvious that $r_{B(C)}(\alpha)$ monotonously decreases in α = 26.65–27.65° interval, that proves the necessity of selection of the largest radius α, since at that the received radiuses of conjugation r_B and r_C are minimum.

Two shells are welded up to a ring using non-standard weld at α = 27±1° angle in disk assembly on variant II.

A calculation of stressed state of the structure second variant is also reasonably to carry out for the

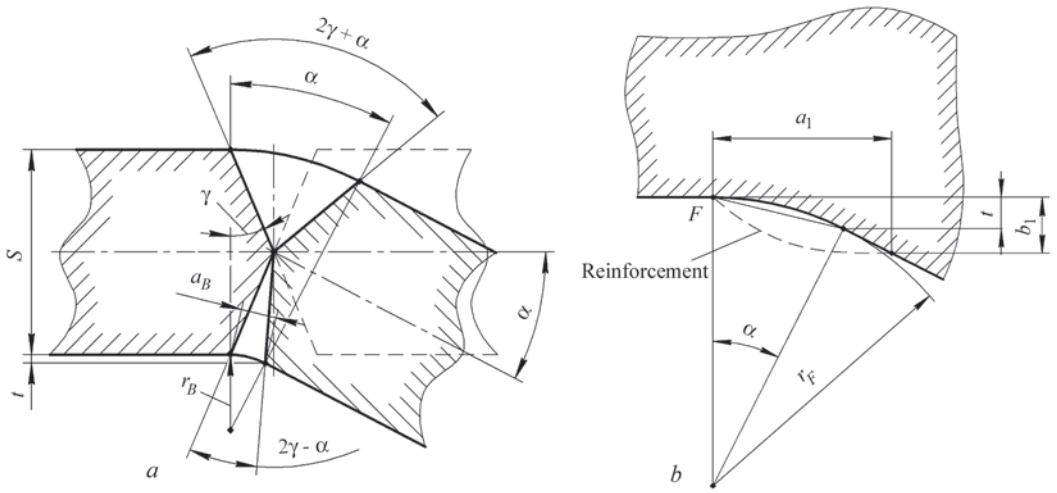

Figure 7. Determination of conjugation radiuses of surfaces of parts for the first (*a*) and second (*b*) variants

worst combination of tolerances. For this it is necessary to obtain the dependence of radiuses of conjugation r_E and r_F on the main parameters *a* and *b* of the weld (Figure 7, *b*).

$$r_E = r_F = \frac{a_1 \operatorname{tg}\alpha - b_1}{\sin\alpha \operatorname{tg}\alpha - 2\sin^2\frac{\alpha}{2}}. \qquad (20)$$

Analysis of dependence (18) shows that in α = 26–28° range the minimum radius corresponds to the minimum value of a_1 and the maximum value of b_1. $r_{E(F)}(\alpha)$ function monotonously rises in the researched interval, therefore, the minimum radiuses r_E and r_F correspond to the minimum value of α.

Inserting in formula (19) assumed values γ = 23° and α = 27.5°, let's determine $r_B = r_C$ = 8.82 mm, and assuming $R = r_B = r_C$ in formula (18), *t* =1 mm is determined.

Inserting in formula (20) a_1 = 14 mm, b_1 = 6 mm and α= 26° values, the smallest conjugation radiuses $r_E = r_F$ = 7.36 mm are received and, assuming $R = r_E = r_F$ in formula (18), *t* =0.74 mm is determined.

Inserting in formula (9) $R = r_B = r_C$ = 8.82 mm and *t* =1 mm, let's determine a_0 = 5.94 mm, then according to formula (16) at β=0° RCF takes α_σ = 1.56 value, and at β = α = 27.5° RCF takes its minimum value α_σ=1.44.

Inserting in formula (9) $R = r_B = r_C$ = 7.36 mm and *t* =0.74 mm, let's determine a_0 = 4.67 mm, then according to formula (17) at β = 0° SCF takes α_σ=1.55 value, and at β = α= 26° SCF takes its minimum value α_σ=1.25.

Computer modelling of stressed state in the zones of stress concentration (Figures 8 and 9) was carried out for validation of the obtained formulae (16) and (17).

Elastic axial tension problem was solved in simulation for steel with physical-chemical properties of steel 20 at 200 °C: modulus of normal elasticity $E = 1.9\times10^5$ MPa, Poisson's coefficient μ = 0.3. The problem was solved for two-dimensional model, representing itself an element of impeller sector of unit thickness. A limitation in form of rigid fixing was applied from hub side, and unit load, distributed on the edge, (Figure 8) was from disk side.

It was determined based on results of the numerical calculation (Figure 9) that the maximum values of SCF for the first and second variants made 1.539 and 1.533, respectively that well agree with the results received using mentioned above calculation method.

From constructions (Figure 10, *a*) it is determined that β = 0° value corresponds to *r* = 500.91 mm and *r* = 784.09 mm values, and β = α = 27.5° corresponds to *r* = 507.02 mm and *r* = 777.98 mm values, thus we can show a curve of radial stresses in the disk of the first variant taking into account stress concentration (Figure 11, *a*).

From constructions (Figure 10, *b*) it is determined that β = 0° value corresponds to *r* = 502.78 mm value, and β = α = 26° corresponds to *r* = 506 mm value,

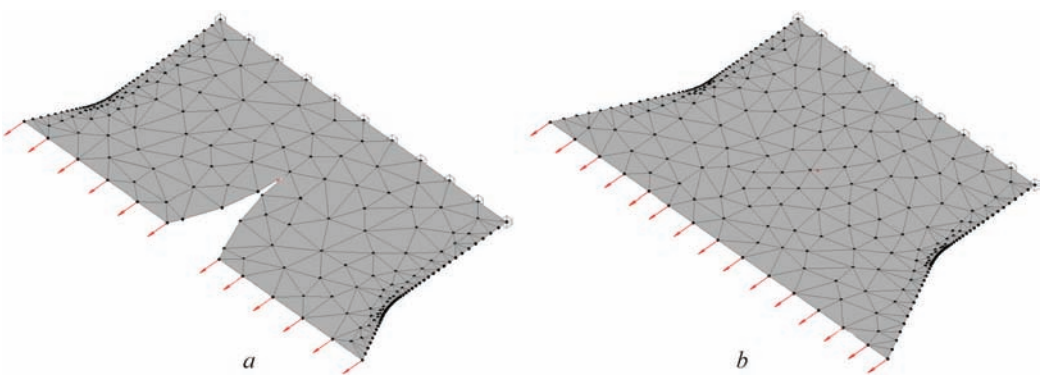

Figure 8. Conditions of loading, fixing and finite element breaking up of fragments of disks of the first (*a*) and second (*b*) variants

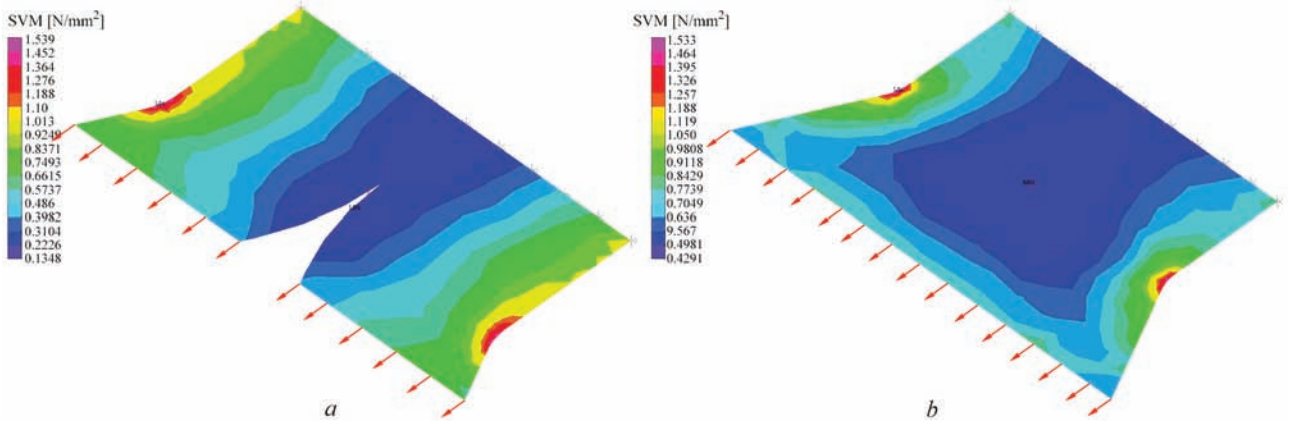

Figure 9. Stress fields in concentration zones of disks of the first (*a*) and second (*b*) variants at axial tension by unit load

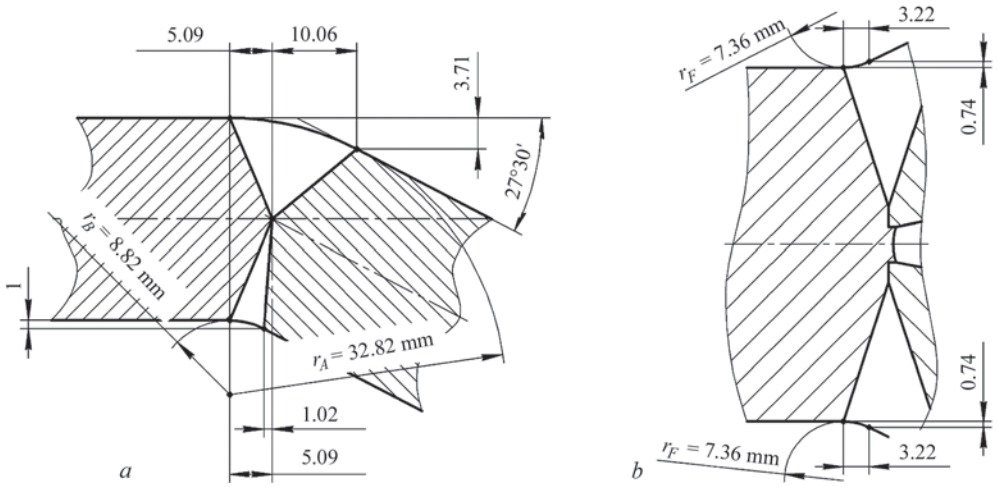

Figure 10. Dimensions in conjugation zone for the first (*a*) and second (*b*) variants of performance of welded disk of smoke exhauster impeller

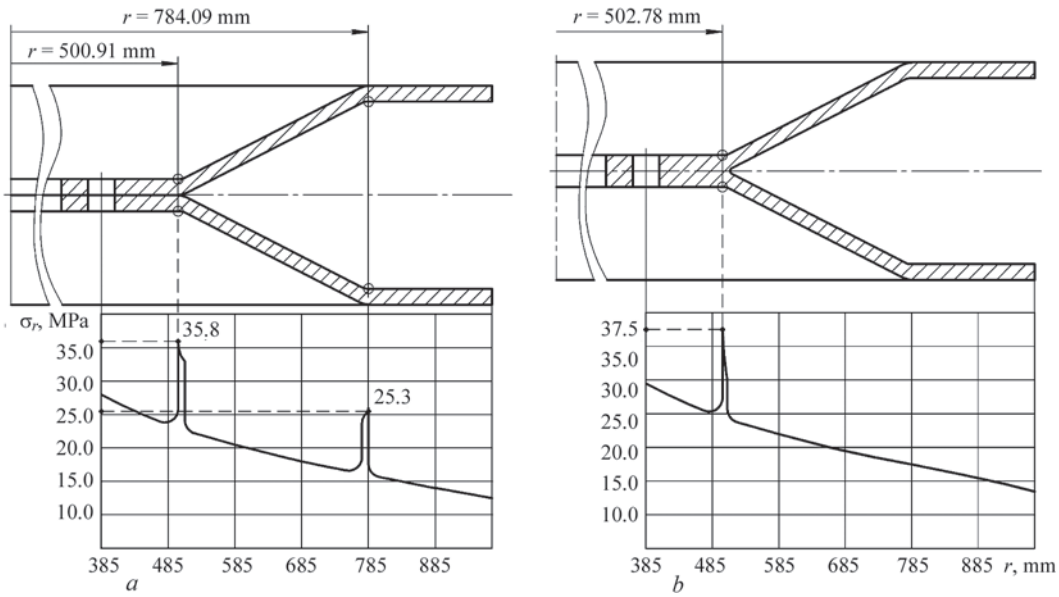

Figure 11. Distribution of radial stresses in disk of the first (*a*) and second (*b*) variants considering stress concentration

thus we can show a curve of radial stresses in the disk of the second variant taking into account stress concentration (Figure 11, *b*).

The curves of radial stresses considering concentration in the weld zone show that the maximum radial stress in the welded disk of the first variant acts in r = 500.91 mm point and makes 35.8 MPa, and in the disk of the second variant it is in the point r = 502.78 mm and makes 37.5 MPa. These values for both variants of

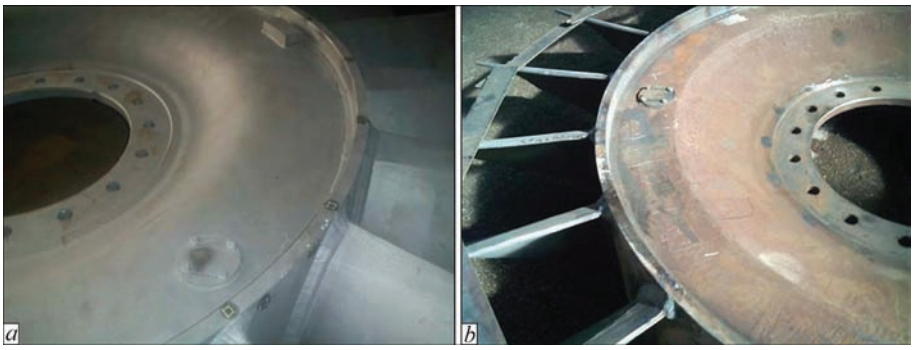

Figure 12. Smoke exhauster impeller with stamped (*a*) and welded (*b*) disk

the welded disk is more than 20 % exceed the value of stress in the hub for corresponding stamped disks.

Analysis of stressed state shows that the maximum stresses in the disks of both variants make not less than $0.2\sigma_y$ (yield strength makes 230 MPa [13] at working temperature 200 °C for steel 20 disk material). Regardless the fact that the maximum stress in the disk of the second variant is much more higher, than in the disk of the first variant, the second variant seems to be more preferable, since possible appearance of cyclic loading in the disk of the first variant provides for the probability of nucleation of fatigue cracks in two zones of stress concentration [14].

Replacement of the stamped structure by recommended variant of the welded disk was virtually realized (Figure 12).

After static and dynamic balancing, the exhauster impeller with the welded disk was put into operation at Ladyzhinsky HPP PJSC «DTEK Zapadenergo».

Conclusions

1. High-efficiency, technological and cost-effective method was developed at «Souyuzenergomash» LLC in scope of program on replacement of foreign component parts by domestic analogues for manufacture of the welded disks of smoke exhauster impellers and two variants of design of these disks structure were proposed.

2. Stuff members of the department of welded structure strength of the E.O. Paton Electric Welding Institute of the NAS of Ukraine developed the algorithm for calculation of disk static strength. It includes determination of service loads, solution of problem on elastic equilibrium of rotating disk as well as evaluation of effect of geometry inhomogeneity in the weld zone on stress distribution.

3. Calculation of stressed state for two variants of the welded disk structure was carried out. As a result, it is determined that the maximum stresses, acting in the welded disks are more than 20 % higher than in the similar stamped parts, however, their value is 5 times lower the yield strength of the disk material at operating temperature.

4. Based on working conditions of the studied parts it is recommended to use a disk structure with lower amount of local stress concentrators, regardless the fact that acting in it maximum stress is somewhat higher, than in alternative design variant.

1. Kishalov, A.E., Kudoyarova, V.M., Markina, K.V. et al. (2012) Analysis of loads applied to elements of gas-turbine engine structure. *Molodoj Uchyonyj*, Vol. 1, 46 (**11**), 52–60.
2. Ryvkin, A.A., Ryvkin, A.Z., Khrenov, L.S. (1987) *Mathematics handbook*. Moscow: Vysshaya Shkola.
3. Timoshenko, S.P., Gudier, J. (1975) *Theory of elasticity*. Moscow: Nauka.
4. Babenko, A.E., Boronko, O.O., Kovalchuk, B.I. et al. (2010) *Procedural guidelines for fulfillment of course and design-graphic works on the subject: Strength of materials (problems and calculation examples) for students of engineering specialities for all forms of education*. Kyiv: Politekhnika.
5. Mozharovsky, M.S. (2002) *Theory of elasticity, plasticity and creep*: Manual. Kyiv: Vyshcha Shkola.
6. Demyanushko, I.V., Birger, I.A. (1978) *Strength calculation of rotating disks*. Moscow: Mashinostroenie.
7. Neuber, H. (2001) *Kerbspannungslehre: Theorie der Spannungskonzentration Genaue Berechnung der Festigkeit*. Vierte Verlag-Berlin: Springer-Verlag Berlin Heidelberg.
8. Verkhovsky, A.V. (1947) Hypothesis of broken sections and its application to calculation of complex configuration rods. *Izvestiya TPI*, 61(**1**), 3–46.
9. Verkhovsky, A.V., Andronov, V.P., Ionov, V.A. et al. (1958) *Determination of stresses in dangerous sections of complex shape parts. Method of nonplanar sections*. Moscow: Mashgiz.
10. Moltasov, A.V. (2013) Application of nonplanar section method for determination of stresses in zones of concentration caused by reinforcement of butt welded joint. *Problemy Prochnosti*, **1**, 159–167.
11. Moltasov, A.V., Klochkov, I.N., Knysh, V.V. (2013) Engineering method of calculation of stress concentration factor in lap welded joint under extension and bending. *Visnyk NTUU KPI. Seriya Mashynobuduvannya*, Issue 69, 150–157.
12. Bugrov, Ya.S., Nikolsky, S.M. (2004) *Higher mathematics*: Manual for institutions of higher education. Vol. 2: Differential and integral calculus. Ed. by V.A. Sadovnichy. Moscow: Drofa.
13. Sorokin, V.G., Volosnikova, A.V., Vyatkin, S.A. et al. (1989) *Grades of steels and alloys*. Ed. by V.G. Sorokin. Moscow: Mashinostroenie.
14. Trufyakov, V.I., Dvoretsky, V.I., Mikheev, P.P. et al. (1990) *Strength of welded joints under alternating loads*. Ed. by V.I. Trufyakov. Kiev: Naukova Dumka.

Received 21.07.2016

doi.org/10.15407/tpwj2016.12.09

ON THE PROBLEM OF PROVIDING ELECTROMAGNETIC COMPATIBILITY OF POWER SOURCES OF RESISTANCE WELDING MACHINES WITH ELECTRIC MAINS

S.K. PODNEBENNAYA, V.V. BURLAKA and **S.V. GULAKOV**
State Higher Educational Establishment «Pre-Azov State Technical University» (PSTU)
7 Universitetskaya Str., 87500, Mariupol, Ukraine. E-mail: office@pstu.edu

In the work the problems of providing electromagnetic compatibility of power sources of single-phase resistance welding machines with three-phase supply mains were studied. The two basic directions were considered: the application of active filter-compensating and balancing devices (AFCBD) and the development of power sources (PS) with the power factor correction (PFC). The application of AFCBD allows using the existing welding equipment, but the high cost limits its wide application. PS with PFC assumes the use of converters either with DC link, or with direct matrix converters, as far as the basic requirement to PS for welding machines is the possibility of generating output voltage of preset shape, amplitude and frequency. In the article the method of control of three phase-single phase matrix converter with six switches was considered, which allows generating the output voltage of rectangular shape of 50 Hz frequency. The selection of frequency was predetermined by application of welding transformer, designed for operation at mains frequency. The shape of voltage was selected from the conditions of providing the minimum losses of power in the mains and inadmissibility of saturation of the welding transformer. The authors suggested also the circuit solution and the method of control of matrix converter with five switches, which during generation of output voltage, synchronized with the mains, allows obtaining the power factor of PS close to one. The analysis of sensitivity of the proposed power source to deviation of voltages was carried out, as a result of which it was determined, that at generation of rectangular voltage it was possible to achieve the stable operation at the voltage deviations of about 10 %, due to which the quality of welded joints was significantly increased. 11 Ref., 3 Tables, 5 Figures.

Keywords: *resistance welding machine, power source, matrix converter, power factor, electromagnetic compatibility*

The power sources (PS) of resistance welding machines are powerful non-linear consumers of electric mains. In most of them the thyristor control circuits are applied. Furthermore, such PS, being mostly single-phase, at their connection to three-phase mains (especially at switching and simultaneous operation of several PS of machines at different phases), have a negative influence on it. This is expressed in growth of asymmetry coefficients and non-sinusoidal voltage [1–4]. The deterioration of quality of supply voltage affects in its turn the quality of welding, moreover, the most significant is the deviation of voltage, which at excess of 15 % results in 100 % rejection (for corrosion-resistant steels 100 % rejection is caused by the deviation of voltage to the amount of more than 10 %) [5]. Thus, the solution of problem of providing electromagnetic compatibility of welding equipment with electrical mains is an urgent problem.

The solution of the specified problem is possible in two directions: the application of additional active filter-compensating and balancing devices (AFCBD) [6], or the development and application of PS with a power factor correction (PFC) [4, 7, 8]. The realization of the first variant allows providing the required (not always single) power factor (PF) of the complex «welding power source — AFCBD», reduces the losses of power in electrical mains, provides symmetrical loading of three phases in operation of single-phase power source in the three-phase mains. The advantage of such approach is retaining of the existing welding PS during the technological process without any modifications. The basic drawback of the first variant is its low profitability, as far as the cost of AFCBD is commensurable with the cost of PS itself.

The other direction for solution of the formulated problem is the PS updating. It has prospects in connection with development of power electronics and appearance of powerful and quick-response power switches, allowing switching the high loads.

In the works [9, 10] the circuit solutions were considered aimed at updating PS by applying thyristor converters of three-phase voltage to a single phase, allowing providing a symmetric (or quasi-symmetric) consumption of currents. The main disadvantage of these circuits is a high ratio of non-sinusoidal currents

consumption (up to 80–90 %) and the need in applying a low-frequency transformer, caused by the decreased frequency of output voltage, generated by the thyristor converter.

For today the more effective is the development of transistor PS, which are designed mainly on the basis of power converters with an intermediate link of direct current (rectifier, DC link, inverter). The connection of such converters to electric mains is carried out through input three-phase LC-filter, isolating the mains from the modulation current components, generated by the converter.

At the symmetric system of mains voltages, the application of uncontrolled rectifier (for example, six-pulse one) provides the consumption of symmetric currents from mains [8]. However, at asymmetrical mains voltages, the symmetry of the consumed currents is also violated. In addition, the spectral composition of currents consumed by the six-pulse rectifier, does not allow providing its electromagnetic compatibility with mains without installation of AFCBD in accordance with the standards established by GOST 13109–97, DSTU IES 61000-3-2:2004, 61000-3-4:2004.

The topologies of inverters, which are the most frequently used for such PS, are bridge, half-bridge and push-pull, as far as they allow providing the absence of a permanent component of magnetic flux in the transformer. The push-pull and bridge inverters generate a bipolar voltage at the output of converter, the maximum value of which is equal to the voltage of DC link. The disadvantage of push-pull inverter is the need in using switches, capable to withstand a double voltage of DC link; among the disadvantages of bridge inverter is an increased number of power switches (four at the bridge against two in the push-pull ones). The half-bridge inverter, consisting of two switches, generates an output voltage, the maximum value of which is equal to half of the voltage of DC link, which is its drawback [8].

The installation of PF corrector on the input of the converter allows providing the sinusoidal currents consumption [7], however it slightly reduces the technical and economic characteristics of the power source in connection with an increased number of controlled power switches.

PS with PFC on the base of converters with an intermediate DC link are quite effective, but their wide application is hindered by the high cost. In addition, there is a problem in reliability of energy storage device in the DC link as well as the need in introducing the special circuits for limiting charge current of capacitors at connection of the power source to mains.

Therefore, for today the investigations are directed mainly to reducing the cost of such PS. It provides possibility to formulate the aim of the article, which consists in development of effective power source for resistance welding machine, providing a high quality of welding process and electromagnetic compatibility with mains.

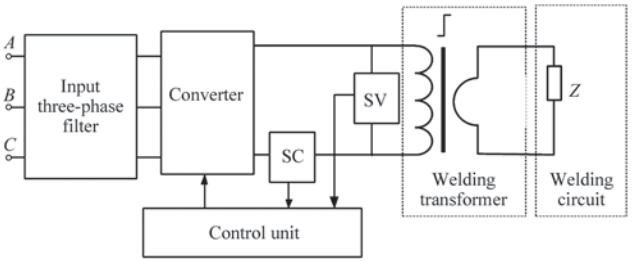

Figure 1. Schematic block diagram of MRW connection to mains

The authors proposed to study PS of MRW, which consists of a welding transformer, a converter, installed into the primary circuit of transformer and an input filter, switched on between converter and mains (Figure 1). As input signals for control of converter, the initial current and voltage serve, measured by the respective sensors (SC, SV), and the mains voltage. As the converter of PS of MRW, it is proposed to use a direct matrix converter (MC), a feature of which is that an intermediate link of direct current (usually — capacitor of high capacity) is absent, which significantly increases the technical and economic indicators of the converter.

Three-phase-single-phase MC consists of six bidirectional switches, each of which switches on one of the phases of mains directly to the load (Figure 2). The bidirectional switches can be designed in the form of two transistors with reverse diodes, having an inverse-series connection, and the controlling electrodes of transistors are connected to a control unit (CU).

It is known that the minimum of power losses in the electric mains at the connection of load to it can be obtained by providing the proportionality between the consumed currents and the corresponding phase voltages [11]. Thus, MC should simulate the symmetrical active load.

The instantaneous active power of three-phase mains is determined as the sum of instantaneous active powers of all three phases:

$$p(t) = p_A(t) + p_B(t) + p_C(t) = \\ = (u_A(t))^2 / R + (u_B(t))^2 / R + (u_C(t))^2 / R, \quad (1)$$

where $p_A(t) = (u_A(t))^2/R$ is the instantaneous phase power A; $p_B(t) = (u_B(t))^2/R$ is the instantaneous phase power B; $p_C(t) = (u_C(t))^2/R$ is the instantaneous phase power C, R is the simulated active load, Ohm; $u_A(t)$, $u_B(t)$, $u_C(t)$ are the instantaneous phase voltages of mains, V.

For symmetrical voltages and load the instantaneous power, consumed by the latter, is a constant value. At the same time, due to absence of energy ca-

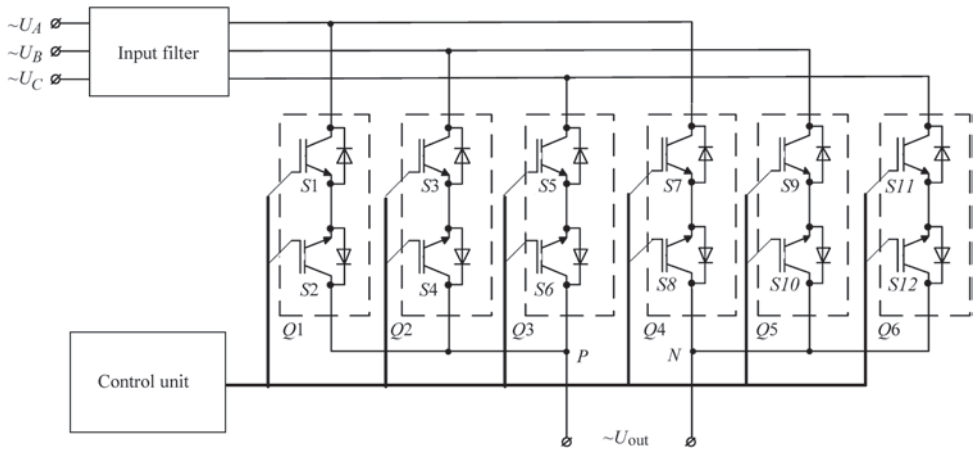

Figure 2. Simplified electric circuit of matrix converter

pacitor, MC itself is not a consumer of active power (excluding the losses of power in the power switches, which in the meantime can be neglected). It follows from this, that to provide a symmetric consumption of currents, MC should operate at a constant active power.

$$P = U(t)I(t) = \text{const}, \tag{2}$$

where $U(t)$ is the output voltage of MC, V; $I(t)$ is the output current of MC, A.

If we neglect the influence of inductance of welding circuit on the output current of the converter, it can be assumed with an admissible error that the symmetrical consumption of MC currents is possible at the generation of constant voltage at its output. Moreover, the constant component of the current, passing through the primary winding of welding transformer, will lead to increase in magnetization and significant power losses.

This can be avoided by providing a change in polarity of MC output voltage in accordance with the expression:

$$\int_0^{T_{out}} U(t)dt = 0, \tag{3}$$

where T_{out} is the period of MC output voltage, s.

At asymmetric system of mains voltages the instantaneous active power of three-phase mains, determined by the expression (1) is not a constant value, then the control of converter can be realized from the condition of the preset active power consumption averaged over the period of mains, which is controlled by changing the simulating active resistance R. Here, the simulating active resistance should not vary during the period of mains not to generate the low-frequency harmonics.

Let us consider the symmetrical voltage system, and, according to the abovementioned assumption, let us carry out the generation of rectangular voltage with 50 Hz frequency at the output of MC. Let us accept the initial phase shift of the voltage phase A as equal to zero. Let us conditionally divide the period of mains into six sectors: to the first and the fourth sector the highest absolute value of the instantaneous voltage of the phase B corresponds (the first is at the negative voltage of the phase B, the fourth is at the positive one), to the second and the fifth — of the phase A (the second at the positive voltage of phase A, the fifth at the negative one), the third and the sixth — to phase C (the third is at the negative voltage of phase C, the sixth is at the positive one).

The duty cycles of the controlling pulses of switches $Q1$–$Q6$ are calculated according to the following expressions:

$$D_1 = \frac{u_A(t)}{RI(t)};\quad D_2 = -\frac{u_B(t)}{RI(t)};\quad D_3 = -\frac{u_C(t)}{RI(t)};$$
$$D_4 = -D_1;\quad D_5 = -D_2;\quad D_6 = -D_3. \tag{4}$$

The selection of the necessary pair of switches for the positive polarity of the output voltage occurs in the control unit in accordance with the Table 1.

A single duty cycle of pulse in the Table means that in the given sector the switch is switched on constantly. To generate the output voltage of negative polarity, the signals of control of switches $Q1$–$Q3$ and $Q4$–$Q6$ change their places with each other (Table 2).

The formation of output voltage with 50 Hz frequency allows achieving one more effect: at synchronization of output voltage with one of the mains voltage (for example, phase A), a number of power switches of converter can be reduced to five (Figure 3). The duty cycles of the controlling pulses of switches of the converter with five switches are calculated in accordance with (4) and are presented in Table 3.

The application of MC with five switches allows preserving all the properties and advantages of classic MC with six switches, excluding the possibility of changing the output frequency, but in view of the overwhelmed majority of welding PS designed for

Table 1. Distribution of control signals of switches depending on number of sector for positive polarity of output voltage

Number of switch	Sector of mains period					
	1	1	3	4	5	8
$Q1$	D_3	1	D_1	0	$1 - D_2 - D_3$	0
$Q2$	$1 - D_3 - D_3$	0	D_2	1	D_2	0
$Q3$	D_3	0	$1 - D_1 - D_2$	0	D_3	1
$Q4$	0	$1 - D_5 - D_6$	0	D_4	1	D_4
$Q5$	1	D_5	0	$1 - D_4 - D_6$	0	D_5
$Q6$	0	D_6	1	D_6	0	$1 - D_4 - D_5$

Table 2. Distribution of signals for control of switches depending on number of sector for negative polarity of output voltage

Number of switch	Sector of mains period					
	1	2	3	4	5	6
$Q1$	0	$1 - D_5 - D_6$	0	$D4$	1	$D4$
$Q2$	1	D_5	0	$1 - D_4 - D_6$	0	D_5
$Q3$	0	D_6	1	D_6	0	$1 - D_4 - D_5$
$Q4$	D_1	1	D_1	0	$1 - D_2 - D_3$	0
$Q5$	$1 - D_4 - D_3$	0	D_2	1	D_2	0
$Q6$	D_3	0	$1 - D_1 - D_2$	0	D_3	1

operation with the transformer of a commercial frequency, it is not a disadvantage.

As a result of mathematical modeling in the package MathCAD the diagrams of input currents, output voltage and current of MC with five switches were obtained (Figures 4, 5). The parameters of MC are as follows: switching frequency is 3.2 kHz, preset output voltage is rectangular, with 50 Hz frequency and the amplitude value of 300 V; the leakage inductance, reduced to the primary winding, amounts to 0.6 mH, active resistance is 2.5 Ohm; inductance of input filter is 0.1 mH, capacitance of input filter is 24 μF. The coefficient of non-sinusoidal input current of the phase, synchronized with the output voltage of the converter, being at the switching frequency after filtering the components, is about 6 %. The power factor is about 95.6 %, the coefficient of asymmetry of input currents by reverse sequence is about 4 %.

Table 3. Distribution of signals for control of switches depending on number of sector for generating output voltage of matrix converter with five switches

Number of switch	Sector of mains period					
	1	2	3	4	5	6
$Q1$	1	D_2	0	1	D_2	0
$Q2$	0	D_3	1	0	D_3	1
$Q3$	D_4	1	D_4	D_4	1	D_4
$Q4$	D_5	0	D_5	D_5	0	D_5
$Q5$	D_6	0	D_6	D_6	0	D_6

The power factor of the described PS of resistance welding machines is much higher than that in the existing thyristor ones, which usually does not exceed 60 % [5]. Moreover, the switching of single-phase resistance welding machine to three-phase mains using the described PS, does not result in arising asymmetry and provides a symmetrical consumption of currents, close to sinusoidal as to the shape.

The application of MC for MRW power supply provides one more positive effect. When switching the welding transformer from the mains directly through the thyristor contactor [10], the maximum voltage, supplied to the primary winding, reaches $\sqrt{3}U_f$. The output voltage of MC is not higher than $1.5U_f$. However, at the rectangular shape of output voltage of MC with the maximum amplitude of $1.5U_f$, the actual value of the first harmonics of voltage will

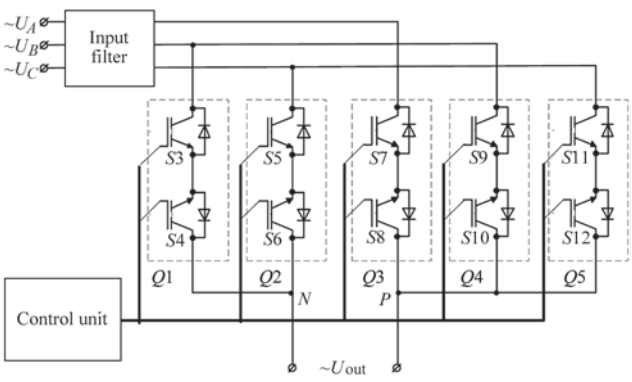

Figure 3. Simplified electric circuit of matrix converter with five switches

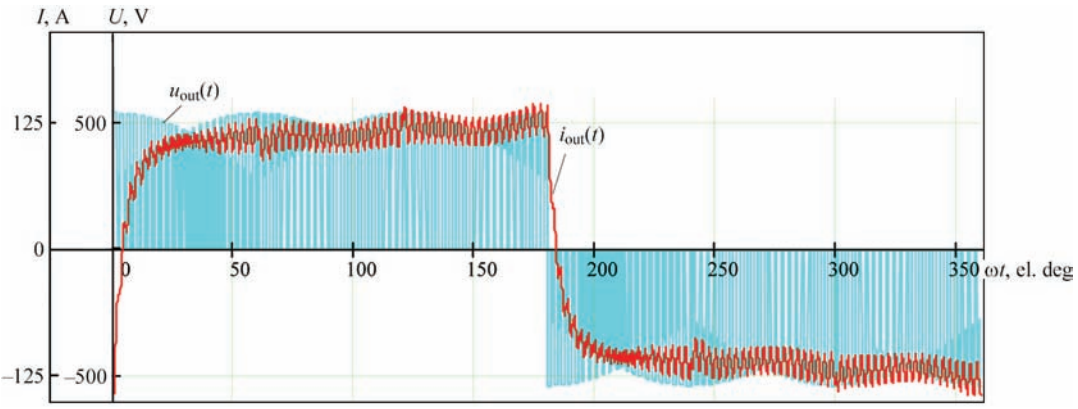

Figure 4. Diagrams of output voltages and current of MC with five switches

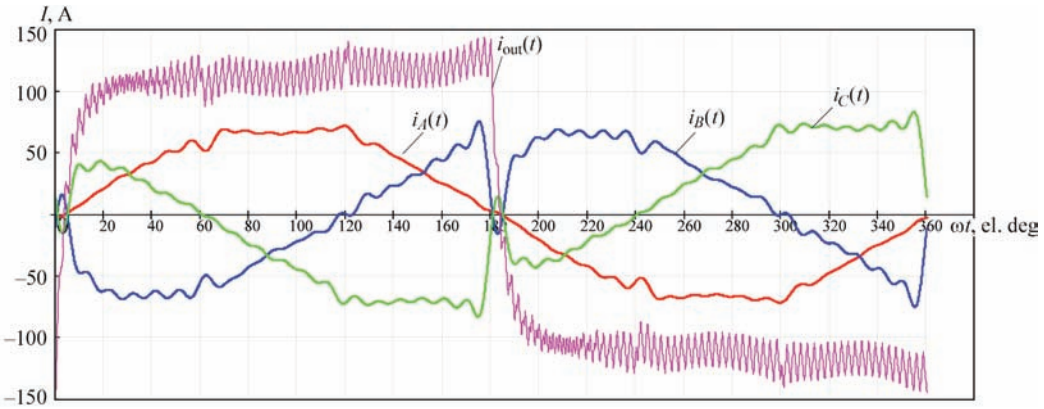

Figure 5. Diagrams of input currents of MC with five switches and its output current

amount to $6U_f/\pi$, that allows reducing the sensitivity to deviations of mains voltage, providing the margin of voltage of about 10 % and increasing the quality of welded joints.

The application of the described converters and the method of their control allowed achieving the high quality of the resistance welding process, thus having provided a high power factor of PS and its electromagnetic compatibility with the mains.

1. Pismenny, A.A. (2014) Improvement of power efficiency of machines for resistance spot welding by longitudinal compensation of reactive power. *The Paton Welding J.*, **1**, 25–29.
2. Rudenko, P.M., Gavrish, V.S. (2013) Thyristor direct converters for supply of resistance welding machines. *Ibid.*, **8**, 54–56.
3. Rymar, S.V., Zhernosekov, A.M., Sidorets, V.N. (2011) Effect of single-phase power sources of welding arc on electric mains. *Ibid.*, **12**, 7–12.
4. Safronov, P.S., Bondarenko, Yu.V., Bondarenko, O.F. (2014) Improvement of electromagnetic compatibility of power sources for resistance welding systems. *Tekhnichna Elektrodynamika*, **5**, 89–91.
5. Vagin, G.Ya. (1985) *Modes of electric welding machines*. Moscow: Energoatomizdat.
6. Podnebennaya, S.K., Burlaka, V.V., Gulakov, S.V. (2012) Decrease of disturbances generated by welding power sources using parallel active filter of higher efficiency. *Visnyk DDMA*, 28(**3**), 221–226.
7. Wagner, M., Kolb, S. (2013) Efficiency improvements for high frequency resistance spot welding. In: *Proc. of 15th European Conf. on Power Electronics and Applications* (EPE), 1–9.
8. Saleem, J. (2012) Power electronics for resistance spot welding equipment. *Mid Sweden University Licentiate Thesis*. Sundsvall.
9. Lebedev, V.K., Pismenny, A.A. (2003) Power system of flash-butt welding machines with a transistor inverter. *The Paton Welding J.*, **2**, 10–12.
10. Lebedev, V.K., Pismenny, A.A. (2001) Power systems of resistance welding machines. *Ibid.*, **11**, 28–32.
11. Podnebennaya, S.K., Burlaka, V.V., Gulakov, S.V. (2013) Peculiarities of regulation of power parallel active filter. In: *Proc. of 11th Int. Sci.-Techn. Conf. of Junior Scientists and Specialists on Electromechanical and Power Systems, Methods of Modeling and Optimization* (Kremenchuk, Ukraine, 9–11 April 2013), 168–169.

Received 14.10.2016

58th INTERNATIONAL WELDING CONFERENCE «TECHNOLOGIES OF THE XXI CENTURY» AND INTERNATIONAL WELDING FAIR EXPOWELDING-2016

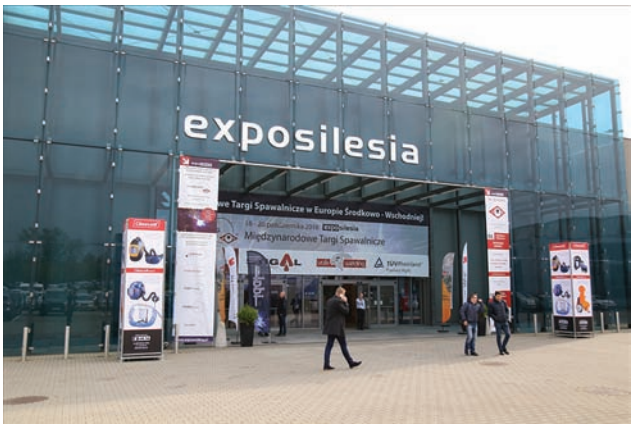

The 58th International Welding Conference «Technologies of the XXI Century» was held on October 18–20, 2016 in Sosnowiec (Poland). The Conference was organized by Poland Institute of Welding and took place at ExpoSilesia Exhibition Center in scope of International Special Fair ExpoWELDING-2016.

ExpoWELDING-2016 Fair. Regular International Special Fair ExpoWELDING-2016 was held on October 18–20, 2016 in Sosnowiec. It is one of the biggest events of welding industry for Central and Eastern Europe. More than 174 companies from Poland, Czech Republic, Germany, Turkey, Netherlands, Slovakia, Ukraine, Canada, Finland, Taiwan and Sweden took part in the Fair work. The largest welding companies of the world were represented at the Fair. Around 5000 specialists of welding industry from Poland and other countries visited the Fair, 40 new products were exhibited. ExpoWELDING-2016 Fair particularly became also a fair of robotization and automation of welding processes applicable to different branches of industry. For the first time Ukraine was represented by a joint booth of five companies, namely E.O. Paton Electric Welding Institute, «TM. WELTEK» LLC (Kiev), «Vita Polis» LLC (Boyarka, Kiev region), «Sumy Electrode» LLC (Sumy) as well as plant of autogenous welding equipment «Donmet» (Kramatorsk).

All Ukrainian companies are already well known in Ukraine as well as out of its borders. Today «TM. WELTEK» LLC is the largest manufacturer of flux-cored wires for surfacing with wide range of materials; «Vita Polis» LLC is the young, but ambitious company specialized in production of wires for welding of carbon, stainless and heat-resistant steels and nickel-based alloys; «Sumy Electrode» LLC is the leading manufacturer of high-quality welding electrodes of special designation.

The joint booth was organized by International Association «Welding» upon an initiative of E.O. Paton Electric Welding Institute and was used for negotiations between Poland and Ukraine specialists. A technology of magnetically-impelled arc butt welding was presented on the booth. It raised interest of the representatives of Poland industry.

Regular XVIII meeting of the Board of International Association «Welding» with the participation of IAW founders, namely E.O. Paton Electric Welding Institute, Poland Institute of Welding, «KZU Group Engineering» (Bulgaria), Institute of Welding «JUG» (Macedonia), was held in course of Fair work. The Board stated the main directions of IAW long term activities and made a decision on having the next XIX meeting of IAW Board in Germany in September 2017.

The participants were awarded with the honorary diplomas of the Fair at awarding ceremony upon Fair work completing. The International Association «Welding» was awarded with a diploma for contribution in international cooperation.

Welding Conference «Technologies of the XXI Century». More than 350 researches and specialists from Poland, Germany, Netherlands, Slovakia, Ukraine and Finland participated in the Conference work. The Conference included a session on «Role of welding in the structures of nuclear power plants» in respect of Poland industry, where five reports were presented. To the beginning of the Conference the plenary papers were published in a special issue of «Biuletyn Instytutu Spawalnictwa» journal No. 5, 2016.

Below is a series of papers presented during the Conference.

Gary B. Marquis — «IIW: developing global best practices for the fatigue assessment of welded struc-

tures». The Intemational Institute of Welding (IIW) acts as the global network of knowledge exchange concerning the joining of materials. One of the working teams, i.e. Committee XIII, is dedicated to new research results and the implementation of innovative technologies in order to avoid fatigue failures in welded structures. Presently, the Committee is developing several new guidelines aimed to increase the fatigue service life of welded structures. One of the guidelines is concerned with the frequent use of mechanical treatment is a method of increasing the fatigue strength of welded structures. The article discusses aspects of the above-named guidelines and the uniqt1e international IIW collaboration enabling the development of these guidelines.

S. Keitel, U. Wolski, U. Mückenheim, Ch. Sondershausen, J. Müglitz — «MIG welding machines for large steel structures». The volume of welding fabrication, geometry and quality standards in the wind power sector require automation. The use of convertional industrial robots is often impossible due to safety, costs, workplace accessibility and programming time. On the other hand , typical processing rasks and post-processing activities such as cutting, arc welding and ultrasonic tests are excessively complex to be mechanised using simple tooling. Small and inexpensive modular devices on rails, known as crawlers, bridge the gap between simple mechanised equipment and industrial robots. Such devices combine easy handling and operational versatility, even in difficult site conditions, characteristic of mechanised equipment with programmability and sensor-controlled movements typical of industrial robots. This article discusses the possibilities and limitations of the above-presented concept in relation to a number of its practical applications.

M. Fiedler, A. Plozner, B. Rutzinger, W. Scherleitner — «Control of mechanical properties of high strength steels through optimized welding processes». The cooling time between 800 and 500 °C is a crucial factor significantly determining the properties of welded joints made of high strength steels. In field welding, the cooling time $t_{8/5}$ can be controlled by heat input even if different wall thicknesses of base materials are used. Modern arc processes with reduced hear input allow obtaining the same with comparable deposition rates and increase the stability of the strength level due to optimized equipment settings. This paper compares conventional GMAW processes, e.g. short arc, spray arc GMAW pulse with new processes such as PMC (pulse multi control) and otl1ers processes in relation to weld properties. Particu1ar emphasis is given to all weld metals and welds. The deliberations presented in the paper allow drawing practical conclusions and formulating recommendations aimed to optimize welding-related properties.

J. Górka, S. Stano — «Laser beam welding of 10 mm thick T-joints made of TMCP steel». The article presents research on the laser·beam welding of 10 mm thick T-joints made of thermomechanically worked high-strength steel S700MC without using a filler metal. The research-relared tests involved making single-sided and double-sided welded joints as well as performing non-destructive tests. The quality of joints satisfied the requirements of quality 1eve1 B according to the PN-EN ISO 13919-l standard. The single-sided welding performed using a beam power of 11 kW enabled the obtainment of 8 mm deep penetration without noticeable displacements in the web. The double-sided welded joints were characterized by correct geometry; the dimensions of pores present in the weld metal satisfied the maximum pore size c1iterion specified for quality 1evel B. The weld microstructure was bainitic-ferritic; the hardness of the weld was by about 60 *HV*1 higher than that of the base material (280 *HV*1). The HAZ revealed a small decrease in hardiness in comparison with that of the base material.

V. van der Mee — «Welding of (super) duplex stainless steels». The article presents and describes in detail duplex steels used in modern sectors of industry (duplex, super duplex, lean duplex and hyper duplex) with particu1ar attention paid to corrosion resistance and primary areas of application. The article also discusses welding-related issues including the preparation of the base material, welding techniques and procedures, requirements concerning heat input as well as pre-weld and post-weld heat treatment. The article emphasizes the growing use of duplex steels, among other things in welded structures, and forecasts their further development.

P. Bernasovský, A. Petráňová — «Failures of high alloy austenitic steel structures — case studies». The article presents failures of structures made of austenitic steels. The first part is concerned with accelerated (centrifugally) cast rubes (∅52.6×5.8 mm) made of steel 25–35 CrNi exposed to high temperature and severe reducing environment (a_c >> 1). The second part of the article presents test results related to a water meter element and a cooling water pipeline made of austenitic steel. In both cases, a relatively short period of service was accompanied by the appearance of

leaks. The tests revealed that the failures were triggered by microbiological corrosion caused by a sulphur reducing bacteria and not by the welding technology applied.

J. Adamiec — «Properties of laser welded tinned tubes made of nickel alloys». The article presents test results concerning properties of ribbed pipes made of the Inconel 625 nickel alloy in terms of their thermal efficiency, resistance to high — temperature corrosion and electrochemical corrosion resistance. It was ascertained that the use of 1ibs (fins) as the extension of heat exchanges surface increases the thermal efficiency of pipes almost by thrice without compromising high corrosion resistance in flue gas atmosphere and electrochemical corrosion.

Booth of Poland Institute of Welding

The improvement of the structure and mechanical properties of electron beam welded joints required the performance of post-weld heat treatment. The best mechanical characteristics of welded joints were obtained after a heat treatment performed in a furnace (annealing at T = 900 ºC for 1 hour and cooling along with the furnace) favouring the obtainment of an almost homogenous structure and the decomposition of metastable phases in the weld and HAZ.

A.A. Golyakevich, L.N. Orlov — «Surfacing performed using flux-cored wire in Ukrainian companies». The article describes experience of extending the service life of various machinery parts by surfacing them with flux-cored wires. High wear resistance during the rolling and straightening of steel is achieved by the formation of a martensitic matrix reinforced with dispersive carbides.

Booth of Fronius company

S.G. Grigorenko, S.W. Akhonin, W.Yu. Belous, R.V. Selin — «Heat treatment effect on the structure and properties of electron beam welded joints made of' high-alloy titanium». The article presents the specific formation of a joint made of high-strength high-alloy titanium alloy (α + β) subjected to electron beam welding in vacuum. Tests involved the use of Ti–Al–Mo–V–Nb–Cr–Fe–Zr specimens obtained through electron melting. The research involved tests focused on the effect of a welding thermal cycle and post-weld heat treatment on structural-phase transformations in the weld metal and HAZ of welded joints. It was revealed that the weld metal and HAZ were composed of a structure dominated by the metastable phase β, which led to the reduction of plasticity and toughness indexes.

Joint booth of Ukrainian companies

Participants of the Conference — «patonovtsy» (representatives of Paton Institute) of different years, *from left to right*: L.N. Orlov («TM.WELTEK» LLC, Kiev), M. Beloev (KZU Group Engineering, Sophia), S.G. Grigorenko (PWI, Kiev)

M. Beloev, N. Lolov — «Selected technological aspects concerning the making of ammonia storage tanks». The article discusses factor s connected with the stress corrosion cracking of ammonia storage tanks and presents the details of a welding technology ensuring the obtainment of the maximum service life of these tanks.

T. Piwowarczyk, M. Korzeniowski, A. Ambroziak, T. Kowal, R. Rutka, M. Karolewski — «Effect of pipe face preparation on the quality of magnetically impelled arc welded joints». The article presents magnetically impelled arc welding — a technology used when making butt joints mainly of elements having circular cross-sections. In addition, the articles indicates issues relate to the preparation of pipe faces and its effect on the quality of welds. The research-related experiment involved the use of selected power transmission elements. The research also included the performance of visual, geometry, metallographic, functional and technological tests of the joints as well as the determination of critical imperfections disqualifying the use of welded joints.

Z. Mikno — «High-frequency invertor welding machine — advantages of new technology». The article presents advantages of inverter welding machines having a high operating frequency of 10 kHz and compares conventional AC 50 Hz welding machines as well as inverter welding machines having operating frequency of 1 and l0 kHz. The article presents research results obtained within a currently implemented project of Programme of Applied Research (PBS3/B4/12/2015).

T. Hejwowski, K. Marczewska-Boczkowska, E. Zięba — «Microstructure, wear resistance and corrosion resistance of coatings surfaced with Ni–Co-base alloys». The article presents results of tests concerning coatings subjected to plasma surfacing involving the use of Co- and Ni-based powder mixtures. The research involved the performance of abrasive wear tests (with corundum abrasive) and adhesive wear tests in the roller-block system. Test concerning electrochemical corrosion were performed in a 3 % aqueous solution of NaCl. The article demonstrates the possibility of making wear resistant coatings of inrermediate chemical compositions.

Awarding ceremony, *from left to right*: A.T. Zelnichenko, Director of IAW; A. Pietras, Director of Poland Institute of Welding, Prof. J. Pilarchik

During IAW Meeting

J. Pikula, M. Lomozik, T. Pfeifer — «TIG method in the multiple repair welding of long-operated components in the power industry». The article presents the results concerning the repair welding of a long-op-

erated waterwall using the mechanized TIG method. The tests were focused on determining the effect of a repair performed in order to remove cracks in welded joints located along flat bars opening on the tube wall side on the structure and hardness of the heat affected zone (HAZ) of a repair welded joint in the waterwall. In addition, the tests investigated the influence of multiple repair welding on the formation of structural notches in the HAZ.

K. Luksa, M. Bednarek — «Weldability of toughened steels used in ballistic shields». The article characterises selected toughened steels used in the production ballistic shields, presents standard requirements in terms of the properties and chemical composition of these steels as well as enumerates and discusses guidance on the welding of such steels. The article also presents the results concerning the comparison of the carbon equivalents (C_e) of selected steels used for ballistic shields and preheating temperatures suggested by steel producers. The analysis of collected information revealed that the above named steels should be welded using low-hydrogen processes ensuring the obtainment of a diffusive hydrogen content below 5 cm^3 per 100 g of the weld deposit. It was also ascertained that sheets having thicknesses above 30 mm should be subjected to preheating and that interpass temperature should not exceed 200 °C. In addition, it was determined that welding should be performed using multiple runs and austenitic high-alloy filler metals, preferably G 18 8 Mn and that gas mixture-shielded welding processes should be performed using argon-based mixtures; preferably 82 % Ar + 18 % CO_2 or 92 % Ar + 8 % CO_2.

S. Stano, J. Adamiec, J. Dworak, M. Urbańczyk — «Laser welding of T-joints made of thin austenitic sheets». The article presents test results concerning the CO_2 and Yb:YAG laser welding of thin-walled T-joints made of steel X5CrNi18–10 (steel 304), X6CrNi18–10 (steel 304H) and XI5CrNiSi25–21 (steel 310) selected as stainless steels potentially useful in the production of ribbed pipes (finned tubes) intended for·operation in boilers of supercritical parameters. Welding tests were performed using two different laser sources, i.e. a CO_2 gas laser and a Yb:YAG solid state laser. The tests involved the determination of the appropriate angle of laser beam insertion into the interface of sheets, enabling the obtainment of properly shaped welds. Non-destructive tests classified the joints as representing quality level B in accordance with standard 13919-1. Selected joints were tested for the distribution of alloying constituents in the joint area. It was ascertained that laser welding made it possible to maintain the uniform distribution of alloying constituents without their significant depletion in the weld area. The tests were financed using the funds of project PBS1/A5/13/2012.

A. Świerczyńska, J. Łabanowski, D. Fydrych — «Effect of linear energy and microstructure on the content of retained hydrogen in welded joints made of superduplex steels». The article presents tests concerning the content of retained hydrogen present in FCAW and SAW welded joints made of superduplex steel. The use of various welding technologies resulted in the obtainment of welds having different microstructures and ferrite contents. Measurements of retained hydrogen present in joints (performed using the complete combustion method) revealed various contents of hydrogen in the base material and in the welds subjected to the tests. Ir was determined that the content of hydrogen in welds made of superduplex steels depends not on1y on the volumetric content of microstructures but also on their composition and welding linear energy.

Dr. A.T. Zelnichenko, IAW

PATON PUBLISHING HOUSE

www.patonpublishinghouse.com

SUBSCRIPTION

«The Paton Welding Journal» is Published Monthly Since 2000 in English, ISSN 0957-798X.

«Avtomaticheskaya Svarka» Journal (Automatic Welding) is Published Monthly Since 1948 in Russian, ISSN 005-111X.

«The Paton Welding Journal» is Cover-to-Cover Translation of Avtomaticheskaya Svarka» Journal into English.

If You are interested in making subscription directly via Editorial Board, fill, please, the coupon and send application by Fax or E-mail.

The cost of annual subscription via Editorial Board is $348 for «The Paton Welding Journal» and $180 for «Avtomaticheskaya Svarka» Journal.

«The Paton Welding Journal» can be also subscribed worldwide from catalogues subscription agency EBSO.

SUBSCRIPTION COUPON

Address for journal delivery _____

_____

Term of subscription since _____ **20** **till** **20** _____

Name, initials _____

Affiliation _____

Position _____

Tel., Fax, E-mail _____

We offer the subscription all issues of the Journal in pdf format, starting from 2009.

The archives for 2009–2014 are free of charge on *www.patonpublishinghouse.com* site.

ADVERTISEMENT

in «Avtomaticheskaya Svarka» and «The Paton Welding Journal»

External cover, fully-colored:
First page of cover (190×190 mm) — $700
Second page of cover (200×290 mm) — $550
Third page of cover (200×290 mm) — $500
Fourth page of cover (200×290 mm) — $600

Internal cover, fully-colored:
First/second/third/fourth page of cover (200×290 mm) — $400

Internal insert:
Fully-colored (200×290 mm) — $340
Fully-colored (double page A3) (400×290 mm) — $500

- Article in the form of advertising is 50 % of the cost of advertising area
- When the sum of advertising contracts exceeds $1001, a flexible system of discounts is envisaged

Size of journal after cutting is 200×290 mm

Editorial Board of Journal «Avtomaticheskaya Svarka» and «The Paton Welding Journal»
E.O. Paton Electric Welding Institute of the NAS of Ukraine
International Association «Welding»
11 Kazimir Malevich Str. (former Bozhenko Str.), 03680, Kiev, Ukraine
Tel.: (38044) 200 60 16, 200 82 77; Fax: (38044) 200 82 77, 200 81 45
E-mail: journal@paton.kiev.ua; www.patonpublishinghouse.com